Packed bed gasification-combustion in biomass based domestic stoves and combustion systems

A Thesis

Submitted for the Degree of

Doctor of Philosophy

in the Faculty of Engineering

by

S Varunkumar

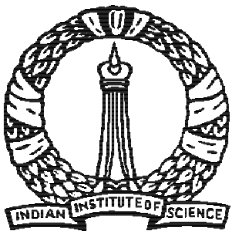

Department of Aerospace Engineering
Indian Institute of Science
Bangalore – 560 012 (INDIA)

17 Feb 2012

Dedicated to my parents

Shri V Sivakumar and Smt. Revathi Sivakumar

Acknowledgements

My heartfelt thanks to Dr N K S Rajan for giving me an opportunity to work in CGPL without which I would not have got a chance to interact and work closely with Prof H S Mukunda. This thesis would not have been possible without their guidance and persistent help. Special thanks to Srinath for helping me with the stove experiments. I thank Dr Dasappa and Prof P J Paul for their support. I am also grateful to the entire team of technicians at CGPL - without their support none of the experiments would have been possible. Thanks to Sheshagiri and his team for helping me with automation and data acquisition. Indranil's video editing skills came handy in creating high quality visual data used in the thesis - my sincere thanks to him. I thank the entire GIS team for promptly attending to problems related to clusters and other computer related issues. My sincere thanks to members of the CGPL students room and other friends at the institute for useful discussions, suggestions and more than that for making my stay at the institute lively and memorable. I extend a very special thanks to my brother, Raman.

Abstract

This thesis constitutes fundamental experimental and computational investigations on gasification and combustion in a packed bed of biomass. Packed bed gasification-combustion in counter-current mode is used in two applications - (1) Gasifier stove in reverse downdraft mode (or equivalently, top-lit updraft mode) that constitutes the idea behind efficient and clean burning domestic stoves. (2) Combustion-on-moving grate for boiler application studied widely in Europe. While a large part of the present study is around domestic stoves, a crucial part of the study aims to address the second application as an extension of the approach taken in the first part to clarify conflicting conclusions of earlier studies and explain the aero-thermo-chemical behavior over the entire range of superficial velocities, V_s (this is velocity of air through the empty cross section of combustion chamber). Operational differences between the two applications lie in the range of superficial velocity - 3.5 to 6 cm/s for domestic stoves and 15 to 30 cm/s for grate combustion. Lower values of V_s are chosen for domestic stoves to limit the particulate emissions; higher values of V_s for combustion-on-grate to maximize the conversion rate.

Present work deals with a fan based gasifier stove, Oorja, built by BP, India (currently transferred to FEPL, Pune) and disseminated to over 400,000 households between 2005 and 2009. The technology was developed at CGPL, IISc and transferred to BP for commercialization. Work reported in this thesis was started to resolve issues of higher CO emissions in char mode operation and occasional smoking during transition from flaming to char mode. The contribution of the thesis is split into two parts. (a) Use of the principles of gasification to improve the performance of the stoves to the highest possible level, balancing between efficiency and ash fusion issues for domestic and industrial applications and (b) fundamental studies to unravel the flame structure in the two-phase gasification-combustion process over the entire range of V_s.

Improving the stove performance

It has been known that in most free-convection based stoves, like three stone fire and others developed over the last two decades, the amount of energy extracted from the stove by a cooking pot, usually measured as water boiling efficiency, is between 15 to 35 % and CO emissions of more than 1.5 g/MJ. Oorja stove had demonstrated water boiling efficiency of 50 % and CO emissions of 0.75 g/MJ. Operational issues noticed in the field provided an opportunity to further improve the performance by conducting detailed thermo-chemical studies. Towards this, the components of water boiling efficiency in different phases and from different modes of heat transfer were determined. Optimizing the ratio of air flow rate between combustion air from top and gasification air through the grate (denoted by R) was the key to improving the performance. The maximum water boiling efficiency obtained was 62% with 0.53 g/MJ CO for a 320 mm diameter vessel; under these conditions, the first phase, termed *flaming mode*, involving pyrolysis-gasification-gas phase combustion contributed 45% to the total efficiency and 0.4 g/MJ CO at R = 4.8 and the second phase, termed *char mode*, involving char surface oxidation-gasification-gas phase combustion contributes 17% and 0.13 g/MJ CO at R = 1.9. Under optimal air flow conditions, efficiency depends on the size of the vessel used; reactive flow calculations were performed with fast chemistry (using mixture fraction approach) in a zone that includes the free space of the combustion chamber and the vessel to obtain the heat transfer efficiency and bring out the effect of vessel size.

Experiments aimed at evaluating the performance of the stove on either side of stoichiometry, revealed that while the stove could be operated on the rich side, *it was not possible to operate it on the lean side* - it was always tending towards the stoichiometric point with enhanced power. Computational studies showed that increased air flow from the top caused enhanced recirculation around the fuel bed bringing more oxygen that reacted closer to the surface and transferred additional heat enhancing the pyrolysis rate, explaining the observed shift towards stoichiometry.

An examination of literature showed that the energy balance for stoves had long remained unexplained (unaccounted losses in stoves were up to 40 %). Using the different components of efficiency obtained from experiments and computations, a heat balance was established to within 5%. This vast improvement in the heat balance is due to the fact that the unaccounted loss in the earlier estimates was

essentially due to poor combustion but was not so recognized. The very significant increase in combustion efficiency in this class of stoves allowed the possibility of estimating other components reasonably accurately. This is a direct consequence of the two stage gasification-combustion process yielding steady flow of gases which contain 80% (gasification efficiency) of the input energy enabling near-stoichiometric combustion with the help of controlled supply of combustion air.

Fundamental studies

Experiments with wood chips (615 kg/m^3) and pellets (1260 kg/m^3) showed that, particle density has no effect on single particle and packed bed combustion in flaming mode beyond the role played through the surface energy balance that involves the product of density of the fuel pieces and the propagation rate, $\dot{r}$. Same is true for single char particles. A transport controlled combustion model taking into account the ash build up over the char surface confirmed this behaviour and showed that, the phenomena follows d^2 law, where d is the equivalent diameter of the fuel particle, consistent with the experimental results and the model. But packed bed of char particles showed distinct dependence on particle density. Differences were traced to poor thermal environment faced by low density wood char pieces compared to pellet char leading to variations in the volumetric heat release rate.

A composite picture of the operational behaviour of the packed bed flame propagation was obtained from the measurements of exit gas composition, bed temperature, temperature of gas phase and condensed phase surface using 100 μm thermocouples, O_2 drop across the flame front using lambda sensor as a function of V_s. The packed bed studies were conducted in insulated steel and glass reactors. These studies clearly showed distinctive regimes in the bed behavior. In the first regime from $V_s = 3$ to 17 cm/s, (a) the propagation rate increases with V_s, (b) the fractions of CO, H_2 are at least 10%, CH_4 drops from 3 to 1%, (c) the oxygen fraction is near zero, (d) the gas phase temperature in the bed is constant at about 1600 K, (e) the condensed phase surface temperature increase from 850 K to 1600 K and (f) oxygen fraction drops from 0.21 to 0.0 within a single particle depth and coincides with the gas phase ignition. The inferences drawn from these data are that (i) the process is diffusion controlled (ii) the bed operates in fuel rich mode, (iii) char participates only in reduction reactions. In the second domain from $V_s = 17$ cm/s up to about 50 cm/s, (a) the propagation rate is nearly constant (b) the mass fractions of CO and

H_2 drops to less than 5%, CH_4 decreases further, (c) oxygen fraction remains near zero, (d) CO_2 increases, (e) gas phase and surface temperatures are nearly equal and increase from 1600 K to 2200 K and match with the equilibrium temperature at that equivalence ratio, (f) oxygen fraction drops from 0.21 to 0 in one particle depth like in the first regime indicating diffusion limitedness in this regime as well, (g) unlike in the first regime volatiles from biomass are convected up to the next layer suppressing a local flame and char oxidation dominates. Beyond $V_s = 50$ cm/s, the propagation ceased to occur. The precise value of the extinction V_s depended on the rate of increase of V_s in this range. A faster change initiated the extinction earlier. Observations showed that extinction began at some location around the periphery and spread laterally. Extinction at one layer was adequate to complete the extinction process.

To explain the observed behaviour a simple zero-dimensional model tracking the heating of a fresh biomass particle upstream of the propagating flame front because of radiative heat transfer was set up. This equation was coupled with the equation for single particle flaming combustion to explain the behavior in the first regime. In order to explain the observed flattening of propagation rate in the second regime, it was found essential to account for the effect of the ash layer building on the oxidizing char particle and the temperature dependence of ash emissivity, on the radiative heat transfer to fresh biomass. The results of the model coupled with the experimental data from all sources on a corrected propagation rate vs. V_s showed a universal behaviour that is considered a very important recognition of the packed bed propagation behaviour.

Combining theory and experiments was needed to explain the extinction. The features are: (a) the presence of the ash layer over the surface that is shown as responsible for maintaining a steady char conversion in a single char particle at low stream speeds, (b) the feature that the ash layer would be blown away at stream velocities of 2.5 to 3 m/s in a single particle combustion, (c) with V_s close to 50 cm/s, local velocities of air flow through the bed can reach 2 to 3 m/s, this value being sensitive to the bed arrangement, with slight shifting or settling of one particle leading to increase of the local velocity at the periphery. Thus, the high local speeds of flow through the bed (more than 2 m/s) was considered responsible for removal of ash layer such that radiation losses would be dominant and cause local extinction of the reaction front at the char surface.

Thus, this study has led to a comprehensive understanding of the gasification-combustion behavior of packed bed in stoves and on grates. It has also led to the evolution of parameters for obtaining high efficiency and low emissions (HELE) from stoves - both domestic and industrial. Most interestingly, it has resulted in recognition of an universal behavior of flame propagation rate through packed bed of biomass.

Nomenclature

Symbols

A/F	Air-to-fuel ratio
c_p	Specific heat (J/kg K)
d_v	Vessel diameter (mm)
d_s	Stove diameter (mm)
Gr	Grashoff number
H	Heat of reaction of carbon with air = 32 MJ/kg
k	Thermal conductivity (W/m^2 K)
$\dot{m}$	Mass burn rate (g/min)
Nu	Nusselt number
p_{O_2}, w	Partial pressure of oxygen at char surface (atm)
q	Cumulative heat transfer to the vessel (W)
q $''$	Heat flux (W/m^2)
R	Ratio of combustion to gasification air
Re	Reynolds number
$\dot{r}$	Propagation rate (m/s)
s	Stoichiometic air-to-fuel ratio of carbon air combustion = 11.5
T	Temperature (K)
t_b	Burn time (s)
t_{ign}	Ignition time (s)
V_s	Superficial velocity (m/s)
V_{ga}	Volume flow rate of gasification air (lpm)
V_{co}	Volume flow rate of combustion air (lpm)

Y_{ox}	Mass fraction of oxidiser

Greek symbols

δ_{ash}	Ash layer thickness (m)
δ_{ffc}	Boundary layer thickness due to free and forced convection (m)
η	Efficiency
ϵ	Emissivity
σ	Stefan-Boltzmann constant = 5.67e-8 ($W/m^2\ K^4$)
ρ	Density (kg/m^3)
ϕ	Equivalence ratio

Subscripts

0	ambient
a	attained
b	bed
c	core
char	char mode
cg	cold gas
e	expected
f	fuel
fla	flaming mode
g	gas phase
ga	gasification
hg	hot gas
ht	heat transfer
p	packing
pb	peak bed
rad	radiation
sh	sensible heat
si	burning surface

ss	ash surface
su	condensed phase surface
wb	water boiling

Contents

List of Figures

List of Tables

Chapter 1

Introduction and earlier literature

The subject of biomass based domestic cooking in developing and emerging countries across the globe has received increasing attention in the last five decades. Much has been written and documented on the subject. Kirk Smith has written over years on the measurements of efficiency and emissions in biomass stoves in several countries (Smith *et al.* (2000*a*,*b*, 2007); Dutta *et al.* (2007)). The International energy agency publishes every year the world energy outlook; the World energy outlook of 2006 (IEA (2006)) specifically addresses several issues of cooking around the globe. The Food and Agricultural Organization (FAO) of the UN has published a series of status documents on the fuel for cooking in several countries (Bogdanski *et al.* (2010)). A joint UNDP World Bank initiative has discussed the access of poor to clean fuels in India. The website `http://bioenergylists.org/` has the collection of enormous literature on stoves built in various countries and technical aspects of the performance by individual developers and some researchers. In India, a national program on improved cook stoves was operated by the Ministry of New and Renewable Energy (MNRE) for 20 years as a subsidy operation on wood burning stoves with a minimum water boiling efficiency (20 %). The work has been reviewed in national sample surveys once in several years (see for instance, NSS, 2004). Recently, an initiative led by UN foundation, 'The Global alliance for clean cookstoves' has been formed with an 'ambitious ten year goal to foster the adoption of clean cookstoves and fuels in 100 million households by 2020' (see Cordes (2011)).

What becomes clear from an examination of these documents is that there is overwhelming concern to develop improved stoves on the part of designers, administrators, policy makers with much expectation but differing unstated specifications. The improved cook stove is expected to use nearly any solid biomass fuel without regard to shape, size or moisture. In the early stages of the program (till about

1990s) it was necessary to develop stoves that did not use electricity for electricity was nearly not available to rural communities who turn out to be the prime users of biomass based fuels. Affordability was a key aspect and stove designs that were based on mud construction received considerable support. The emissions of smoke and particulate matter for sure, carbon monoxide in some cases were considered worthy of being removed from the kitchen space even if these were generated in the combustion process. This led to chimney based designs acquiring popularity. An examination of the designs in the stove web site shows that most designs were the creation of enthusiasts for very little science ascribable to the designs seems documented.

Most available designs can be classified into (a) chimney based designs built using mud and clay, (b) clay based portable stoves, (c) metal stoves and (d) inner ceramic and outer metallic arrangement based design. A second classification would be based on mode of air supply, free convection based air supply for combustion or fan based forced convection air supply. The chimney based systems and all earlier generation portable stoves have free-convection based air supply. The fan based air supply based stoves are very recent. These aspects will be discussed in detail below.

1.1 Chimney based designs - free convective air supply

One of the three-pan mud stove designs that received scientific inputs on heat transfer is the ASTRA Ole at the Indian Institute of Science by Lokras *et al.* (1983). The stove in shown in Fig. 1.1a. This chimney based three-pan stove showed a water boiling efficiency of 40 % under laboratory conditions and up to 30% under field conditions (see Shastri *et al.* (2002)). In this stove *combustion efficiency* has not been the focus. The ASTRA Ole was built in large numbers, 500,000 up to 1993 (see MNES & IIT (1993)), initially with the support of the government and subsequently in a semi-commercial mode. A large number of masons were trained to build them to specifications and building these stoves was their livelihood support. A further point about chimney based stoves is that they are built around a cooking vessel. There must be no possibility of air leakage between the vessel and stove, for this unintended leakage will affect the combustion and heat transfer processes. Even if the entire system is flawless at the time of construction, there will be mild separation

between the metal vessel and the clay-mud edges of the stove over a period of time due to repeated cyclic thermal expansion and contraction. This will lead to leakage that will reduce the efficiency. Added to this, if power is considered inadequate, the user might introduce more fuel leading to fuel-rich combustion and loss in efficiency. In fact monitoring groups after some years of installation have determined the mean performance being much lower than expected (Shastri *et al.* (2002)). What more, at instances of high power, there will be leakage of smoke through the interface thus partly not obviating the classical problem of smoke that the 3-stone fire is supposed to be saddled with. These issues are not simply limited to ASTRA Ole, but generic to the chimney based designs.

A Chinese design developed by Daxu corporation (shown in Fig. 1.1b) seems to have attracted attention through Ashden award in 2007. The statement on the award states '...Most families in China still cook using stoves that burn coal or wood which has led to severe deforestation and dangerous levels of indoor air pollution, particularly from coal use. Crop waste is widely available in China yet very few stove designs have been able to burn this waste effectively. The Daxu stove is not only designed to burn crop waste, either loose or in briquettes, it is also 40% efficient, produces hardly any smoke, cuts cooking and heating costs by 50% ...'

Paul Anderson describes this stove in a separate article composed from a number of sources as variant of TLUD (top lit updraft) stove design (see subsequently for a description of this design as it is the same as the reverse downdraft stove, the subject of this thesis) with two pan heat extraction possibility and with a chimney. A direct examination of the elements as seen from Fig. 1.1 shows that even though the system is loaded and lit at the top, unless the entire top surface is lit completely, it will not work like a classical TLUD stove. Further, the airflow rate is a direct function of free convective pumping resulting from the chimney and can vary during the operation. This feature coupled with ill-defined combustion process will not ensure the correct air-to-fuel ratio that promises high combustion efficiency as well as low emissions. If the emissions were indeed low, why would the chimney be required to eliminate the exhaust gases from the kitchen area? It appears from the design that the fuel burning zone can be opened as desired allowing the hot gases to exit from the combustion chamber. The data concerning the stove are briefly set out in Table 1.1 drawn from a presentation of the data by Charren and Bryan Wilson (Colarado State university).

Figure 1.1: Stoves with chimney - a) Three pan Astra ole developed at IISc, b) Daxu stove developed in China

Table 1.1: Operational parameters of Daxu stove

Fuel consumption rate (kg/h)	1.6 - 2.6
Cooking power (kW)	2.2 - 3.4
Heat efficiency (%)	32 - 43

The fuel consumption rate in Table 1.1 in kg/h is not consistent with the power in kW indicated therein - the consumption rate of 1.6 to 2.6 kg/h implies a power of 6 to 9.5 kW allowing for a lower limit of the lower calorific value (LCV) of 13 MJ/kg. The stove size shown in the photographs appear to be consistent with larger power level. Hence, it is not clear to what extent the efficiency values can be relied upon.

1.2 Portable stoves - free convective air supply

Portable stoves offer a solution that seems to adopt to cooking habits in some parts of India. In summer, cooking is done outside in the courtyard to reduce the additional heat from the stove and in winter, inside to help keep the living environment warm. More importantly, these stoves enable factory based production and hence the possibility of accurate realization of the intended design in all the stoves. There are two versions - ceramic built around moulded clay product fired in a furnace to lead to a terra-cotta like product (fired at around 900 °C) and a metal version. Also a combination of ceramic inner construction and an outer metal construction is possible. A wide range of stove designs are in vogue.

An important class of portable ceramic stoves are *rocket stoves*, developed by Dr. Larry Winiarski and studied extensively by Dean Still and team at the Aprovecho research centre for the past three decades. The most recent version of the rocket stove is StoveTec, with an efficiency of about 35%.

Figure 1.2 shows several designs that have been tested by Bhattacharya et al. The efficiencies are about 25 % or less and a minimum CO emissions of 1 g/MJ and higher efficiency not always meaning lower emissions.

Amongst the simpler metal versions that were built in large numbers under an MNES (now MNRE) subsidy program is the stove called Priagni, shown in Fig. 1.3a, once very popular in India. This stove has an efficiency of 26% (MNES & IIT (1993)). According to this report, Harsha, a portable metallic single pot stove without chimney (shown in Fig. 1.3b), was designed as an alternative to Priagni stove that was specifically suitable only for fuel wood. Harsha was designed to burn multiple fuels like dung cakes, agro-residues etc., and can be used with vessels of diameter 18-26 cm. This stove distributed to about a million households and has an efficiency of about 25% (MNES & IIT (1993)).

There are several variants of this class of design that do not fundamentally alter the combustion or heat transfer process and extensive tests have been performed on these class of stoves to determine their efficiency and emissions (see for instance Jetter & Kariher (2009); MacCarty *et al.* (2010)). The difference between clay and metal versions is that clay versions are cheaper, but fragile even though they may last longer than metal versions when handled carefully. Clay versions are generally heavier and absorb more heat. Longer cooking cycles will lead to efficiency differ-

Figure 1.2: Several designs of mud, clay and ceramic stoves from Indo-Chinese countries tested by Bhattacharya *et al.* (2002)

Figure 1.3: Some metal stoves - a) Priyagni b) Harsha

ences that are not significant. Most of this class of designs will lead to efficiencies between 20 and 30%, peak being 35% when the fuel sizing and loading are 'proper'. It is not immediately obvious what arrangement of sizes will give the best performance. Also the emissions of CO will be more than 1.5 g/MJ. Laboratory tests

and field results can be widely different simply because in the field the fuel size, shape and moisture are not what they are intended to be, in addition to the way the fuel wood pieces are loaded or rearranged from time to time, both of which affect efficiency and emissions.

It remained to Emmons & Atreya (1982) to bring out the fundamentals of wood combustion with specific reference to stoves; however, this work seems to have had little influence on stove designers (one hardly finds reference to this work in later literature) and most designers were continuing to optimize the heat transfer efficiency without actually addressing combustion efficiency issue. Attempts have been made to understand the combustion, flow through the stove and heat transfer using controlled experiments and modelling, but restricted to simplified geometries and natural convection driven systems (for instance Kohli *et al.* (1993); Ravi *et al.* (2002); Agenbroad *et al.* (2011)).

Mukunda *et al.* (1984) sought to model single wood sphere combustion and also intended to design stoves of high efficiency (Mukunda *et al.* (1988)). Some designs of 1 kW were built with water boiling efficiencies of 40%. Recognizing the difficulties in raising the efficiencies beyond this value and also realizing that kerosene and LPG stoves have high efficiency ($\sim$ 70%) and low emissions of CO (0.2 to 0.4 g/MJ), they studied the principal reasons for the high efficiency achieved in a single pan LPG stove and why wood stove efficiency is inferior to the levels achieved in kerosene and LPG stoves. What became evident is that unless the air-to-fuel ratio was near stoichiometry at least on the average, it is not possible to achieve efficiencies close to 40% that they got in their stove. That this is far from possible achievable levels was due to the oscillating combustion temperatures ($\sim$ 700 to 900 K) being far below the stoichiometric value ($\sim$ 1900 K); unless until the temperatures achieved went close to the stoichiometric values achieving higher efficiencies would be impossible. It was further verified that either with kerosene wick stoves or LPG stoves, the flame was steady and the achieved temperatures were about 1700 to 1800 K. It was also uncovered that when the stove design that provided 40% efficiency was scaled to work at 2.5 to 3 kW, the efficiency did not go beyond 35 %. This was inferred as due to a combination of shorter residence time under the bottom of the vessel and the lower flame temperatures due to poor quality of combustion that the system allowed for. The comparison with kerosene and LPG stoves is thought doubly important. Firstly on the basis of scientific enquiry, to determine what

limits achieving efficiencies as high as kerosene or LPG. Secondly, in the development ladder, LPG stoves occupy the highest level and various socio-economic studies have shown that the deprived groups have a highly enhanced sense of self-esteem when they possess LPG stoves (Larson & Kartha (2000)); any stove that comes close to LPG stove would receive much higher acceptability in the users perception. The high flame temperature obtained by operating the stove near stoichiometry brought out by Mukunda *et al.* (1988) controls the heat transfer to the vessel within the limited bottom area available and hence must be as high as possible to obtain high efficiency. LPG and kerosene stoves use this principle and therefore have very high efficiencies and very low emissions. But stove designs based on free convective air supply and biomass loaded as and when it is thought fit into the hot combustion chamber will function with air-to-fuel ratios that can be very rich or very lean. The former conditions lead to sooting and the latter to smoking. Also parts of the fuel over the stove may still be cold leading to air flow out of the chamber without participation in the combustion process while other areas are deprived of air.

The importance of high combustion efficiency in biomass stoves is brought out from the view point of environmental compatibility in Smith (1994, 2002). The important conclusion is *'unless biomass is used with very high combustion efficiency, zero carbon balance cannot be ensured'*. This is of serious concern when it comes to the impact of biomass combustion on global warming. It has been shown in his study that a biomass stove with 89% combustion efficiency (that can be considered high for a traditional biomass stove) emits for every 1000 g of biomass, 440 g of carbon as CO_2 and 60 g of carbon as CO (43.5 g), CH_4 (8 g), non-methane hydrocarbons NMHC (7 g) respectively and rest as respirable suspended particles (RSP). The Global Warming Potential (GWP) of these products of incomplete combustion (PICs) with 20 years life span is 470, higher than that of CO_2 (440) and this shows that *'an efficiently burning fossil fuel stove has lesser GWP compared to a poorly burning biomass stove'*. Therefore, any biomass stove must have very high combustion efficiency and hence very little PIC emission to cause meaningful intervention.

1.3 Transition to forced convection stoves and gasifier stoves

While most stove developments around free convective air supply were taking place, Reed & Larson (1996) had built a fan based stove from an earlier version described in La Fontaine & Reed (1993), that burnt a fixed bed of wood chips and provided a quality of combustion vastly superior to those of free convective designs that permeated the world of stoves. This design is similar to the rice hull gasifiers developed in China as early as 1967 (see Bhattacharya (2005)). Scientific study on this gasifier was done by Kaupp (1983) and they showed that to obtain gases of maximum calorific value the equivalence ratio for gasification must be close to 0.25. Schematic of rice hull gasifier is shown in Fig. 1.4.

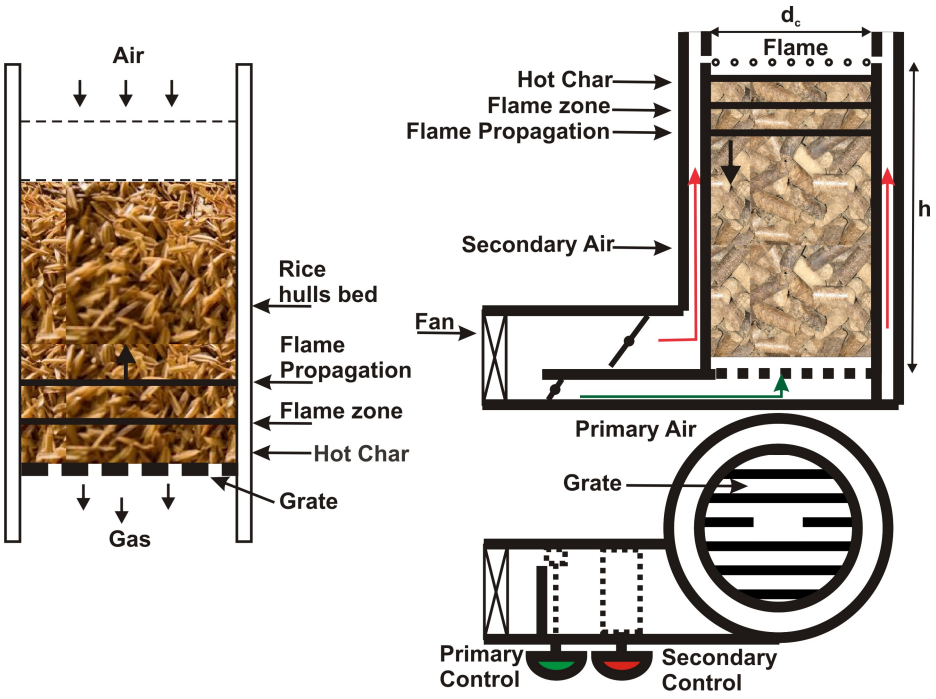

Figure 1.4: Packed bed gasification systems - Rice hull gasifier is shown on the left. Note that the air is drawn from the top; Reverse downdraft system is shown on the right - air for gasification flows from bottom to top

Apart from rice hull the reactor can also be used for the thermo-chemical conversion of other biomass like pellets and wood chips. If in this reactor the gasification air is allowed to flow from bottom to top so that the generated gas, called *producer*

gas, can be burnt on the top of the bed with a second stream of combustion air, the heat generated can be utilised for cooking applications. This configuration is shown on the right side of Fig. 1.4 and is known as top lit updraft (TLUD) (sought to be popularised by Anderson *et al.* (2007)) or equivalently reverse downdraft system (REDS). This configuration is similar to the combustion-on-grate system widely used in Europe for large scale heating and power generation application (for a detailed review of literature on this see Section 1.5).

The cost of this stove was thought unaffordable in most developing countries partly due to the high cost of the fan and the power that it was drawing to operate the fan (10 W); non-availability of electricity in rural areas was considered a stumbling block for the wider acceptability of this class of stoves. A free convective based alternative was built by Mukunda and colleagues later but was abandoned due to an appreciation that the quality of combustion was inferior to that of fan based version (see Biomass stoves under technologies section of the IISc laboratory website `http://cgpl.iisc.ernet.in` for a description of various designs built and tested at the laboratory). It was only in 1999 that the computer based fans became available at relatively low price and these were intended to be adopted for use in stoves. Utlising the fan for supplying the air for gasification and combustion with possible control of the power was the conceptual part of the solution. It was necessary to define the parameters concerning power and energy to convert the concept to a design. The cooking duration was set at one-hour drawing from field studies. These power and energy values were deduced from experiments including cooking as 2.5-3 kWth and 0.6 to 0.7 kg biomass with the water boiling efficiencies at about 50%. Also wood chips with a density of 300 to 400 kg/m^3 were to be replaced by pellets of much higher density (700 to 800 kg/m^3) to enable compact combustion process much like a LPG gas stove. It was around these ideas that stoves were built and tested at the laboratory (see Mukunda *et al.* (2010) for details).

Around this time, much international interest was shown in developing advanced cooking solutions and one development that is somewhat unique is the Phillips stove (see Philips (2006)) shown in Fig. 1.5. This stove needed considerable attention on the part of the user since the loading of the fuel was to be done at a periodicity of 3 to 4 minutes. This stove belongs to the category of in-situ combustion stoves and are no different from furnaces in principle. Biomass is ignited and sufficient amount of air (about 6 kg per kg of typical biomass) is supplied around the fuel

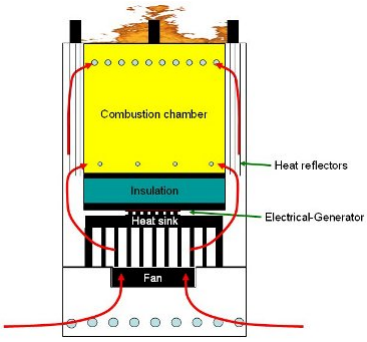

Figure 1.5: Philips wood stove - in-situ combustion stove

zone. This leads to simultaneous de-volatilisation and char combustion. Claimed as near-smoke-free, it has a measured laboratory efficiency of 40% and a level of emissions governed by the loading cycle. The stove when marketed showed that it was much beyond the affordability of those who were likely to use the stove and therefore did not find market favor. Part of the reason is that simpler and cost effective solutions have been worked out for the power supply using rechargeable storage batteries (for example, as a part of the commercialization of the IISc design by First Energy Private Limited - see Mukunda et al, 2010) instead of local power generation by thermoelectric system; the first associated with power generation is offloaded to much cheaper rechargeable batteries.

Figure 1.5 shows the Phillips combustion stove with a 100 mm combustion chamber diameter and loading of small pieces of biomass with air supply from a fan that is run by electricity obtained from thermo-electric generation using the heat of the bottom of the chamber. The series of holes towards the bottom of the combustion chamber supply air for combustion.

1.4 The gasifier stoves

The background to gasifier stoves has been discussed above. The technology developed at IISc was transferred to BP, India in 2005. The ownership later moved to First Energy Private Limited, Pune. In the first four years, more than 400,000 stoves were sold commercially.

Figure 1.6 shows the Oorja stove. The inside shown on the right indicates a ceramic combustion chamber with grate at the bottom and combustion air-supply

Figure 1.6: Oorja 1.3 – FEPL's domestic gasifier stove

holes at the top. The air for gasification is supplied from under the grate. It can be loaded with 700 gm of pellets and its power level can be varied between 2.4 to 3.5 kW and its measured water boiling efficiency is 50% and CO emissions is 0.7 g/MJ.

1.4.1 Flaming and char mode

The stove has two modes of operation, namely, *flaming and char mode*. Flaming mode is characterized by propagation of ignition front through the packed bed against the air flow (counter-current mode) resulting in heating and de-volatilization of fresh biomass followed by combustion of volatiles with the incoming primary air. The products of sub-stoichiometric combustion of volatiles contain mainly CO, CO_2, H_2, H_2O, CH_4 and some higher hydrocarbons (tars). Typical biomass contains about 75% volatiles and 25% fixed carbon on a moisture and ash free basis. This fixed carbon in the form of char is left over after the process of de-volatilisation and the gases from sub-stoichiometric combustion of volatiles pass through this hot char bed ($\sim$ 900 K) and undergo reduction reactions, mainly, $C + CO_2 \rightarrow 2CO$ and $C + H_2O \rightarrow CO + H_2$, resulting in the generation of producer gas rich in combustible gases like CO (15%), H_2 (12%), small amounts of CH_4 (2-3%) and other higher hydrocarbons (2-3%). In this process, once the flame front reaches the grate almost all the volatiles present in the biomass are released and about 20% char is left on the grate. The air coming in through the grate causes surface oxidation of char and generates primarily CO and CO_2 and little H_2. CO_2 so generated passes through the hot char on top and can undergo reduction with carbon to form CO. This is the second phase and referred to as the *char mode*. The power level of the stove is dependent on the air flow rate through the bed. This controls the gasification process. Higher

air flow rate implies larger superficial velocity (air flow velocity through the empty chamber cross section) that causes higher flame propagation rate through the bed in a direction opposite to the air flow and hence greater gasification rate and larger power. The power in the char oxidation period is about quarter of the power in the flaming mode at fixed air flow rate through the bed. This raises issues of poor utilisation in char mode - a subject addressed in detail in this thesis.

One of the key issues with this stove was to produce fuel pellets of quality (and supply it to widely distributed users, a subject not discussed here). Internationally, solid stock of trees (of densities of 500 kg/m^3) that are felled are ground into fine form and then pelleted to high densities $\sim$ 1000+ kg/m^3. Such an approach is far more energy intensive than can be justified - in processing the solid into powder form and then pelleting to high densities, certainly in a developing country context. Also, national fuel related surveys in India (see Mukunda *et al.* (2010)) have shown that the agro-residues are used far more inefficiently than firewood. This is because agro-residues come with much wider range of shape, size and density apart from moisture content than firewood. Getting good combustion and thermal performance from agro-residues requires that they be processed into pellets ensuring control on all the aspects noted earlier limiting the moisture content as well as ash fraction. Hence FEPL established pellet making machinery for agro-residues like groundnut shell, bagasse, de-oiled rice bran and a number of other minor residues from agricultural operations. Collection and transportation of these residues would affect the ash fraction because of pick of sand and grit from field locations and considerable efforts were needed to limit them to values less than 10%. Also year-to-year upward variation of the raw biomass costs led to increased cost of the final product.

In this period, problems that were observed in the field systems were largely related to the second phase of operation (char mode) when the power delivered by the stove was too small for use or on occasions the flame would extinguish, a feature that was traced largely to higher ash fraction in the pellets. Also the life of the metal version was no more than about 1000 hot hours or about one and a half years. Several versions of the stove were developed particularly (a) to allow larger amount of pellets to be loaded (up to 800 gms) (b) to reduce the power and energy consumed by the fan, and (b) to introduce ceramic version that extends the life to beyond three years. Further, commercial users (hotels and community kitchens) created a demand

scenario for larger power stoves. The principal driving factor was that while domestic LPG subsidies and enhanced cost of pellets due to reasons discussed earlier did not provide the needed commercial incentive for domestic users to use these stoves, the higher costs of LPG for commercial applications allowed the possibility of this segment using larger sized stoves for heavy cooking applications. This needed an examination of issues when the power was scaled up. Hence the key questions raised were: would a scale up alter the thermo-chemical environment favorably or would it throw up issues, is there any further limitation on the stove efficiency achieved in the laboratory and field systems (the field systems also gave efficiencies close to laboratory values because the user has little opportunity to alter the performance except make a choice of power level occasionally). Some of the deviations in the thermo-chemical performance particularly in the char mode that were observed on the domestic stove (called Oorja 1.3) had inadequately been understood and hence, needed study. Energy balance for the stove, to track the energy flow from biomass to vessel through various processes in flaming and char mode like, gasification, gas phase combustion and heat transfer to vessel is an important missing link in the process of understanding. This is also evident from the work of Sharma (1993), which shows unaccounted for energy loss as high as 40%.

The study that has evolved into this thesis was started with these primary aims. During the course of the study it was found that the behavior of the stove *in the char mode* with wood chips was vastly different from high density pellets. This led to an investigation of the causes for the difference. Staring with individual pieces of pellets and wood spheres, the differences were traced to the bed operation in the char mode. It was also necessary to determine how the bed was behaving at different superficial velocities. During this exploration, it was uncovered that the European work of Gort (1995); Ronnback *et al.* (2001); Harttanainen *et al.* (2002); Porteiro *et al.* (2010*a*) were largely at much higher superficial velocities ($>$ 10 cm/s) than the domestic stoves were designed for (3-6 cm/s). The reason for the emphasis of low superficial velocities for domestic stoves is to limit the fine particulate emission. The choice of high superficial velocities in European investigations was to enhance the conversion rate (measured by the flame front propagation rate, $\dot{r}$) to the extent possible - for, the use was as a fuel bed on travelling grates in boilers which anyway had electro-static precipitators for particulate removal before the exhaust stream was let out into the atmosphere. Also since for high superficial velocities the amount of char

left after the propagation front reached the grate is very little fraction of the initial mass (see Yang *et al.* (2004)), these studies did not distinguish between flaming and char mode. A study of these papers showed several internal inconsistencies that needed experiments over a range of superficial velocities beyond what would normally be used in domestic stoves. This enhanced the scope of the investigations over the entire range of superficial velocities even up to extinction.

1.5 Propagation of flame front in packed beds

Packed bed gasification-combustion finds application in large scale combustion devices for utilisation of biomass to generate power. The actual configuration used is a moving grate furnace and is shown on the left of Fig. 1.7. When the frame of reference is fixed to grate the system becomes equivalent to a fixed-bed configuration shown on the right side of Fig. 1.7. To obtain high conversion rates, the superficial velocity employed in these systems are at least 15 cm/s.

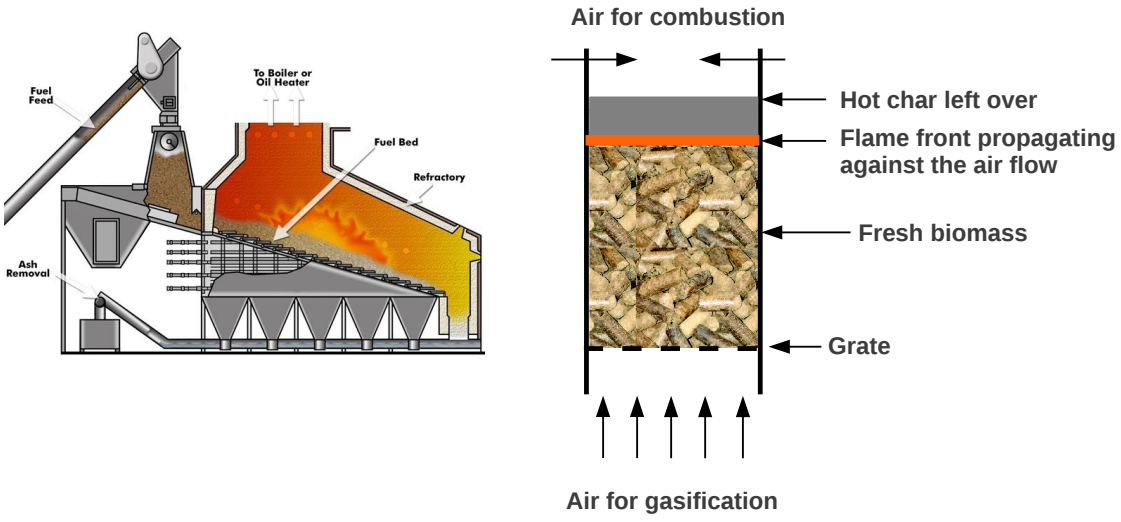

Figure 1.7: Left - Moving grate furnace; Right - equivalent fixed-bed system after change of frame of reference to the grate

Extensive experimental and modeling results exist for the counter-current flame propagation through a fixed bed of biomass. Superficial velocity (V_s) has been identified as the most influential parameter affecting the fuel mass flux ($\dot{m}_f$), bed

temperature (T_b) and exit gas composition (Fatehi & Kaviany (1994); Reed *et al.* (1999)); the other parameters affecting the conversion process are density, moisture content, ash content and particle size of biomass. Fatehi & Kaviany (1994) have done experimental as well modeling studies to bring out the effect of V_s on $\dot{m}_f$ and T_b. By assuming that the reaction front thickness (δ_f) is large compared to the particle diameter (d), a volume averaged pseudo-homogeneous 1-d model (see Dosanjh *et al.* (1987); Gort (1995)) is developed by them. By treating the propagating front as analogous to a premixed flame they have used classical asymptotic analysis with the limitation of treating diffusion controlled rates in terms of activation energy for mass diffusion. The experimental results along with the model results are shown in Fig. 1.8 and the agreement for the chosen kinetic parameters is good.

Figure 1.9 shows the influence of choice of kinetic parameters on the predicted bed temperature and propagation rate. A change of frequency factor by over ten orders of magnitude has very little influence on the predicted results. Change of activation energy from 150 kJ/mol also has negligible effect on the predicted results up to a air pore velocity of 0.3 m/s, which corresponds to a superficial velocity of 15 cm/s. Beyond 15 cm/s the scatter in the experimental data is itself about 30%, something which is not observed in the experimental results presented in the current work. So the effect of activation energy shown in Fig. 1.9 might not have any physical significance. Moreover, if the principal idea of reaction control were true, the propagation rates would show strong dependence on the nature of biomass because the kinetic parameters are strongly dependent on the presence of elements like sodium and potassium which are naturally present in widely differing proportions. This is not true as is evident from Fig. 1.9. Based on their experiments, they have classified the operating regimes into a oxygen limited fuel rich part and a fuel limited fuel lean part (see Fig. 1.10).

Porteiro *et al.* (2010*a*) report experimental results of $\dot{m}_f$ and T_b variation for the entire range of V_s (up to extinction) for eight different types of biomass with different moisture and ash contents. The results are reproduced in Fig. 1.11.

Based on the results, the operating regimes are classified into three regions, namely, *fuel rich oxygen limited* combustion up to 17 cm/s, *fuel rich fuel limited* combustion up to 35 cm/s and a *convective cooling dominated* region to the right of 35 cm/s (see Fig. 1.12).

Though this classification is claimed to be an extension of that of Fatehi &

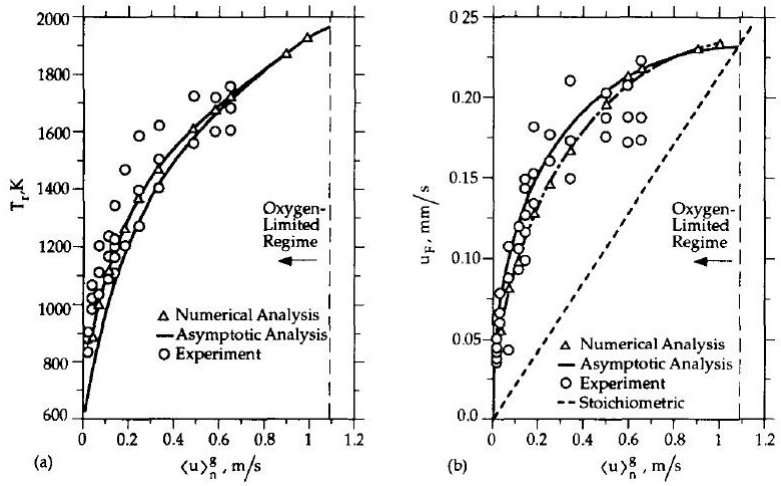

Figure 1.8: Variation of a) the adiabatic flame temperature b) propagation rate with superficial velocity - experimental and model results from Fatehi & Kaviany (1994)

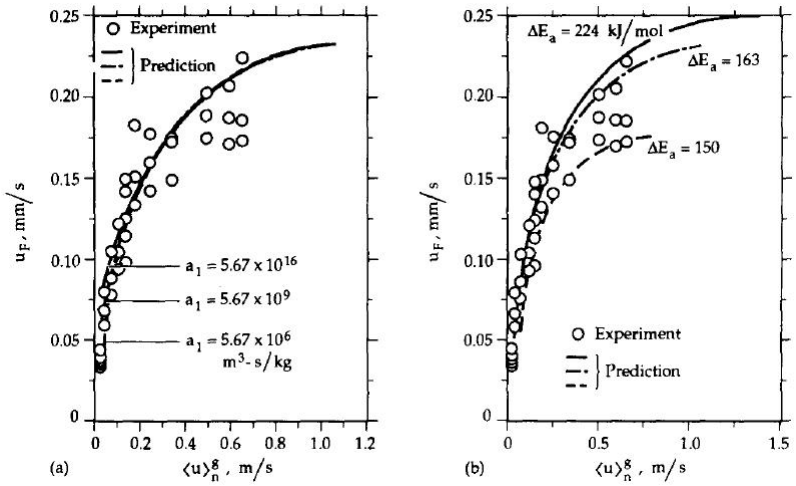

Figure 1.9: Effect of a) frequency factor b) activation energy on the predicted values of flame front velocity from Fatehi & Kaviany (1994)

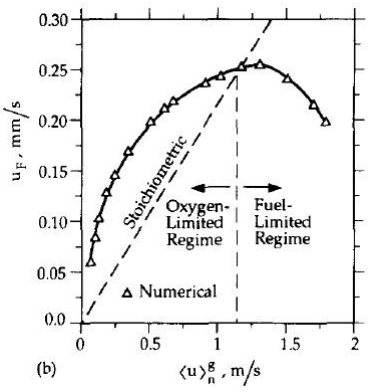

Figure 1.10: Classification of operating regimes Fatehi & Kaviany (1994)

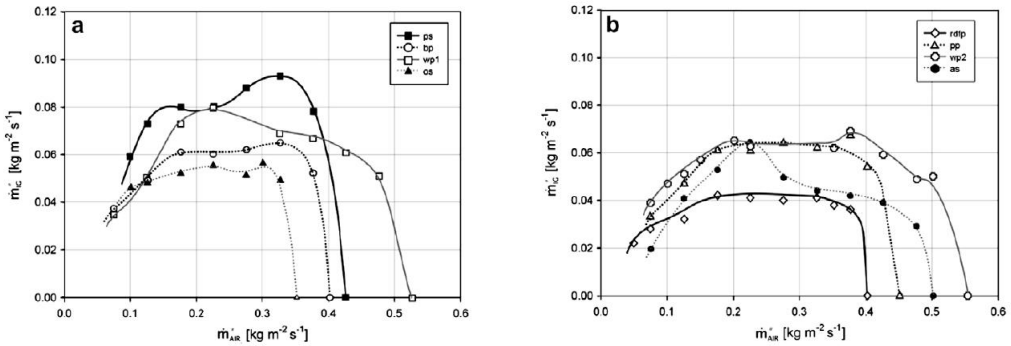

Figure 1.11: Fuel mass flux variation with superficial velocity from Porteiro *et al.* (2010*a*). ps - pine shavings, as - almond shell, os - olive stone, rdfp - RDF pellet, pp - poplar pellet, bp - brassica pellet, wp1 - wood pellet 1, wp2 - wood pellet 2

.

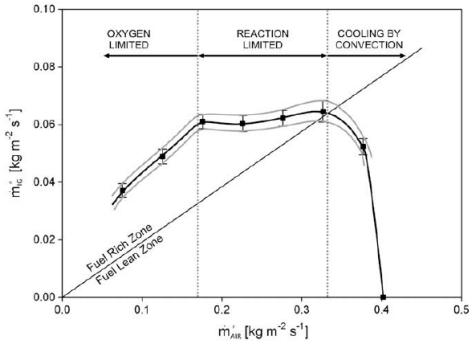

Figure 1.12: Classification of operating regimes proposed by Porteiro *et al.* (2010*a*)

.

Kaviany (1994), the idea of fuel rich fuel limited zone used here appears incorrect; there is no such regime in ref. Fatehi & Kaviany (1994). There are also difficult-to-justify char stoichiometry ideas in Porteiro *et al.* (2010*a*), discussed in detail in Chapter 5 of this thesis.

Gort (1995) reports experimental results for $\dot{r}$, T_b and exit gas composition (CO, CO_2, O_2 and C_xH_y only) for 10 mm wood samples with 10% moisture as a function of V_s. The classification is similar to that of Porteiro *et al.* (2010*a*) excepting that the oxygen limited regime in Fig. 1.12 is titled *partial gasification* since some char is left behind in the process.

Based on experiments similar to Porteiro *et al.* (2010*a*), Ronnback *et al.* (2001) propose a different classification. In addition to $\dot{m}_f$ and T_b, they have also measured the exit gas composition and used it as a basis for classification. The classification proposed has three regimes, namely, *(i) sub-stoichiometric combustion with incomplete consumption of oxygen*, same as oxygen limited regime in Fig. 1.12, *(ii) sub-stoichiometric combustion with complete consumption of oxygen*, same as the fuel limited regime in Fig. 1.12 and *(iii) over-stoichiometric* combustion from a superficial velocity of about 40 cm/s, similar to the convective cooling dominated regime in Fig. 1.12. Their conclusion (i) is based on a short duration oxygen data over the bed ($\sim$ 4 mins) with instruments whose response time is comparable to 4 mins. The effect on this on the measurement and proposed classification will be brought out in Chapter 5.

The influence of other fuel related parameters like density, particle size, moisture

content etc, have been studied using experiments and modeling (see for instance Yang *et al.* (2004); Ronnback *et al.* (2001); Gort & Brouwers (2001); Johansson *et al.* (2007)). By using wood pieces of 8, 12 and 34 mm, Ronnback *et al.* (2001) show that there are no perceptible differences beyond experimental errors. Ryu *et al.* (2006) experimentally investigated the effect of fuel type, equivalence ratio and particle size on the fixed bed combustion of biomass in the superficial velocity range of 6-11 cm/s. That the ignition front speed is found to be inversely proportional to bulk density is considered somewhat surprising by them even though it is clear that this follows simply from the surface heat balance condition (see analysis in chapter 5). Work of Thunman & Leckner (2005) also shows that influence of density on the dynamics of propagation is negligible.

The effect of ash has had relatively little attention compared to other fuel related parameters. It appears that Cooper & Hallett (2000); Ryan & Hallett (2002) are the only people who have incorporated the effect of ash by modifying the mass and heat transfer coefficients and the effective thermal conductivity (which also includes the effect of radiation). Present work takes into account the effects of ash and identifies its role in the gasification-combustion-extinction behavior of the packed bed.

Recently Collazo *et al.* (2011) have explored a three-dimensional model to explain the features of packed bed combustion. The model is complex and invokes kinetics for char-oxygen reaction. Also the heat transfer from the gas phase flame above the bed is taken to be ignition source, while in fact it is the radiation from the hot char bed that is the ignition source (see Fatehi & Kaviany (1994)). The temperature-time profiles are much sharper in the experiments compared to predicted ones (see Fig. 1.13). That the reason for this could be a near-diffusion control of the process and that their assumed kinetic influence would have been stronger and perhaps unrealistic is not recognized in the work. Moreover, the gasification reactions of CO_2 and H_2O with char and the effect of ash on radiative heat transfer are not taken in to account in this model. It is concluded by Collazo *et al.* (2011) that 'although this model shows close agreement with experimental data, it is based on certain assumptions or hypotheses that limit its direct application to other facilities'. But it is not clear which particular assumptions or hypotheses they are referring to or what the other facilities are. This raises the question, why a transient three-dimensional model is to be contemplated even before certain crucial fundamental processes like the effect of ash, gas phase and condensed phase processes are understood? In the

light of these questions, a simpler approach to deal with these issues is considered in this work (see Chapter 5).

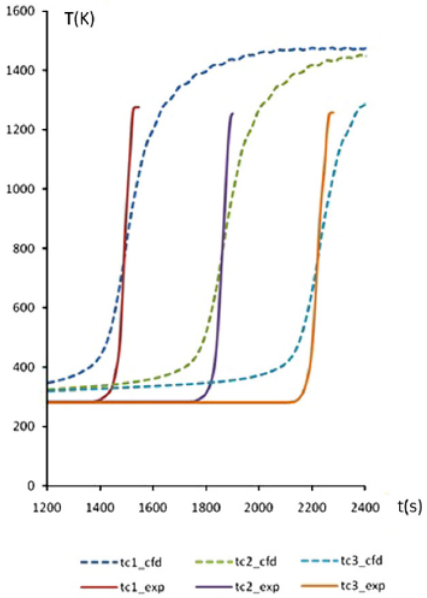

Figure 1.13: Temperature profiles of a propagating ignition front - experimental and modelling results from Collazo *et al.* (2011). Solid lines - experiments; dashed lines - computation

In summary, the key issues that have remained unaddressed are: a) the differences in perception of the behavior of the packed bed in different zones, b) the implication that there are significant differences in the propagation rate between various fuels, and c) the essential features of a model to reconcile the data seeking possible universality of the behavior and propose a prediction procedure for the propagation rate with justifiable inputs. It is also felt important to explore a zero-dimensional model that captures as many experimental features as feasible.

Summarizing the motivation for this work,

i. It was begun after the domestic stove Oorja 1.3 was commercially sold to about 400,000.

ii. Issues of performance loss and ash fusion in the final phases were reported. While the problem area in practice was traced to higher ash fraction, this

threw up issues of lower efficiency in the char operational period that needed investigation.

iii. It was noticed that pellets with ash fraction less than 10 % performed in a very superior way in the char operational period compared to wood chips. This needed understanding of the differences in their behavior.

iv. Scale up to larger power levels was needed. The role of char operational period vis-a-vis flaming period was to be elucidated for performance optimization.

v. The issue of performance optimization vis-a-vis vessel size was to be elucidated.

vi. Investigations on packed bed combustion at superficial velocities including values higher than in domestic stoves had several unexplained features (like constancy of propagation rate and bed temperature beyond a certain superficial velocity) and other conceptual inconsistencies that needed to be rationalized. This needed both experiments and modelling.

1.6 Thesis organisation

The thesis organisation is shown in Fig. 1.14.

Chapter 2 contains details of experimental methods used, various measurement techniques, equipments used with their characteristic features like response time etc., and their limitations.

Chapter 3 deals with detailed thermo-chemical evaluation of the stove performed using experiments and computations. Different components of efficiency of the stove, namely, gasification efficiency, water boiling efficiency and CO emissions from the stove are determined experimentally. Break up of water boiling efficiency and CO emissions in flaming and char mode for different equivalence ratios is presented to demonstrate the importance of near-stoichiometric operation. The results are then used to identify avenues for improvement of performance of the stove. Insights obtained were used in the design of large scale community stoves and are shown to perform with an efficiency of 65% and CO emissions of just 0.4 g/MJ. The importance of optimal power level for obtaining maximum efficiency is also demonstrated in this chapter. These insights are used to show that the efficiency of the existing domestic stove can be improved by about 5%. The gas phase combustion process

of producer gas with secondary air in the stove is modelled using mixture fraction method to bring out the effect of vessel size on the effectiveness of heat extraction and hence on the efficiency of the stove. Crucial flow features like the stagnation point boundary layer at the bottom of the vessel, the recirculation zone caused by impinging jets in cross flow etc., are brought out in this chapter with the help of reactive flow computations using CFX commercial software. The chapter ends with energy balance for the stove.

Chapter 4 deals with issues related to the difference in combustion behaviour of pellets and wood in char mode. Detailed experiments with single particles have been performed to identify whether the unusual effect is related to individual particle combustion or a property of the packed bed of char particles. A simple transport controlled model is also developed for the combustion of single char particle and the effect of ash layer on conversion process is brought out.

Chapter 5 deals with experimental and modelling study performed to understand the behavior of flame front propagation through a packed bed of biomass for the entire range of superficial velocity. The universality of this process is the key finding of this study and the resolution of existing conflicting perceptions on the operation of packed bed. Details of ash effect which forms the crucial part of the model and other features related to gas phase and condensed phase processes are brought out in this chapter.

Chapter 6 contains an overview and concluding remarks.

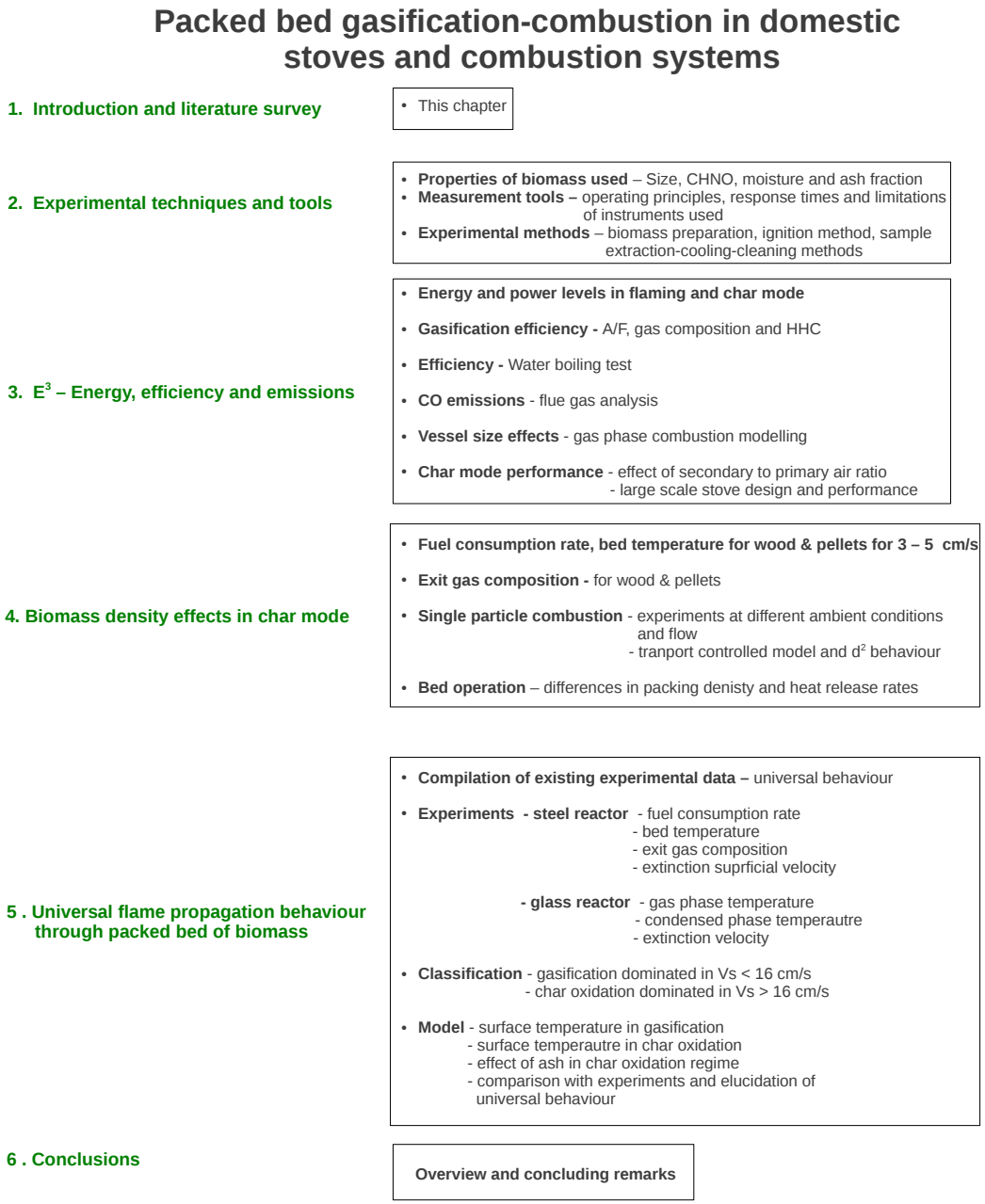

Figure 1.14: Thesis Organisation

Chapter 2

Experimental techniques and tools

This chapter describes various experimental techniques used in the study of gasifier stove and packed bed gasification-combustion processes. Details of the various types of biomass used in the study along with typical experimental procedure followed and measurement tools used are presented.

2.1 Biomass types and properties

Seven types of biomass of various shapes, sizes, densities and ash content were used in this entire study and Fig. 2.1 shows a picture of them. This includes two types of wood chips with similar properties but with different densities, two types of agro-residue pellets with similar properties but with different ash content, wheat and thin wood flakes. All the biomass used were dried at 105°C for 24 hrs to ensure uniform moisture content (6-10%). Table 2.1 summarises the relevant properties of all the biomass used.

Extensive data on propagation rate obtained by Porteiro *et al.* (2010*a*) is used for comparison with the model results in Chapter 5 of this thesis. So a picture of all the biomass used in their experiments is taken from their paper and shown in Fig. 2.2.

Figure 2.1: Photograph of all the biomass used in the study

Figure 2.2: Photograph of all the biomass used by Porteiro *et al.* (2010*a*)

2.2 Experimental techniques

The entire set of experiments can be grouped into two categories : 1) experiments specific to stove, namely water boiling tests, flue gas analysis etc., to determine var-

Table 2.1: Properties of different biomass - proximate and ultimate analysis

Biomass	Wood chips	Pellets	Wheat	Thin wood chips
Density, kg/m^3	615, 850	1260	1200	350
Size, mm	12*12*15	8 dia, 15-20 length	4 (avg)	12*12*4
Bulk density, kg/m^3	462, 650	794	1000	300
Proximate Analysis				
Volatile content*, %	87	82	80	80
Char*, %	13	18	20	20
Ash content, %	1	1%, 10%	1	1
Moisture content, %	10	6	6	10
Ultimate analysis*				
C	44.4	42.5	39.4	40.4
H	6.3	5.7	4.3	6.1
O	48.8	51.6	55.7	52.4
N	0.6	0.2	0.7	1.1
	$CH_{1.7}O_{0.79}$	$CH_{1.62}O_{0.93}$	$CH_{1.62}O_{0.93}$	$CH_{1.62}O_{0.93}$
A/F(stoichiometric)	5.2	4.5	5	5.2

* - moisture and ash free basis

ious components of efficiency and CO emissions and to establish energy balance, 2) experiments on biomass packed bed aimed at understanding the flame propagation behaviour.

2.2.1 Energy, efficiency and emissions experiments

Cylindrical stainless steel tube of diameter 100 mm and length 130 mm insulated with glass wool with a grate at the bottom was used in the experiments. The dimensions used conform to that of the domestic Oorja stove. The experimental set up used for water boiling tests and flue gas analysis is shown in Fig. 2.3. Two inlets, one at the bottom for gasification air and one at the top for combustion air were provided. The gasification air enters the stove through the grate. The combustion air issues into an annular chamber concentric with the 100 mm cylinder and is then distributed across the cross-section of the stove through eighteen holes of 5 mm dia punched in the 100 mm cylindrical tube. Diverging channels with an angle of 8° were used upstream of the flow entry regions to ensure uniform velocity

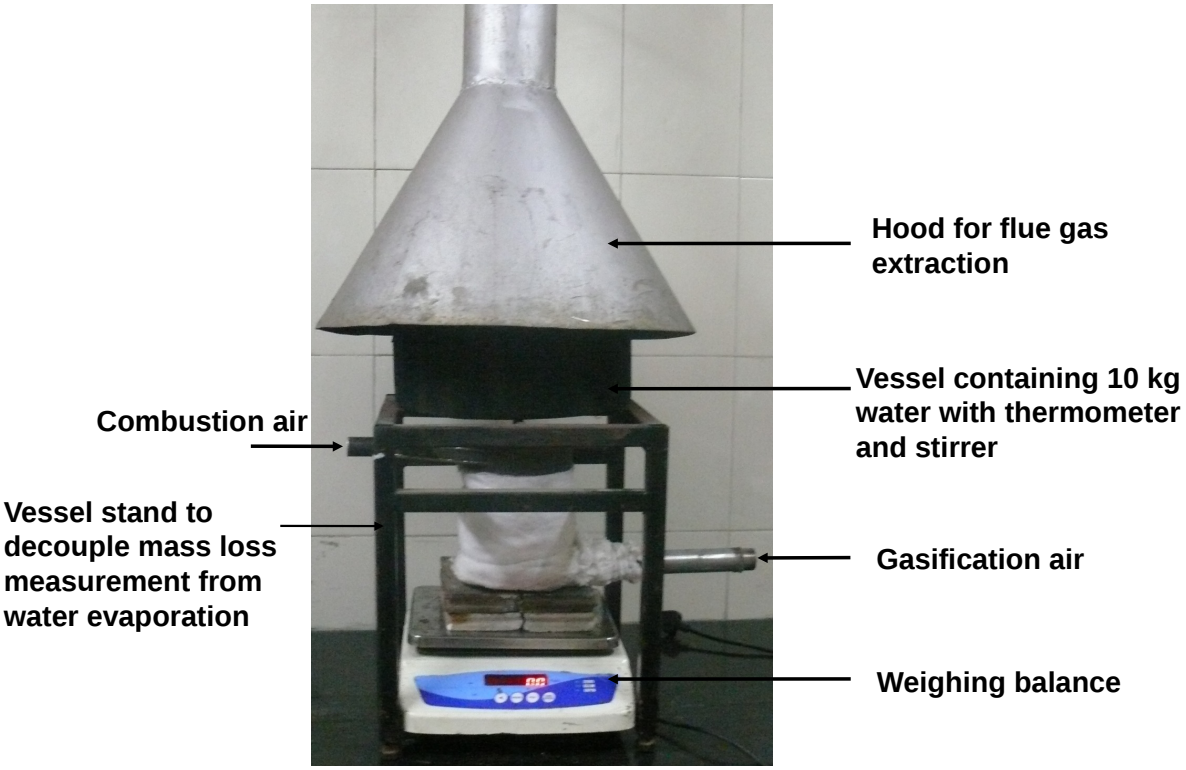

Figure 2.3: Experimental set up for water boiling tests and flue gas analysis

profiles. The uniformity of flow through combustion air holes was checked using a hot wire anemometer and the deviation from the mean velocity was found to be within 5%. The symmetry of the flame on top of the bed during the experiment is also indicative of the uniformity of gasification and combustion flows. Stove experiments were performed only with low density wood chips and 10% ash agro-residue pellets. This entire set up is mounted on a fine balance of 0.5 g accuracy to measure the fuel mass loss with time to estimate the power level of the stove. The balance is interfaced to a computer using RS232 port for continuous data acquisition.

Biomass was loaded into the cylindrical chamber and the amount loaded depended on the density (see Table 2.1). The ignition process involved placing some kerosene soaked waste cotton over the bed and lighting the cotton. This was followed by supplying a fixed amount of gasification air entering from the bottom of the grate and combustion air through the eighteen holes on the top. The flow rates were measured and controlled using calibrated rotameters and needle valve assembly. This set up allows for operating the stove under different equivalence ratios by using a fixed amount of gasification air and varying the amount of combustion air. Experiments can also be done at different power levels by adjusting the gasification air appropriately. A schematic of the experimental set up is shown in Fig. 2.4.

About two minutes after ignition, a 320 mm dia cylindrical aluminium vessel filled with 10 lt of water is placed on a steel stand positioned in such a way that the vessel is at a height of 2.5 cm from the stove top and centred about the stove. This decoupling of vessel from the stove is required to eliminate the effect of water evaporation on fuel mass loss measurement (see Fig. 2.4). The vessel is closed with a lid-stirrer-thermometer arrangement to enable periodic stirring to ensure uniform temperature while measuring the temperature using a thermometer. Water boiling tests were conducted according to the Indian Standards 13152. A hood of appropriate dimensions conforming to IS13152 was used to collect flue gas samples to be analysed for CO using Quintox flue gas analyser. Extracted flue gas was cooled and cleaned for dust and other suspended particles using a condenser-cotton-$CaCl_2$ (see Fig. 2.4) filter before entering the analyser. Two vessels of similar dimensions are required to complete the test. The first vessel is removed when the water reaches 95° C and immediately the second vessel is placed on the stove. The second vessel is removed once the mass left in the stove is less than 1% of the initial mass (excluding the ash). The amount of water evaporated was estimated by using a 0.5 g accurate

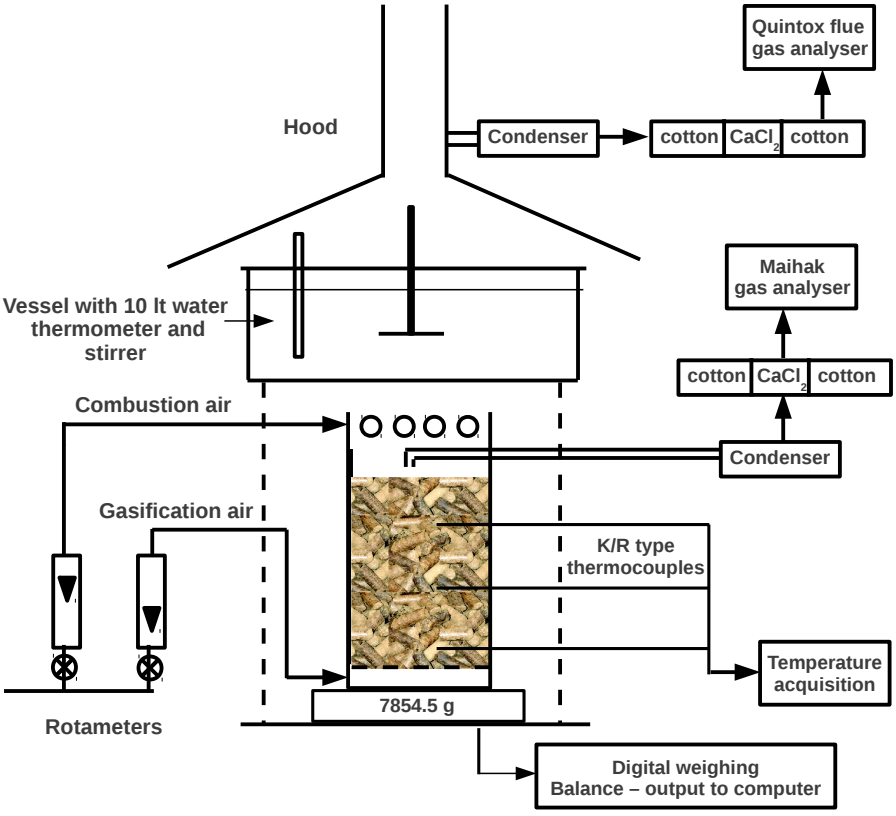

Figure 2.4: Schematic of the stove experiment

weighing balance immediately after the vessels were removed from the stove.

Experiments aimed at determining the gasification efficiency required measurement of composition of the gases issuing out of the packed bed. In these experiments *combustion air was blocked* to eliminate its influence on the gasification and sample extraction process. K-type thermocouples of size 1.5 mm were introduced at regular intervals along the length of the reactor to measure bed temperature and propagation rates. Gas samples were extracted at a location 10 mm above the bed using a 6 mm dia stainless steel tube and a set up similar to the one used for flue gas analysis was used for cooling and cleaning (see Fig. 2.4). The samples were analysed using Maihak and Cubic gas analysers connected in series (see later sections for details about the analyser). The gas composition, bed temperature and mass loss measurements were done for both flaming and char mode.

2.2.2 Packed bed experiments

Initial set of experiments done to estimate the gasification efficiency were restricted to superficial velocity range of 3-6 cm/s corresponding to power of 2.5-5 kW, the operating range of the stove. In order to elucidate the behaviour of packed bed in the entire range of superficial velocity, from 3-60 cm/s, separate set of experiments was performed. Also maximum temperature encountered in the stove experiments was not more than 1250 K and the use of K-type thermocouples is justified. With flow rates ranging from 3-60 cm/s, the temperature can be expected to reach values more than 1500 K (maximum temperature that can be measured with K-type). Therefore, K-type thermocouples used in stove experiments were replaced with 0.4 mm R-type thermocouples (can measure up to 1850 K) for bed temperature measurements.

Apart from fuel consumption rate, exit gas composition and bed temperatures which can be obtained from the set up explained in the previous section by increasing the gasification air flow rate, further measurements like reaction zone thickness, O_2 drop across propagating flame front, gas phase and condensed phase temperatures demanded experiments to be done on transparent reactor. For this purpose a 100 mm dia 150 mm long borosilicate tube was attached to a steel base with provision for controlled gasification air supply. At three equally spaced locations along the length of the tube, 4 mm holes along with extension tubes were provided for measurement access and sample extraction (see Fig. 2.5). The gas phase flame temperature was measured by placing a 100 μm R-type thermocouple in the gap between two particles

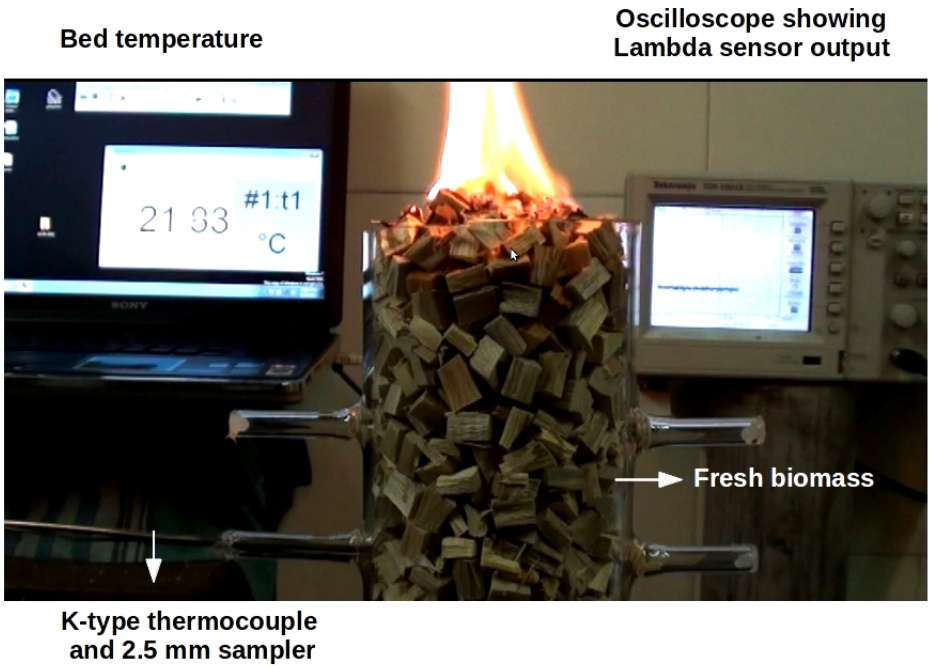

Figure 2.5: Photograph of the glass reactor

and by slightly moving it into the thin diffusion flame in between the particles. The condensed phase surface temperature was measured by pressing the thermocouple against the particle surface.

For oxygen drop measurement across a propagating flame front, a gas sampler of 2.5 mm dia and a 1 mm dia K-type thermocouple were positioned close to each other, as shown in Fig. 2.5, to detect the changes as the flame front moved past this point. The samples extracted were analysed using a lambda sensor (more on lambda sensor a little later).

2.3 Measurement tools

The following subsections contain details about the operating principles, capabilities and limitations of the measurement tools mentioned above.

2.3.1 Temperature measurements

Thermocouples of either 1 mm K-type or 0.4 mm R-type, depending on the range of temperature measurement, were introduced at regular intervals along the length of the bed for measuring the bed temperature. K-type can measure up to 1530 K and R-type can measure up to 1850 K. Error introduced because of radiation loss is not significant for these measurements because the thermocouple is surrounded by high temperature environment. 100 μm R-type thermocouples were used for precise measurement of the gas phase and condensed phase surface temperature in the packed bed. Specific experiments aimed at estimating the error introduced in the gas phase temperature measurement due to surface radiation from the condensed phase were performed with 100 μm aspirated thermocouples. Since the difference in temperature measured with aspirated and bare thermocouple was not more than 20 K, bare thermocouples were used for the rest of the measurements.

2.3.2 Gas composition measurement

Three types of composition measurements with disparate range and time scales were required for various studies conducted. Therefore three different measurement tools were used and the details are presented in the following paragraphs. A picture showing all the three gas analysers along with their response time is shown in Fig. 2.6.

Maihak and Cubic gas analyser

Maihak and Cubic gas analysers are used in series to measure the exit gas composition from the bed. It measures the volume fraction of CO, CO_2, H_2, CH_4 and O_2 only. The measurement range is 0-25% for CO, CO_2 and O_2, 0-20% for H_2, 0-10% for CH_4. The analysers uses non-dispersive infra red (NDIR) sensors for CO, CO_2 and CH_4, paramagnetic sensor for O_2 and thermal conductivity based sensor for H_2. The analyser was calibrated using standard gas composition cylinders at a flow rate of 1 lpm before each set of experiments and the analyser was flushed with ultra high pure N_2 before and after each set of experiments. The accuracy of the analysers was estimated by using a standard cylinder of different composition from the one used for calibration and was found to be within 1% for all the components analysed. The response time of the analysers was determined by alternatively switching between standard cylinders and UHP N_2 and measuring the time it takes for the analysers to

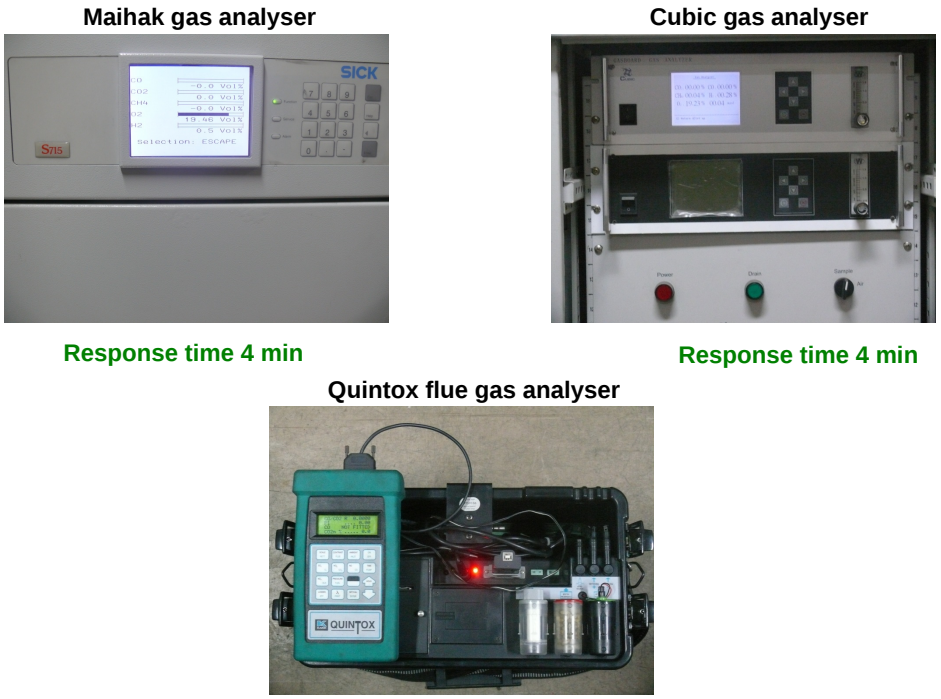

Figure 2.6: Three types of gas analysers used in the study

switch from one composition to the other within a error band of 1%. The time was estimated to be about 4 mins. The flow rate of gases to the analyser was maintained at 1 lpm, the same flow rate used for calibration.

Quintox flue gas analyser

Flue gas samples extracted from the hood placed above the stove vessel arrangement (see Fig. 2.4) was analysed for CO, CO_2 and O_2 using Quintox flue gas analyser. Quintox flue gas analyser measures CO, CO_2 using NDIR sensor and O_2 using a chemical cell. The measurement range for CO is 0-10% with a resolution of 0.01% and 0-25% with 0.1% resolution for O_2. An inbuilt pump samples gases from the hood and the device is calibrated using a standard gas mixture of known composition.

Lambda sensor

Measurement of O_2 drop across the propagating flame front requires a sensor with a response time around 10 sec and since the response time of both Maihak and Quintox analysers is of the order of few mins, a lambda sensor, shown on the left side of Fig. 2.7), was used for this purpose. The set up used for sample analysis is shown on the right side of Fig. 2.7.

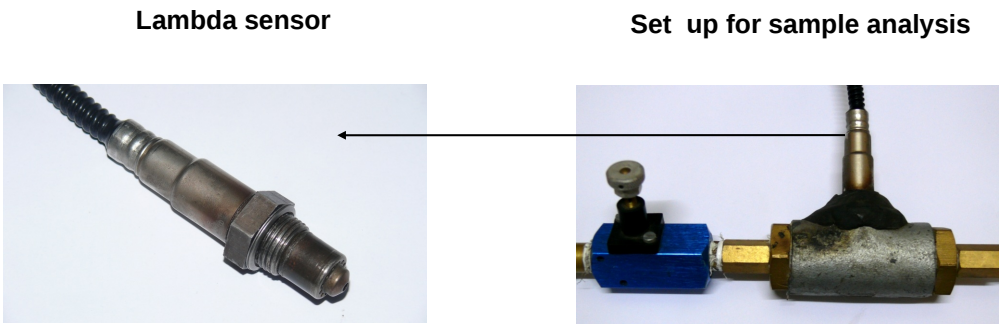

Figure 2.7: Sensor for O_2 measurement across the flame front. Left - picture of lambda sensor. Right - set up used for sample analysis

The response time of this sensor is less than one second and the gas transport time was found to be the limiting factor here. This time was made as low as 10 sec by using a gas sampling probe of 2.5 mm dia and 0.5 m length combined with a glass condenser. Use of glass condenser has the following advantage - as the flame front approaches the sampling location, volatiles start to evolve and can be used as a tracer to estimate the time of sample transport from the reactor to the sensor. The sensor output range is 0-2 V corresponding to 21-0% O_2. The sensor was calibrated using standard gas containing known fraction of O_2 and the response in the 0-21% range was found to be linear. The total response time is composed of the time of transport of sample to the sensor of 10 s and the sensor response time of < 0.5 sec). The choice of these sizes accounted for the process time scales which is about 100 s for a 10 mm particle size. The reaction zone thickness and the location of flame front were obtained from the videos taken. Sample videos are posted at `http://cgpl.iisc.ernet.in/videos/`.

Table 2.2: Measured quantities and corresponding equipments

Measured quantity	Equipment used
Packed bed mass loss with time	30 kg capacity weighing balance with 0.5 g accuracy
Volumetric flow rates of gasification and combustion air	variable area rotameters
Temperature of water in the vessel	thermometer
Single particle mass loss with time	200 g capacity balance with 1 mg accuracy
Peak bed temperature	1 mm K-type or 0.4 mm R-type thermocouple depending on the range of measurement
Gas phase and condensed phase temperature	100 μm R-type thermocouple
Exit gas composition from the bed	Maihak gas analyser
CO emissions from the stove	Quintox flue gas analyser
O_2 drop across the propagating flame front	Lambda sensor

2.4 Summary

All the measurement tools used along with the experimental techniques were presented in this chapter. Table 2.2 summarises the quantities measured with their corresponding measurement tool.

Chapter 3

E^3 - energy, efficiency and emissions

The earlier chapter described the experimental tools that have been used in the investigations in this work. The present chapter is concerned with aspects related to the measurement of the components of energy balance, efficiency and emissions. To enable these, measurements are made of gas composition, water boiling efficiency and flue gas analysis. Gasification efficiency of the stove is compared with that of the gasifier to bring out the similarities and differences. Measured efficiency and CO emission are split into flaming and char modes to identify the causes of poor char mode utilisation. Consequent upon this, methods to improve the performance in char mode are presented. The effect of vessel size on the heat extraction is modelled by simulating the gas phase combustion process and the results are compared with experiments. Certain crucial gas phase flow features like stagnation point boundary layer at the bottom of the vessel and the role played by recirculation on the restoration of stoichiometric operating conditions are also brought out.

3.1 Energy and power levels in flaming and char mode

Figure 3.1 shows a typical mass loss with time plot for pellets at a superficial velocity of 3.5 cm/s. Two distinct modes, flaming and char, can be identified from the plot. Photographs of the flame in flaming and char mode are shown in Fig. 3.2. Sharp change in slope of mass loss with time combined with drastic reduction in flame intensity observed in the experiments (see Fig. 3.2) are indications of transition from flaming to char mode. Some features of the plot are as follows : 1) it can be noted that the mass loss with time is nearly linear in flaming mode that extends up to about 42 minutes; this implies that the *operating power of the stove is nearly constant* in this time period, 2) Transition to char mode starts at around 42 minutes

and in the initial phase of char mode there is very little consumption of fuel; this is related to the cooling effect created by combustion air discussed in detail later. The mass loss in the char mode is about 15 % of that in the flaming mode. The power delivered is about 25 % of that in the flaming mode; this difference is due to the fact that the calorific value of char is about one-and-a half times that of biomass.

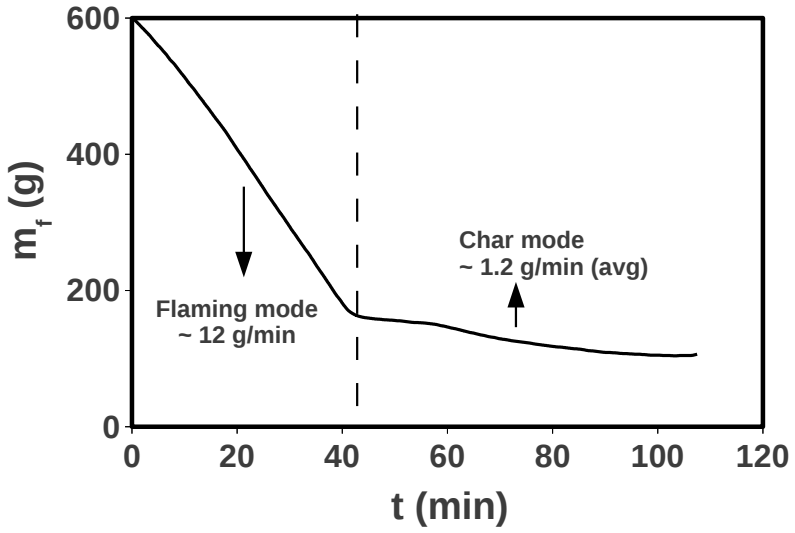

Figure 3.1: Mass loss vs. time with pellets at $V_{co} = 3.5$ cm/s

Table 3.1 shows fuel consumption, energy and power corresponding to the mass loss plot shown in Fig. 3.1. Energy consumed in the flaming mode is calculated as the difference between total energy and energy consumed in char mode, by assuming char calorific value to be 28 MJ/kg. Power level is estimated from average slope of mass loss curve in each mode.

It can be noted that the power levels and energy values in flaming mode and char-burning mode are widely different. Energy delivered in the flaming mode is about 70% of the total energy. Therefore, it was found logical to split the total efficiency and emissions of the stove into contribution from flaming and char mode. This, as will be shown later, will help identify avenues for improvement of stove performance. Before that, it is important to estimate how efficient the first step, the gasification process? This is discussed in the next section.

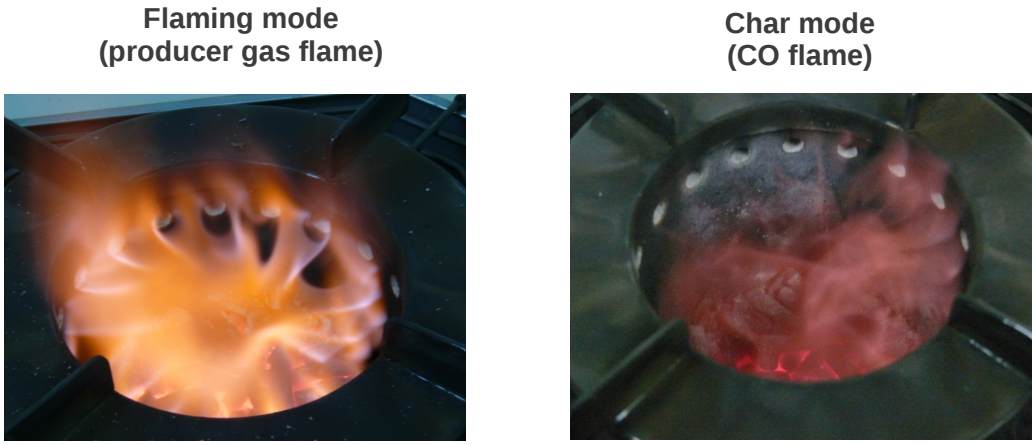

Figure 3.2: Gas phase flame in the stove. Left : Flaming mode. Right : Char mode

Table 3.1: Mass, Energy and Power behaviour, $\dot{m}_{fla}$ = fuel consumption rate at 17 g/min gasification air flow rate; combustion air flow blocked

Mode	Fuel (g)	$\dot{m}_f$ (g/min)	Cal Value (MJ/kg)	Energy (MJ)	Time (min)	Power (kW)
Flaming	413*	11	13.4**	5.5	40	2.3
Char	90#	1.2##	28	2.5	70	0.6

Cal value of biomass = 16 MJ/kg, * = excluding 6% moisture
** = deduced, # = excluding 70 g ash
= average value over the char mode

3.2 Gasification air-to-fuel ratio

Table 3.2 shows gasification air-to-fuel ratio (A/F) and bed temperature (T_b) measured for three different gasification air mass flow rates, corresponding to a superficial velocity range of 3-5 cm/s with wood as fuel. Combustion air flow is blocked in these experiments to avoid influence on the gasification and sample extraction process.

This simple result obtained from air-flow and fuel mass-time data confirms the known fact that the A/F of gasification is constant in the range of flow rates considered. This condition is required for obtaining gas of highest possible calorific value (Kaupp & Goss (1984)). It is important to recognise this fact because the A/F is not

Table 3.2: Gasification A/F and bed temperature (T_b) with wood as the fuel, V_{ga} - air flow rate, $\dot{m}_{fla}$ - fuel consumption rate in flaming mode,

V_{ga} (lpm)	V_s (cm/s)	$\dot{m}_{fla}$ (g/min)	A/F	T_b (K)
15	3.2	10	1.5	996
18	3.8	12	1.5	1096
24	5.1	16	1.5	1206

1.5 for all range of air flow rates as shown in Reed *et al.* (1999). Therefore this serves as a check for optimal performance of any gasifier stove. Measured bed temperature increases with increase in superficial velocity. These two phenomena, namely, constant A/F and increasing bed temperature, are consistent with the internal heat balance in gasification process. As the air flow is increased heat release rate will increase because more of pyrolysis products are burnt. But this will not increase the temperature of char bed directly because the endothermic reduction reactions ($C + CO_2 \rightarrow 2CO$ and $C + H_2O \rightarrow CO + H_2O$) will cause reduction in temperature rise. Also the amount of gas passing through char bed undergoing endothermic reduction reactions will increase and therefore consumption of char will increase. This net effect results in a constant A/F even with increase in mass gasification rate.

3.3 Gas composition and gasification efficiency (η_{ga})

Table 3.3 shows gas composition and gasification efficiency for flaming mode operation with wood corresponding to fuel consumption rates shown in Table 3.2.

Table 3.3: Gas composition (volumetric) and gasification efficiency (η_{ga}) at different wood consumption rates

$\dot{m}_{fla}$ g/min	CO %	CO_2 %	CH_4 %	O_2 %	H_2 %	T_g K	H_c MJ/kg	η_{ga} %
10	8	19	1.5	2.80	1.6	996	2.0	41
12	12.3	20	2.5	1.30	5.2	1096	2.7	57
16	13	18	2.5	0.83	7.5	1206	3.1	66

Table 3.3 shows that gas composition improves with increase in mass gasification

rate; this is expected because the amount of gas reduced by char bed increases and that means more of CO_2, H_2O get converted to CO and H_2 and more tar gets cracked into simpler components.

Gasification efficiency is defined as the ratio of energy contained in the gases generated in the gasification process to the input energy in the flaming mode. Energy input in the flaming mode is estimated using the same method used in calculating energy in Table 3.1. Contribution of sensible enthalpy is also taken into account while calculating energy content of producer gas. Maximum gasification efficiency obtained is 66%. However, classical downdraft gasification systems show a cold gas efficiency of 80 % and a corresponding hot gas efficiency of $\sim$ 96 %, when the sensible enthalpy carried by all the gases (CO, CO_2, H_2, CH_4, N_2) including H_2O at 800 K is taken into account (the exact value of the composition is presented later). The only difference between gasifier and stove is the presence of a relatively thick char bed in gasifier as compared to a stove. Absence of this in the case of stoves is responsible for higher volume fraction of CH_4 (2-3%) in stoves as compared to 1-2% in a classical downdraft gasifier. With thick char bed, cracking of higher hydrocarbons (referred to as HHC) like tar is very effective in a classical downdraft gasifier. Even in a downdraft gasification systems, it is inferred that the fraction of HHC will be higher whenever CH_4 is greater than about 1.5 %. Such a situation is therefore most likely in the stove gasification process and a preliminary elemental balance revealed a carbon imbalance of 10% and a hydrogen imbalance of 20% at 5 cm/s superficial velocity. Since the gas analyzer used in experiments cannot detect any hydrocarbon other than CH_4, a complete elemental balance for the gasification chemical reaction was carried out. Also, since the water vapour in the gases is condensed before the analysis, the heat carried away by water vapour is not accounted for in the calculation of the gasification efficiency. This applies to both stoves and gasifiers. Using equations obtained from the elemental balance and the measured composition on dry basis, a methodology was developed to simultaneously calculate the HHC and water vapour fraction. The details are given in the following paragraphs.

3.3.1 Elemental balance

In order to enforce elemental balance the amount of carbon, hydrogen and oxygen consumed in the flaming mode is required. To calculate this the amount of char left at the end of flaming mode is required and was found to be 18% (ash and moisture

free) of the initial mass from experiments. Using this fact along with the CHNO of wood, $CH_{1.72}O_{0.88}N_{0.00248}$, and that of char $CH_{0.28}O_{0.07}$ obtained by outsourcing it to a chemical laboratory, the amount of carbon, hydrogen, and oxygen consumed in the flaming mode was estimated. CHO consumption for a typical experiment with 400 g of wood is set out in Table 3.4. Amount of hydrogen and oxygen present in the biomass in the form of 10% moisture is accounted for in calculation by adding it to flaming mode hydrogen and oxygen consumption. Nitrogen from biomass is not included in the calculation because it is negligible compared to nitrogen from the air.

Table 3.4: Energy and CHO consumption in flaming and char mode

	Amount (g)	C (g)	H (g)	O (g)	Energy (MJ)
Biomass	396*	161.2	27.5	207.3	5.7
Flaming	332#	105.8	26.2	200.0	3.9
Char	64	55	1.3	7.3	1.8

* - ash free basis; # - 10% moisture added

Using the air flow rate measured with rotameter and the above mentioned details, the gasification reaction can be written as,

$CH_{1.72}O_{0.88}N_{0.00248}$ + 0.17 H_2O *(10% moisture)* + 1.61$(O_2$ + *3.76* $N_2)$ → aCO + bCO_2 + cH_2 + dH_2O + eCH_4 + 6 N_2 + 0.36 $CH_{0.28}O_{0.07}$ *(18% char)*

By assuming that the only hydrocarbon present is CH_4, the energy equivalent of other HHC was estimated by solving the element balance equations (Eq. 3.1, 3.2, 3.3) obtained from the gasification reaction. CHO of the char on the product side is taken in to account in the equations. Here e refers to CH_4 produced in the gasification reaction plus the CH_4 equivalent in energy to other hydrocarbons.

$$C : a + b + e = 0.64 \tag{3.1}$$

$$H : 2c + 2d + 4e = 1.96 \tag{3.2}$$

$$O : a + 2b + d = 4.24 \tag{3.3}$$

There are three equations and five unknowns (a, b, c, d and e). But the volume fractions of CO, CO_2 are known on dry basis from the experiments and this gives the following two equations corresponding to 16 g/min wood consumption (see Table 3.3),

$$a/(a+b+c+e+6) = 0.13 \tag{3.4}$$

$$b/(a+b+c+e+6) = 0.18 \tag{3.5}$$

The five equations were solved by initially assuming the water fraction in the exit gas to be 10% and by iteratively correcting this estimate, so that the final composition satisfies the elemental balance equations and Eqs. 3.4, 3.5. Methane was added to account for the unbalanced carbon; hydrogen remaining after this was added to H_2O to balance the oxygen. The final composition for 16 g/min wood consumption along with the gasification efficiency is shown in Table 3.5 for both hot and cold gas.

Table 3.5: Composition corrected using Atomic balance

	CO %	CO_2 %	CH_4 %	H_2 %	H_2O %	Cal value (MJ/kg)	η_g* (%)
Hot gas	9.6	13.3	3.9	10.0	21.6	4.6	96
Cold gas	12.3	17.0	5.1	12.3	-	3.3	69

* - basis is flaming mode energy input - 11 MJ/ kg biomass

Comparing with the composition presented in Table 3.3 the methane equivalent of HHC is around 2-3%. It contributes about 16% to gasification efficiency and methane alone contributes 14%, including the sensible part. Volume fraction of water vapour in the exit gases is about 20% and contributes 6-7% to the gasification efficiency. It is important to note that the sensible part alone contribute about 28% to the gasification efficiency.

3.3.2 Comparison with downdraft gasifiers

Typical gas composition obtained from a large downdraft gasification system is 20% CO, 18% H_2, 1.5% CH_4, 12% CO_2 on dry basis and the gasification efficiency of this

cold gas is 80%. A point to note here is that, in a classical downdraft gasification system the char extracted under these conditions is $\sim$ 2% of the initial mass and amounts to only 3% of total energy. So neglecting this does not affect the gasification efficiency calculation. Superficial velocity in the operating range of gasifier $\sim$ 13 cm/s. The gases come out of the gasifier at approximately 800 K and the composition of the wet gas, calculated using a procedure similar to the one described earlier, is 17.6% CO, 15.7% H_2, 1.4% CH_4, 10.6% CO_2 and 12.1% H_2O. Gasification efficiency corresponding to this composition including the sensible enthalpy is 96%. Sensible part alone contributes only 14% as compared to 28% in stoves. This shows that the heat losses associated with gasification in both the systems is about 4% and the sensible enthalpy compensates for the poor composition obtained from stoves as compared to a gasifier.

A natural question at this juncture is 'What will be the cold gas and hot gas efficiency of top lit updraft, that is, stove at a superficial velocity of 12-13 cm/s?'. A comparison is presented in Table 3.6.

Table 3.6: Gasification efficiency of large downdraft gasifiers and TLUD systems

System	Input energy (MJ/kg biomass)	η_{cg}^{*} (%)	η_{sh}^{**} (%)	$\eta_{hg}^{\#} = \eta_{cg} + \eta_{sh}$ (%)
TLUD 5 cm/s	11.0	69	27	96
TLUD 12 cm/s	13.2	54	39	93
Downdraft gasifier	15.4	81	16	96

* - cold gas; ** - sensible heat contribution; $^{\#}$ - hot gas

Figures 3.3, 3.3, 3.5 show a schematic of different components contributing to the gasification efficiency for all the three cases considered along with the gas composition on wet and dry basis.

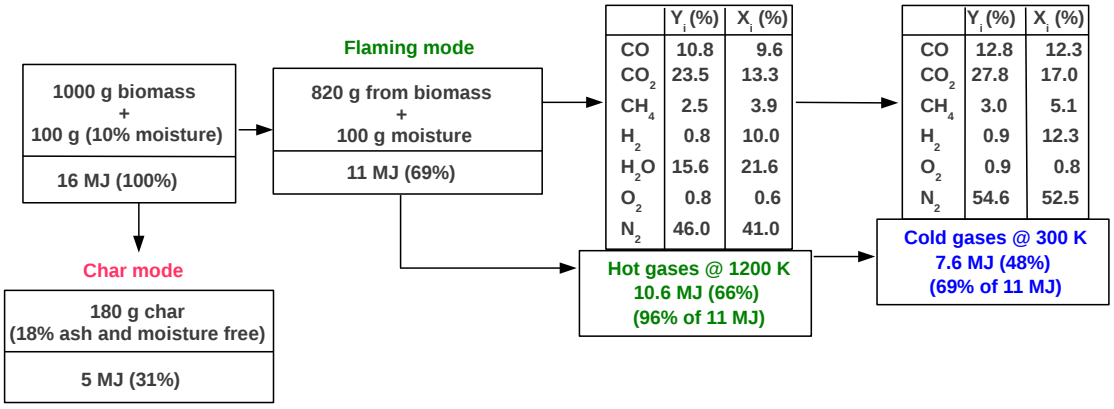

	Y_i (%)	X_i (%)
CO	10.8	9.6
CO_2	23.5	13.3
CH_4	2.5	3.9
H_2	0.8	10.0
H_2O	15.6	21.6
O_2	0.8	0.6
N_2	46.0	41.0

	Y_i (%)	X_i (%)
CO	12.8	12.3
CO_2	27.8	17.0
CH_4	3.0	5.1
H_2	0.9	12.3
O_2	0.9	0.8
N_2	54.6	52.5

Figure 3.3: Gas composition and gasification efficiency corrected using elemental balance at 5 cm/s for TLUD stove. A/F = 1.5. Y_i - mass fraction; X_i - volume fraction

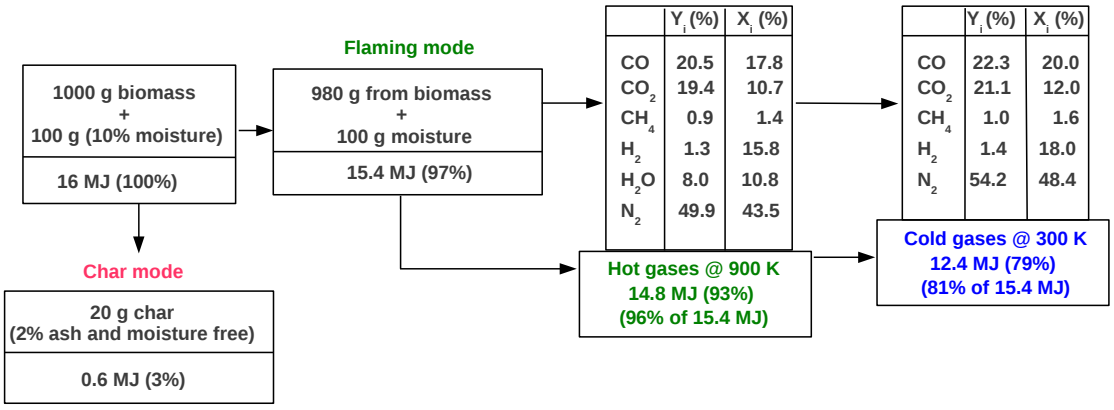

	Y_i (%)	X_i (%)
CO	20.5	17.8
CO_2	19.4	10.7
CH_4	0.9	1.4
H_2	1.3	15.8
H_2O	8.0	10.8
N_2	49.9	43.5

	Y_i (%)	X_i (%)
CO	22.3	20.0
CO_2	21.1	12.0
CH_4	1.0	1.6
H_2	1.4	18.0
N_2	54.2	48.4

Figure 3.4: Gas composition and gasification efficiency for a downdraft re-burn gasification system. A/F = 1.7. Y_i - mass fraction; X_i - volume fraction

A few points are worth noting here, which are as follows,

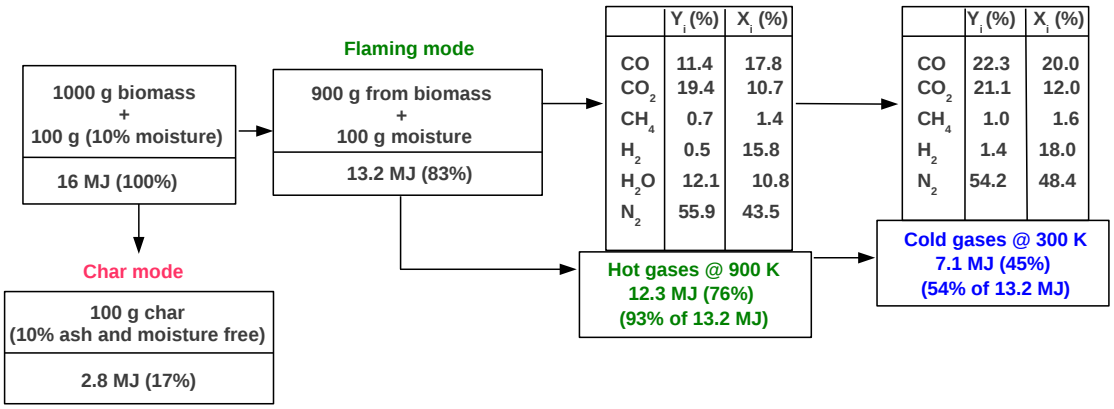

Figure 3.5: Gas composition and gasification efficiency corrected using elemental balance at 12 cm/s for TLUD stove. A/F = 2.4. Y_i - mass fraction; X_i - volume fraction

i. In a top lit system like in stove the cold gas calorific value is about 3.3 MJ/kg and that of hot gas is 4.6 MJ/kg. The difference is 1.3 g/MJ.

ii. In the case of a bottom lit gasifier, the difference between the hot gas and cold gas calorific value is only about 0.3 g/MJ. This parameter itself is an indicator of the performance of the gasifier, where the aim is to get cold gas with as high caloric value as possible.

iii. Comparison of gasifier with a top lit system operating at the same superficial velocity of about 12-13 cm/s (see Fig. 3.5) brings out the role played by the thick hot char bed in generating high calorific value gas in a downdraft gasifier.

In this section an important component of stove efficiency, namely gasification efficiency was established. Similarities and differences between a stove and a gasifier was brought out using hot and cold gas efficiencies. The following section deals with the water boiling efficiency and other related aspects.

3.4 Water boiling efficiency

This section presents results of water boiling test performed to estimate the efficiency of the stove in flaming and char mode. To assess the importance of near

stoichiometric operation, experiments were performed at different equivalence ratios by fixing the gasification air flow rate and by varying the combustion air flow rate. The range of flow rates used and equivalence ratios expected and attained are shown in Table 3.7. Here equivalence ratio (ϕ) is defined as the ratio of actual fuel-to-air ratio to that at stoichiometry. An important point to note is, the gasification A/F is not 1.5 any more as in Table 3.2. This shows the influence of combustion air on the gasification process. As the combustion air flow rate is increased further to achieve overall lean conditions, the influence of combustion air on the gasification process causes shifting of operating point towards stoichiometry. Last two rows in Table 3.7 show an interesting feature - *the stove cannot be operated on the lean side*. When flow rates are adjusted to obtain lean condition, operating point shifts toward stoichiometric point through increase in the burn rate. Explanation for this behaviour is obtained from the results of CFD calculations presented later (see Section 3.9.7).

Table 3.7: Expected and attained equivalence ratio, ϕ_e and ϕ_a, V_{ga}, and V_{co} = volumetric flow rates of gasification and combustion air, A/F = $(V_{ga} + V_{co})/\dot{m}_{fla}$, $(A/F)_{stoichiometic} = 5$

V_{ga} (lpm)	V_{co} (lpm)	$\dot{m}_{fla}$ (g/min)	ϕ_e (expected)	$\dot{m}_{fla}$ (measured) (g/min)	ϕ_a (attained)
15	40	13.3	1.18	13.3	1.18
15	50	13.3	1.01	13.3	1.01
15	54	13.3	0.94	14.5	1.03
15	58	13.3	0.80	14.7	0.99

Energy utilisation from the stove was estimated by measuring the temperature of 10 kg water in a vessel heated by the stove. From the knowledge of heat transferred to the vessel, mass burn rate and calorific value of the fuel, the water boiling efficiency was calculated. This water boiling efficiency of the stove was split into flaming and char mode efficiencies by using water temperature data and energy delivered in each mode (Table 3.1). Experiments were performed with wood (615 kg/m^3) and pellets (1260 kg/m^3) for two equivalence ratios and the results are shown in Table 3.8. Repeated experiments (about 15) showed that the uncertainty in heat transferred to the vessel is about 1%.

Table 3.8: Water boiling efficiency and CO emissions at two equivalence ratios ($\eta_{wb} = \eta_{fla} + \eta_{char}$; η'_{fla} and η'_{char} are flaming and char mode efficiencies with energy in the volatiles and in the char as the basis respectively. Power level corresponds to data given in Table 3.1)

ϕ	η_{wb} (%)	CO (total) (g/MJ)	η_{fla} (%)	CO (flaming) (g/MJ)	η_{char} (%)	CO (char) (g/MJ)	η'_{fla} (%)	η'_{char} (%)
				Wood				
1.0	44	1.0	40	0.43	4	0.57	54	15
1.2	42	0.88	36	0.65	6	0.23	48	23
				Pellets				
1.0	45	0.95	41	0.4	4	0.55	55	16
1.2	43	0.8	37	0.6	6	0.2	49	24

3.5 Flaming and char mode efficiency

In Table 3.8, basis for calculating η_{fla} and η_{char} is the calorific value of biomass (16 MJ/kg). The quantities η'_{fla} and η'_{char} are efficiencies derived as the ratio of heat absorbed by vessel to the energy delivered in the respective modes. These will indicate how the heat transfer process has been effective in the two separate segments of operation. Table 3.8 shows that efficiencies (η_{wb}, η_{fla} and η_{char}) of the stove with wood and pellets are about the same. Low efficiencies in char mode are also evident; however, when the stove is operated in fuel rich mode ($\phi = 1.2$), char mode efficiency and CO emissions calculated for this segment alone appears better than for the stoichiometric case. This indicates that air flow rates corresponding to rich flaming mode operating conditions are more favourable for char mode than the air flow rates corresponding to stoichiometric flaming mode conditions. Also mass loss with time (see Fig. 3.1) shows that at an air flow rate corresponding to typical flaming mode power level of 12 g/min, the peak char mode burn rate is 2 - 3 g/min. Since 70% of total input energy is delivered in flaming mode, the stove is designed in such a way that it ensures stoichiometric operation in the flaming mode. This air flow rates remain unchanged as the transition to char mode takes place, but the composition of the fuel changes to $CH_{0.28}O_{0.07}$. This factor leads to very lean conditions in char mode to an equivalence ratio, $\phi = 2.5$ and the combustion air instead of aiding completion of combustion will cause dilution leading to quenching. Effect of these

factors on efficiency and emissions and ways to improve the performance in char mode are explained after a consideration of CO emissions in these modes.

3.6 CO emissions

Quintox flue gas analyzer was used to measure the volume fraction of CO, CO_2 and O_2. Biomass is the only source of carbon and hence the only source of CO and CO_2. After combustion, the primary carbon products are only CO and CO_2. From the mass burn rate of biomass, the absolute mass of CO emission in g/MJ of energy input was calculated using the volume fractions of CO, CO_2 and O_2. Table 3.8 shows CO emissions from the stove with wood chips and pellets as fuel, at two different equivalence ratios.

Total emission from rich operating point is low compared to stoichiometric operating point. This appears surprising at first sight. However, issues become clear if the efficiency and emissions are split into flaming and char mode segments and compare them against the corresponding emissions. This shows that the results conform to the intuitive behaviour expected from thermo-chemical considerations - higher combustion efficiencies correspond to lower emissions. An important point to note is *combustion efficiency corresponding to 0.4 g/MJ CO emissions is about 99.3%*. A typical free convection driven biomass stove will have a combustion efficiency of about 89% (see Smith (1994)). As explained earlier, lower char mode combustion efficiency and higher emission under stoichiometric flaming mode conditions compared to rich flaming mode operating point are because of the adverse cooling effect created in the char mode by combustion air. Reduction in the power level is not accompanied by change in the air flow rate to ensure stoichiometric operation in char mode, leading to very lean operation. Any reduction in CO emission must therefore address the char mode rigorously.

3.7 Modifications to improve the performance in Char mode

The reasons for poor performance of the existing design in char mode compared to flaming mode were brought out in the previous sections. The reduction in mass burn rate as the transition to char mode takes place leads to very lean conditions; this was argued to be the reason for poor utilisation. In order to make the operating

Table 3.9: Effect of R = V_{co}/V_{ga} on the efficiency, ϕ_{char} = Char mode equivalence ratio, $\dot{m}_{char}$ = Char mass burn rate

V^*_{ga} (g/min)	V^*_{co} (g/min)	R	$\dot{m}^{**}_{char}$ (g/min)	ϕ_{char}	η_{wb} (%)	η_{fla} (%)	η_{char} (%)	CO (g/MJ)
12	58	4.8	3.0	0.5	51	45	6	1.00
18	52	2.9	4.4	0.7	56	45	11	0.75
24	46	1.9	6.2	1.0	62	45	17	0.53

* - air flow rates changed only in the char mode

* - in flaming mode V_{ga} = 12 g/min, V_{co} = 58 g/min for all the three experiments

** - peak burn rate

conditions close to stoichiometric, gasification air flow rate was increased by keeping the total flow rate constant, when the transition to char mode happens (the flow rates are not altered during flaming mode). This leads to an increase in burn rate and the cooling effect of combustion air is also brought down. Results presented in Table 3.9 show the effect of changing flow rates in the char mode on efficiencies and emissions. In this table R represents the ratio of combustion to gasification air flow rates. As R is reduced from 4.8 to 1.9, the equivalence ratio moves closer to stoichiometric operating conditions from very lean conditions. Water boiling efficiency of the stove increases with decrease in R as the contribution from char mode increases from 4% to 17%.

Carbon-monoxide emission and mass loss with time for experiments performed at different values of R are shown in Figs. 3.7 and 3.6. The following features need particular attention.

i. Mass loss plot shows similarity of flaming mode power level for all three cases considered, 11 g/min.

ii. At these air flow rates it can be seen from the plot (see Fig. 3.6) that in char mode flame cannot sustain because of inadequate power level and combustion air cooling. Hence quenching takes place and about 100 g of char (rest 50 g is ash) is left un-burnt.

iii. As transition to char mode takes place, decrease in the ratio of combustion to gasification air flow rate is reflected in char consumption rate increasing from about

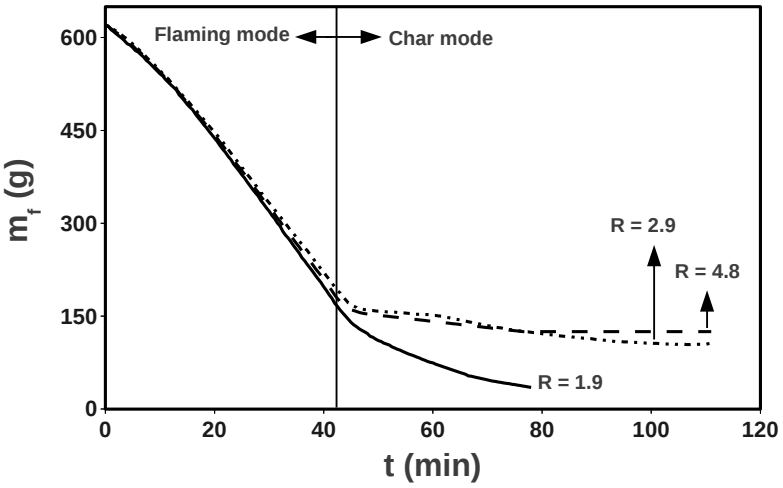

Figure 3.6: Effect of R on mass burn rate of char at a mass burn rate of 11 g/min

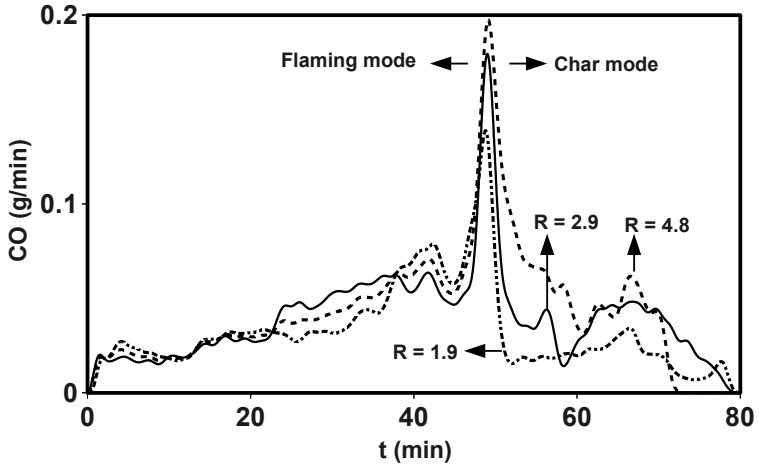

Figure 3.7: Effect of R on CO emissions at a mass burn rate of 11 g/min

3.0 g/min to 6.2 g/min. This results in shifting of A/F towards stoichiometric point as indicated in Table 3.9 and leads to complete consumption of char without quenching.

iv. CO from flaming mode is same for all three cases, reinforcing the similarity of flaming mode operation.

v. Transition to char mode is evident from the spike in CO. The spike is associated with the sudden change of energy release mode from volatiles combustion to surface char oxidation.

vi. After the spike, CO emission is higher with R = 2.9 compared to R = 1.9 case, consistent with the A/F shift.

3.8 Implications for the commercial Oorja stove

Since the combustion to gasification air ratio (R) must be maintained close to 4.8 (see first row in Table 3.9) to obtain maximum efficiency in flaming mode, design modifications are required with regard to char mode operation to implement the insights obtained from Table 3.9. To explore the extent to which performance can be improved with the existing design, experiments were done on Oorja 1.3 at the two power levels dictated by the design, 3.5 and 4 kW and the results are shown in Table 3.10. Clearly higher power level in char mode leads to 5 % increase in efficiency. These results bring out another crucial fact that optimum power level in flaming mode is also important in extracting more energy from the stove (see row 1 and 2 in Table 3.10). Low power level in flaming mode combined with high power level in char mode leads to an increase in water boiling efficiency by 5%, ie., from 55% to 60%. As shown in Table 3.9, if the char burn rate can be increased to 6 g/min, efficiency can go up to as high as 65%.

3.8.1 Scaled up versions

Recently demand created by commercial large scale kitchens led to the development of scaled up versions of Oorja. Two versions, K30 with a peak power of 15 kW and K60 with a peak power of 25 kW were designed. These designs along with the domestic version are shown in Fig. 3.8. The insights obtained from the experiments

Table 3.10: Efficiency of Oorja stove

Flaming Power level	Char Power level	$\dot{m}_{fla}$ (g/min)	$\dot{m}_{char}$ (g/min)	η_{fla} (%)	η_{char} (%)	η_{wb} (%)
High	High	16	4	40	15	55
Low	Low	14	3	45	10	55
Low	High	14	4	45	15	60

reported earlier in Table 3.9 were used in this design. Two separate fans, one for gasification and other for combustion were used in this design, which allows for independent control. Therefore the speeds were adjusted to give a R value of 5 in flaming mode and 2 in char mode to get the maximum efficiency possible. Efficiency of 65% and CO emission of 0.4 g/MJ for vessel to stove diameter ratio of 2.2, were obtained with these stoves. The point to note is that these values indicate performance that is nearly as good as an LPG stove. About 2500 of these stoves are already in operation in the field.

3.9 Vessel size effect - Gas phase combustion modelling

Efficiency numbers presented in the previous sections were obtained for a 320 mm vessel. This efficiency is composed of two parts, namely, gasification efficiency and heat transfer efficiency. Unlike gasification efficiency, which depends only on the superficial velocity through the stove, the heat transfer is strongly dependent on the flow field around the bottom portion of the vessel. This is the reason for strong dependence of water boiling efficiency on the size of the vessel. Therefore it is important to understand in detail the convective heat transfer from hot gases to the vessel. Another feature of the stove which demanded complete flow field details was the effect of recirculation zone on the restoration of stoichiometric operation observed in the experiments. Towards this, detailed thermal and flow field profiles were obtained by solving the conservation equations in a domain comprising the portion of the stove above the fuel bed and the vessel.

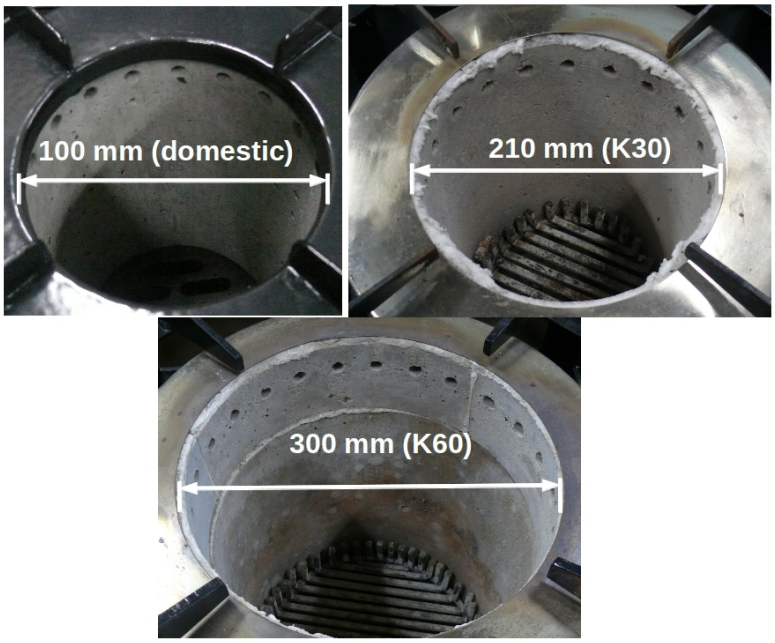

Figure 3.8: Domestic and scaled up versions of Oorja

3.9.1 Flow regime, domain and boundary conditions

In order to simulate the flow in a stove it is required to know whether the flow is laminar or turbulent. The stove is essentially a cylinder of diameter 100 mm and 18 circular jets on its circumference. Average biomass burn rate is 13 g/min and the stoichiometric A/F is 4.9. Therefore for stoichiometric operation, total flow through the stove is 76.7 g/min. The flow Reynolds number with the stove diameter (100 mm) as the characteristic length is $\mathrm{Re}_d = \rho \mathrm{Vd}/\mu = 4\mathrm{m}/\pi \mathrm{d}\mu = 301$. This is very small compared to Re_{crit} (for transition to turbulent flow) for flow through a cylindrical duct constituting the combustion chamber. But there are 18 jets coming into the cross-flow and the critical Reynolds number of jet is small. Reynolds number based on jet diameter and the mass flow of combustion air is $\mathrm{Re}_{d_j} = \rho \mathrm{Vd}/\mu = 4\ \dot{m}_{air}/\pi \mathrm{d}\mu = 391$. Even at this Reynolds number, the jet could be turbulent. But the jets are issuing into a chamber that has a high viscosity (due to high temperatures in the combustion chamber). The net behavior is close to laminar flow - the physical appearance is of a mildly dancing diffusion flame.

In actual stove the combustion air is supplied using a fan which blows air into a plenum and then it enters the combustion chamber through 18 circular holes on the circumference of the chamber. Issues of axi-symmetry and nature of inflow velocity profile were determined by simulating the cold flow through the plenum and the stove combustion chamber. The flow domain used for the calculation is shown in Fig. 3.9. Structured grid with 0.15 million cells was used to compute the flow field. Mass flow inlet boundary condition for the main inlet, zero pressure gradient for the outlet and no slip no penetration boundary condition for the walls were used. The results are presented in Fig. 3.10.

There is some asymmetry in the velocity profile but does not appear significant. Since the interest is in the overall thermal behaviour, velocity profile obtained from ensemble average of the data at each point along the radius was used to approximate the velocity profile and the simulations were performed. For the ease of computation a 20 ° sector with one combustion air inlet was simulated assuming symmetry and a parabolic velocity profile was assumed for air inlets. The computational domain along with the boundary conditions used are shown in Fig. 3.11.

Gas phase combustion process in the stove is non-premixed and therefore the chemical reactions were assumed to be *mixing controlled*. Calculations were made with additional transport equation for the mixture fraction and algebraic equation

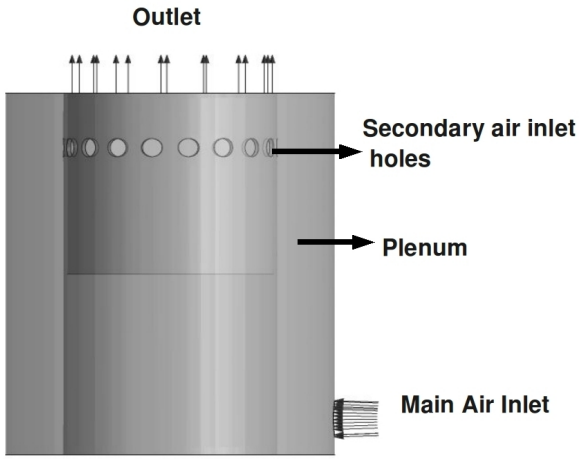

Figure 3.9: Computational domain for calculating combustion air distribution

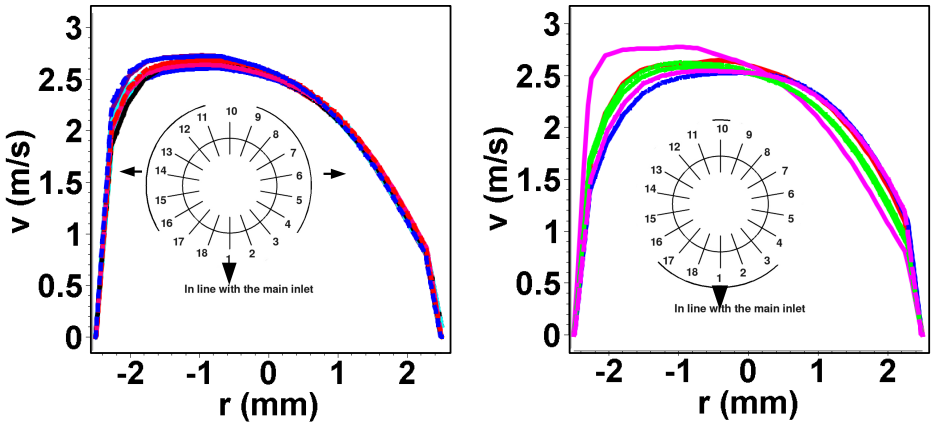

Figure 3.10: Combustion air inlet velocity profile

for mass fractions of various components. Heat transfer due to radiation from the gases and the stove walls was modelled using discreet transfer equations.

A few preliminary computations showed that the stagnation boundary layer at the bottom of the vessel requires a fine grid. Capturing this with good resolution is crucial because the aim of the computation is to determine the vessel wall temperature gradient. The wall heat flux along the bottom of the vessel is shown for three different grids in Fig. 3.12. A grid with 0.26 million nodes (220 mm diameter vessel) and 0.2 mm size in the direction normal to the vessel wall resolved the boundary layer with sufficient accuracy. The point to note is that the coarse grid

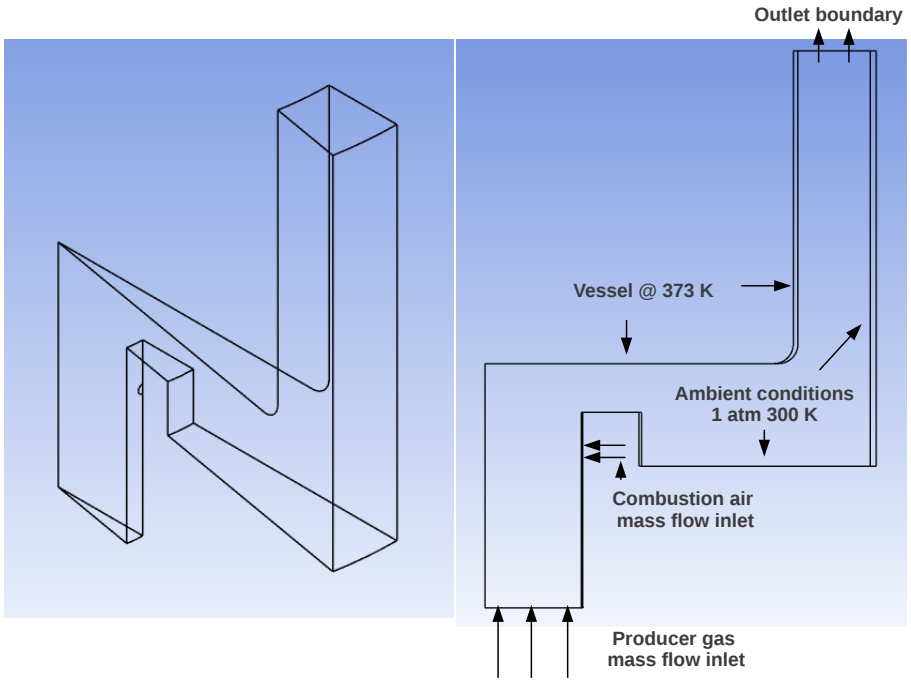

Figure 3.11: Computational Domain and Boundary Conditions

had problems resolving the flow features close to the stagnation point. It was found that this would not affect the prediction of total heat transfer, because the relevant area involved is small close to the stagnation point.

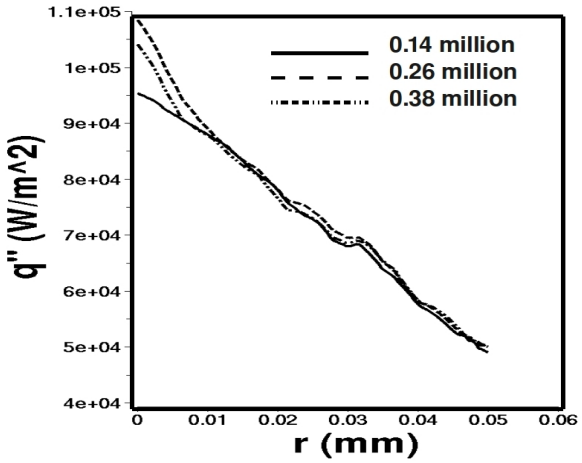

Figure 3.12: Grid independence test

3.9.2 Flow structure

Figure 3.13 shows path traced by fluid particles from combustion air inlet. The vector length represents the velocity magnitude and is coloured with temperature field. The front view shown on the right shows the jet impingement and recirculation zone.

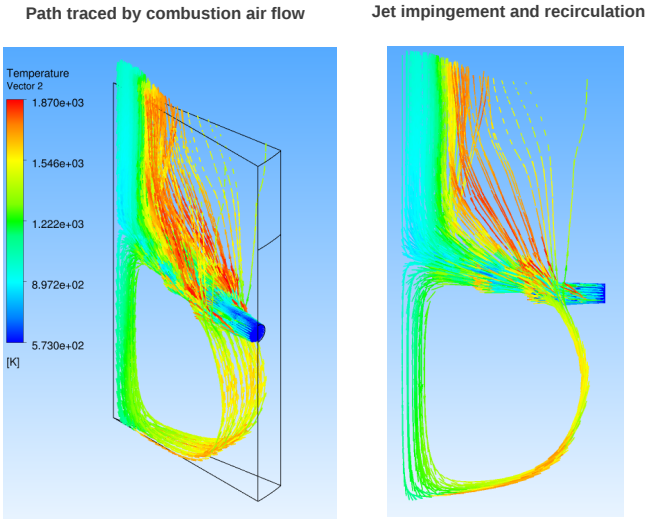

Figure 3.13: Path traced by fluid particles from combustion air inlet - Left - isometric view; Right - front view

Figure 3.14 shows velocity vectors on the centre plane coloured with temperature. The structure of the recirculation zone and that of the exhaust plume are brought out in Fig. 3.15. The stagnation zone visible above the jet in the centre plane is because of recirculating flow moving past the incoming air jet creating a wake like flow (see Fig. 3.16).

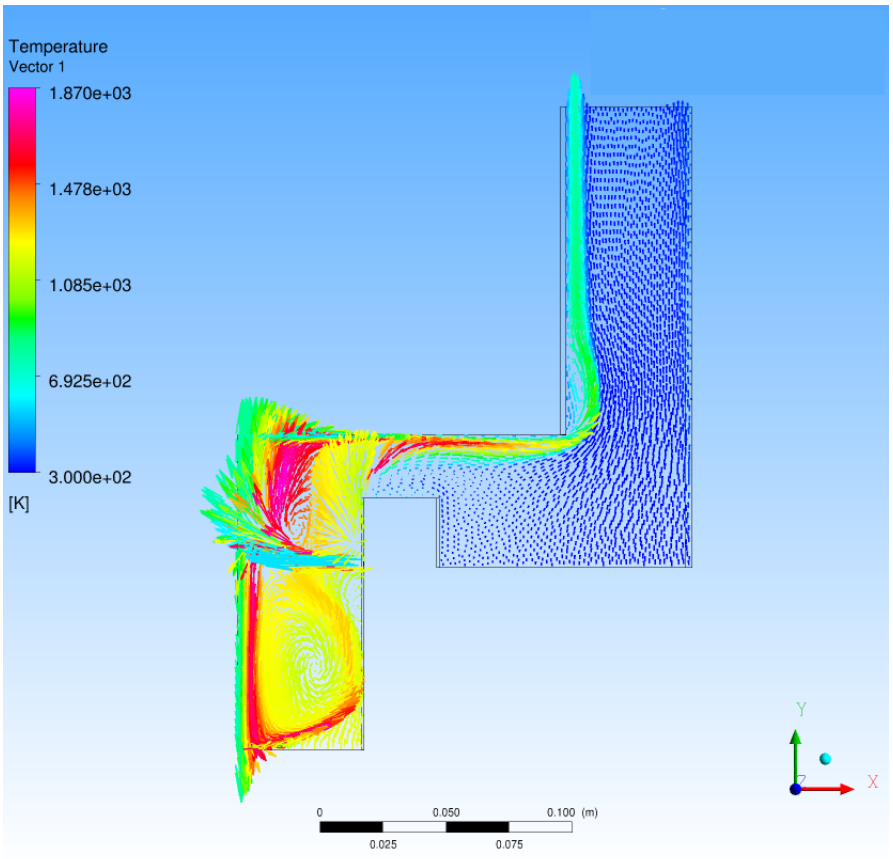

Figure 3.14: Vector plot of the recirculation zone - coloured with temperature

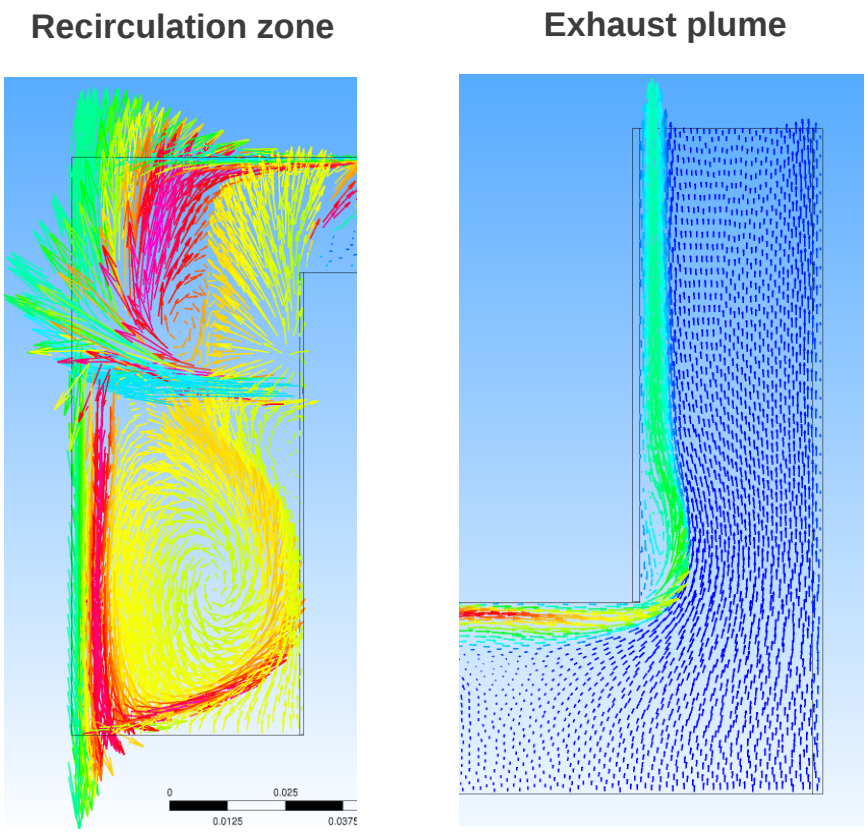

Figure 3.15: Recirculation zone and the exhaust plume from the stove

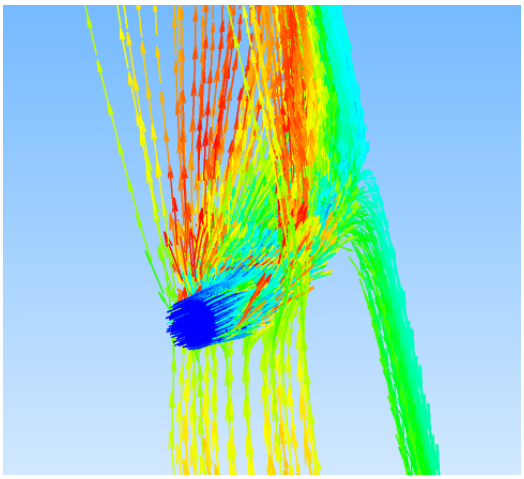

Figure 3.16: Wake region above the jet

Figure 3.17 shows temperature contours on a plane parallel to the air inlet direction located at a height such that it coincides with the centre of the jet. The high temperature zone indicates presence of flame in the jet shear layer, where the air and fuel mix and react.

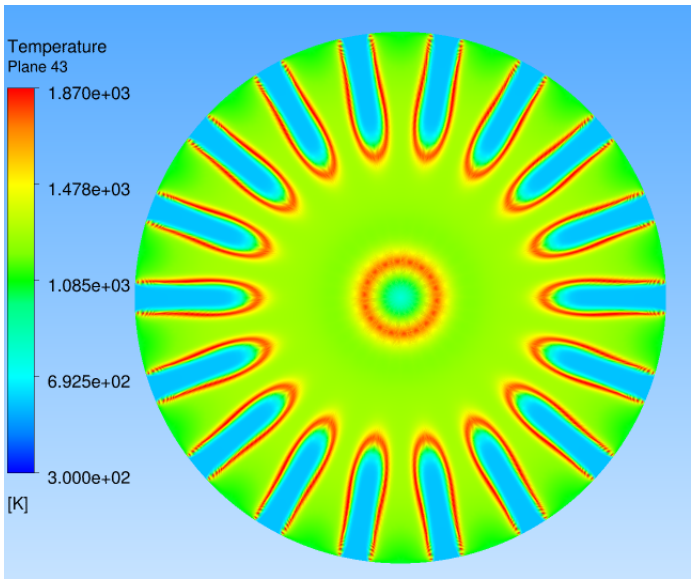

Figure 3.17: Temperature contour showing flame in the jet shear layer

Figure 3.18 presents a comparison between pictures of the flame takes frome xperiments and constructed from CFD calculations using volume rendering.

Figure 3.19 shows velocity field in the recirculation zone and below the vessel. Velocity close to the vessel surface is about 2 m/s near the centre and drops as radius increases. This is also clear from the grid independent stagnation point boundary layer profiles shown in Fig. 3.20 for different points along the vessel wall. From the plot (Fig. 3.20) it is inferred that the gradients are strong within 1-2 mm from the wall and decrease away from the stagnation point along the vessel wall. Therefore the heat flux is maximum near the stagnation point.

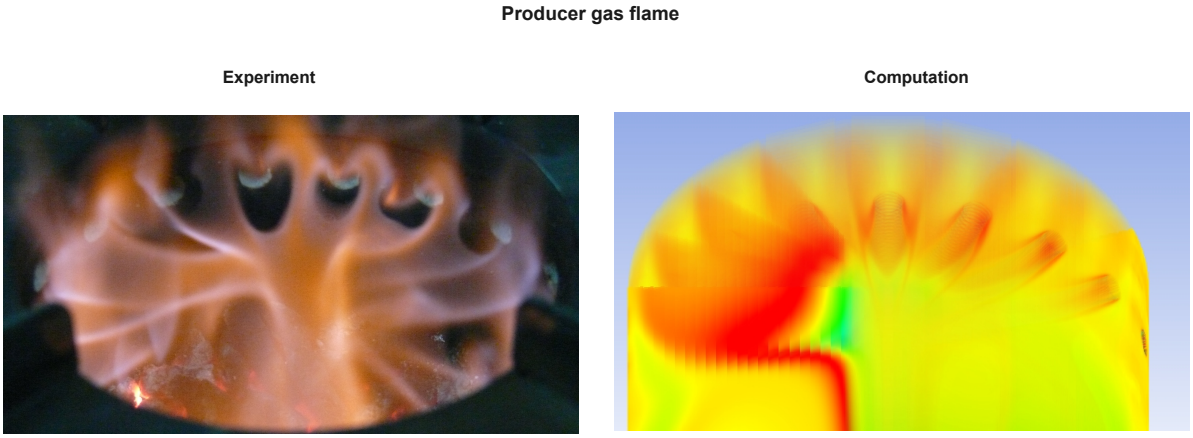

Figure 3.18: Left - photograph of producer gas flame from experiments. Right - 3-D flame picture constructed using volume rendering from CFD calculations. Important common features in the two pictures - combustion air entering as jets from the stove wall is seen. Visible thin flame in the jet shear layer is seen. Jet impingement leading to recirculation is also seen clearly.

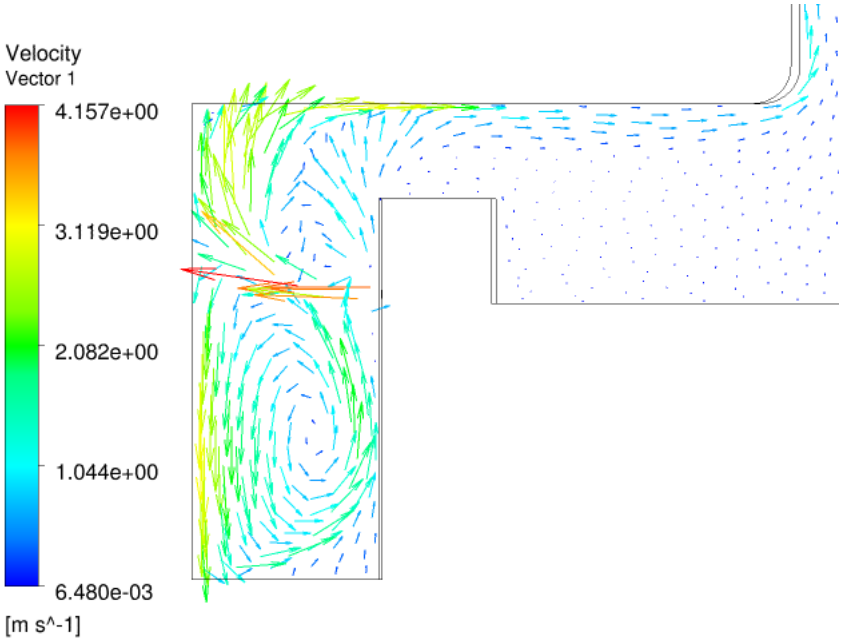

Figure 3.19: Velocity field in the stove

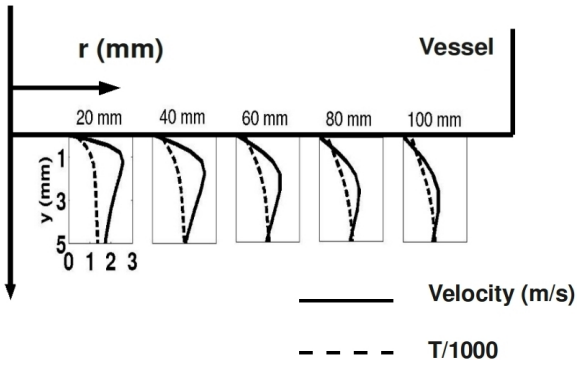

Figure 3.20: Stagnation point boundary layer profile

3.9.3 Heat transfer to vessel

The total heat transfer to the vessel up to radius r is given by eqn. 3.6. Fig. 3.21 shows the wall heat flux, the area of the vessel and the heat transferred to the vessel up to radius r as a function of radius of the vessel.

$$q = \int_0^r q'' 2\pi r dr \tag{3.6}$$

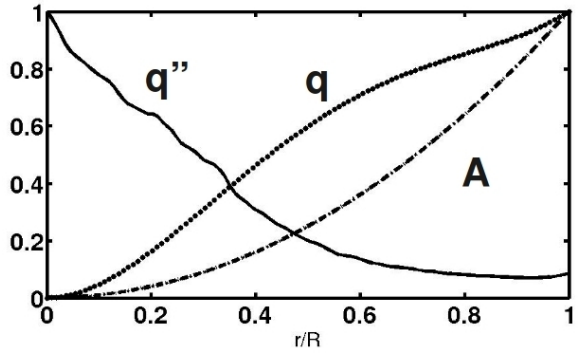

Figure 3.21: The variation of heat transfer along the radius of the vessel

Once the quantity $\dot{q}''$ is obtained the convective heat transfer efficiency can be obtained. The heat transferred to the vessel side wall was included into $\dot{q}$ for calculating η_{ht}. Computations were performed for vessels of 220, 260 and 320 mm diameter that are the kind of dimensions of practical cooking vessels determined from field studies. Table 3.11 presents the results of the computations.

Table 3.11: Efficiency

d_v (mm)	η_{ht} (%)
220	51.2
260	66.4
320	72.2

The results indicate better utilization of heat as the vessel size is increased. Introducing swirl is sometimes claimed to enhance the heat transfer to the vessel. Calculations done with 30° swirl showed marginal changes in the heat flux along the radius and on integration, the heat transferred to the vessel seemed unaffected by the swirl.

Radiation from hot char bed left over by the propagating flame front is an important component of heat transfer to the vessel and must be calculated for determining the flaming mode contribution to the overall efficiency, given by Eq. 3.7. The methodology used to determine η'_{rad} is explained below.

$$\eta'_{fla} = \eta_g \eta_{ht} + \eta'_{rad} \tag{3.7}$$

3.9.4 Radiation heat transfer efficiency (η_{rad})

The heat transfer from the hot char bed to the vessel was determined theoretically. The geometry used in the calculation is shown in Fig. 3.22.

To estimate the radiative heat transfer to the vessel from the char bed, the fraction of energy emitted by surface 1 intercepted by surface 3 is to be calculated. For this, the view factor F13 is required. For this geometry the view factors are known from standard charts provided by Incropera & Dewitt (1996) and is shown in Table 3.12.

Table 3.12: View Factors

L (mm)	F13
50	0.38
75	0.25
100	0.20

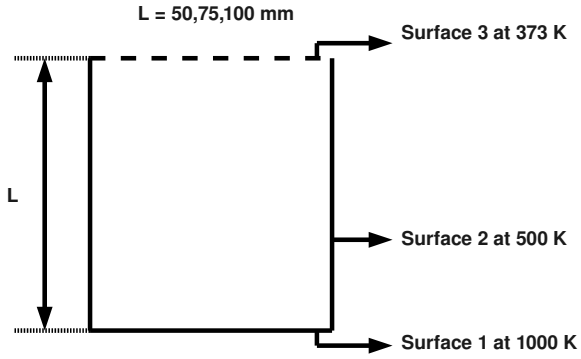

Figure 3.22: Model for theoretical prediction

Char was assumed to be a blackbody at 1000 K. The theoretical radiative heat transferred is calculated from flux intercepted by surface 3 using Eq. 3.8. The quantity $A1$ is the area of surface 3.

$$q_{rad} = 5.678 * 10^{-8} \times A1 \times F13 \times (1000^4 - 343^4) \tag{3.8}$$

Since the depth at which the char bed surface is located changes during stove operation, calculations were done for three different depths and the average was taken as the contribution of radiation from the char bed. The results are set out in Table 3.13.

Table 3.13: Radiative Heat Transfer

L (mm)	q_{rad} (W)
50	167
75	110
100	90

Average heat transfer rate is 122 W. This theoretical estimate was put to test using experiments. Instead of biomass loaded in the chamber, the chamber was sealed and evacuated using a vacuum pump to 550 mm of Hg below atmosphere. Base plate was maintained at 1000 $\pm$ 50 K and the heat transferred to water was calculated as before. Measured heat transfer rate was 160 W. This is slightly higher than the average number estimated from theory. In experiments there is a possibility

of other modes of heat transfer like natural convection and conduction (because of direct contact). Taking into account these factors the measured values are not very far from the theoretical values. Therefore from combination of experiments and theory the contribution of radiation to flaming mode efficiency was estimated to be about 4±0.5 % and therefore about 2.5±0.5 to the overall efficiency of the stove.

Now that all the components of the efficiency are determined, the overall efficiency picture is as shown in Table 3.14.

Table 3.14: Overall Efficiency

d_v (mm)	η_{ga} (%)	η_{ht} (%)	$\eta'^{*}_{fla} = \eta_{ga} \times \eta_{ht}$ (%)	η'^{*}_{rad} (%)	$\eta^{**,\#}_{fla}$ (%)
220	96	51.2	49.4	4	38
260	96	66.4	64.0	4	48
320	96	72.2	69.6	4	52

* - flaming mode energy input as the basis

** - total energy input as the basis

$^{\#}$ - radiation contribution of 2.5% included

3.9.5 Comparison with experiments

Computational results presented in Table 3.15 bring out the effect of vessel size on the heat extraction process. Vessel with 320 mm dia gives the highest efficiency amongst cases considered and demonstrates the importance of using vessels of appropriate sizes to obtain optimal efficiency.

Table 3.15: Vessel size effect - Experiment and CFD

d_v (mm)	η_{fla} Experiment* %	η_{fla} CFD %
220	33±2	38
260	40±2	48
320	45±2	52

*-cal value of biomass 16±0.5 MJ/kg

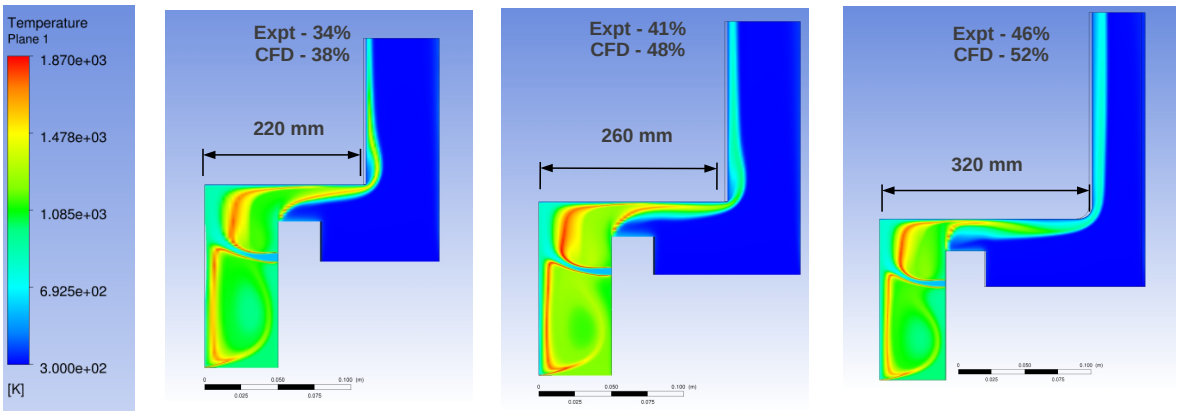

Figure 3.23: Effect of vessel size on heat extraction

Computational results over predict the efficiency by about 7%. This is related to the use of fast chemistry with only CO_2 and H_2O as the only products of combustion. This implies that the there are no CO emissions. But experiments show that 0.4 g of CO is emitted in the flaming mode for every MJ of energy input in the form of biomass. This brings up an important question - *'how far from fast chemistry assumption are the processes in the stove?'* One can expect that the peak temperature attained in the stove will be less compared to that in the fast chemistry calculations assuming complete conversion. The peak temperature is about 1870 K in the calculations assuming fast chemistry. Preliminary computation with finite rate chemistry shows a peak temperature of about 1730 K and a flaming mode efficiency contribution of $\sim$ 46%, a number within 2% of the experimental value. Therefore this difference of 140 K is thought responsible for the over prediction of efficiency by 5%.

Preliminary finite rate calculations show a CO emission of 0.5 g/MJ. This agrees well with the experimentally determined value of 0.4 g/MJ. Carbon-monoxide estimated from the equilibrium conditions corresponding to 1730 K indicates 0.02 g/MJ. This shows that the CO oxidation process in the stove is far from equilibrium and therefore kinetically controlled. Therefore a fast chemistry calculation appears reasonable for capturing the vessel size effects. A finite rate calculation is demanded to model precisely the CO oxidation and obtain efficiencies to within 2% of the experimental results. This work is currently being pursued and part of the future work.

3.9.6 Efficiency dependence on d_v/d_s

The effect of vessel size on heat extraction was brought out in the previous section. The results of Mukunda *et al.* (2010) are set out with additional results of 100 mm model stove with optimal R and those of larger stove in terms of the ratio of vessel diameter to the stove combustion chamber diameter in Fig. 3.24.

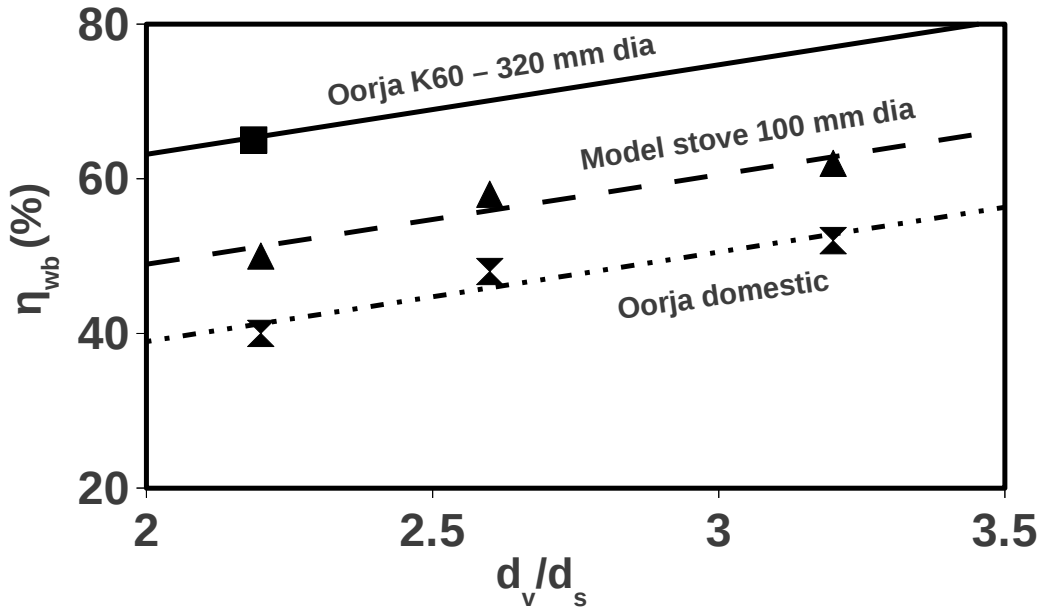

Figure 3.24: Variation of efficiency with vessel to stove diameter ratio. Data points - experimental results. Lines - linear fit

Efficiency increases nearly linear with ratio of vessel to stove dia. Efficiency of K60 for d_v/d_s of 2.2 is extrapolated using the slope determined from the Oorja and model stove data to $d_v/d_s = 3.2$. The efficiency thus estimated is 77%. Therefore, with optimal value for R in flaming and char mode and with vessel of appropriate sizes, it is possible to reach efficiencies as high as 77%, comparable to that of LPG stoves.

3.9.7 Effect of recirculation on A/F

The experimental fact that the stove cannot be operated on the lean side was brought out earlier (see Table 3.7). This was attributed to the increase in the intensity of recirculation caused by the increase of combustion air flow rate to attain lean conditions. To quantify this effect, computations were performed corresponding to conditions presented in second and fourth row of Table 3.7. Figure 3.25 and 3.26 show the convective heat and oxygen flux in the vertical direction calculated for the two cases. Oxygen flux plot is shown only up to a radius of 0.01 m because it is zero beyond that point. Also convective heat flux is shown only for the part where the transport is towards the bed.

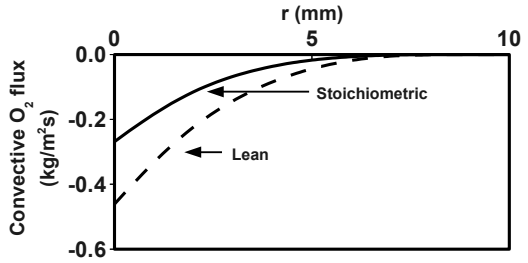

Figure 3.25: Convective oxygen flux towards the fuel bed for stoichiometric and lean cases

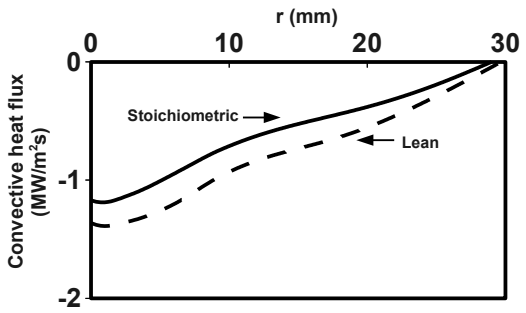

Figure 3.26: Convective heat flux towards the fuel bed for stoichiometric and lean cases

Both heat and oxygen transport to the fuel bed surface is enhanced because of the increase in combustion air flow rate. This leads to increase in the pyrolysis rate and restoration of stoichiometric operating conditions.

3.10 Ash fusion problem

As mentioned earlier, the problems of smoking at the transition from flaming to char mode and on occasions to ash fusion were the motivation for taking up this study. Biomass coming from agro-residues carries with it some potassium and sodium largely arising out of the use of fertilizers. The presence of potassium has been known to create ash fusion problems due to the reduction in ash fusion temperature (Bryers (1996)). It is useful to recognize that woody materials do not pose a serious concern in terms of ash fusion because very low ash content in the fuel. Further, additional problems are created because the process of collection brings with it mud and grit. These have led to pellets with ash content generally about 10%, but on occasions even up to 13 %. Operation of stoves at high ash fractions leads to a transition process from flaming to char mode in which the air-to-fuel ratio imbalance (the stoichiometric ratio increasing from about 6 to 11) leads to weak thermo-chemical conversion of char. This causes smoking. Once the char mode operation stabilizes, the presence of potassium in more-than-acceptable proportions can cause ash fusion because of the reduction in ash fusion temperature discussed earlier. Pursuing the issues at greater depth did not seem meaningful because the problems were sporadic in earlier stages and when the pick-up of mud and grit was minimized, the problems got reduced substantially. It is also to be recognized that ash fusion problem increases with V_{co}. Thus, operationally, it is desirable to limit the range of V_{co} to less than 16 cm/s. Larger V_{co} values help in increasing the propagation rate and limiting to values below this V_{co} help in reducing ash fusion problems.

Another factor that must be taken into account is the fact that flow velocities past the char particles increase because the presence of the grate implies reduced porosity. Hence, the recommendation has been to choose a grate with maximum acceptable porosity.

3.11 Energy Balance

Establishing energy balance which tracks the flow of energy from biomass through different processes like gasification, gas phase combustion, convective-radiative heat transfer to vessel, is one of the primary aims of this work. It is a valuable tool in examining possibilities to improve the stove performance. This problem has been

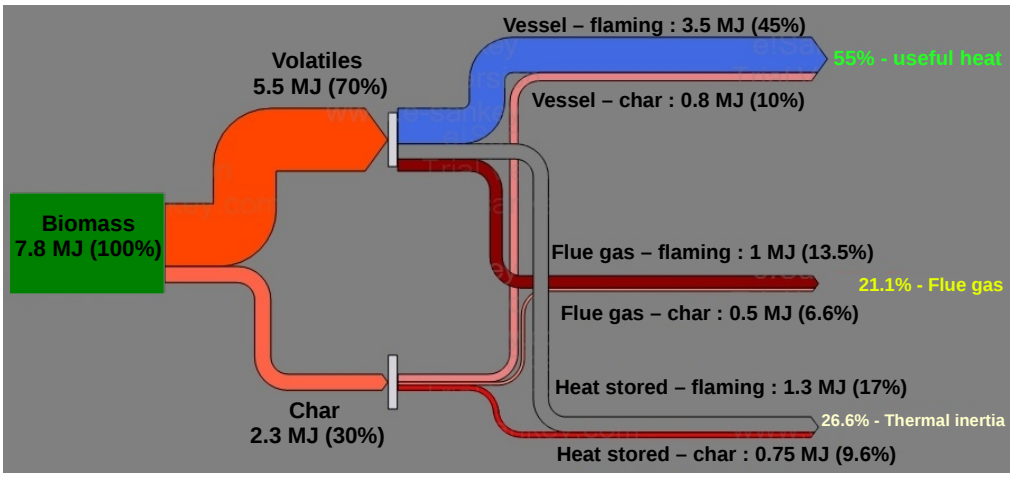

Figure 3.27: Energy balance on the stove

addressed in Sharma (1993); however, there are gaps in the energy balance to the extent of 40%. Figure 3.27 shows energy balance obtained from experiments and computations. Using the data from Table 3.9 for R = 2.9, a sample calculation is demonstrated. 600 g of pellets loaded into the stove contains 50 g moisture and 60 g ash. Therefore the total energy content of the fuel loaded is 7.8 MJ (490 g*16 kJ/g). Table 3.9 shows that 56 % of this total energy, i.e. 4.4 MJ is transferred to the vessel. 4.3 kg of flue gas with heat capacity 1100 J/kg K leaves the stove at an average temperature of 650 K as estimated from CFD calculations and measured in experiments. This accounts for 1.5 MJ i.e. 20% of the total energy. The stove walls along with 60 g of ash left at the end are together at around 600 K and the energy stored in this accounts for 20%. About 5% of total energy is lost to the surroundings by heat loss from the stove outer wall and this completes the energy balance with an uncertainty of 5%.

3.12 Summary

This chapter has presented a complete thermochemical evaluation of the reverse downdraft gasifier stove. Constancy of gasification A/F in the operating regime is established and the value is 1.5, optimal for obtaining gases of highest calorific value. Measured dry gas composition is used along with elemental balance to show that

the hot gas efficiency is about 96%. The system was compared with the classical downdraft gasifier to show that the hot gas efficiency is the same in both of them and the difference lies only in the split up between calorific value part and sensible enthalpy part. In stoves sensible enthalpy contributes 28% towards the gasification efficiency whereas in gasifiers it is just 14%. The chapter has also addressed issues that can help increase the utilization efficiency (water boiling efficiency) and combustion efficiency that helps reduce the CO emissions. Towards this, the components of the efficiency of the stove, namely, flaming and char mode, are established with experiments. The experiments have also shown that the stove cannot be operated in the lean regime and is attributed to the recirculation enhancement caused by increase in the combustion air flow. Modelling results are shown to support this observation. The difference in combustion dynamics between the flaming and char mode is brought out. A stove designed to operate with stoichiometric conditions in the flaming mode cannot do so in the char mode at the same flow conditions because these lead to extremely lean conditions in char mode operation; this is traced to the change in the fuel composition and hence the mass burn rate. This fact combined with fixed flow rates is shown to be the reason for char mode efficiency being one-third of flaming efficiency, leading to higher CO emissions. The ratio of combustion to gasification air flow rate (R) is about 5 for stoichiometric operation in the flaming mode and the value of R that leads to stoichiometric operation in the char mode is shown to be 1.9. Operating the stove with a R value of 5 in the flaming mode and 1.9 in the char mode leads to highest efficiency and lowest emissions. The value of R was implemented in the design of larger versions of the Oorja stoves, K30 and K60 and efficiencies as high as 65% and CO emissions of 0.4 g/MJ were obtained. These studies also provided crucial inputs with respect to appropriate power levels to increase the efficiency of the domestic version, Oorja 1.3, by an additional 5% - 10%.

The gas phase combustion and heat transfer processes were modelled to bring out the effect of vessel size on the heat extraction. A 320 mm dia vessel was shown to yield much higher efficiency on a 100 mm stove as compared to a 220 mm and 260 mm, elucidating the importance of vessels of appropriate size in obtaining high efficiency. The computational results agree well with the experimental results. Experimental and computational results were used to construct an energy balance for the stove to track the energy flow from biomass to the vessel, with an uncertainty

of just 5%.

Chapter 4

Biomass density effects on flaming and char mode

Chapter 3 dealt with the detailed thermo-chemical evaluation of the stove and aspects related to efficiency and CO emissions. Combustion-to-gasification air flow ratios required for optimal performance in flaming and char mode were determined. These experiments performed with wood chips (615 kg/m^3) and agro-residue pellets (1260 kg/m^3) revealed an interesting fact. Flaming mode dynamics, quantified by fuel mass burn rate and peak bed temperature, were same for wood and pellets. But the behaviour of char mode showed dependence on the biomass used, with particles of higher density showing higher mass burn rate and temperature. Visual observation also confirmed this fact and the difference in the combustion intensity in char mode is clear from Fig. 4.1. A large amount of data on practical stoves with pellets having ash content of 8 to 10 % showed char burn rates of 3 to 4 g/min and when run with wood pieces showed a char burn rate of 2 to 3 g/min. This chapter presents results of experimental and modelling studies aimed at resolving this problem.

Figure 4.1: Photographs of wood char combustion (left) and pellet char combustion (right) in the stove

4.1 Earlier work

In examining the relevance of earlier work seeking explanation for the above observations, it appeared that Evans & Emmons (1977) are perhaps the only researchers who have conducted a rigorous and thorough study of the combustion of wood chars of the kind typically used in domestic applications. The study has been on a one-dimensional stagnation point flow configuration and the measurements have included burn rate, surface temperature, and heat and mass transfer coefficients. The range of velocities is more than 5 m/s as there is extinction below this value. It is interesting and perhaps, remarkable that wood chars burn in one-dimensional spherical configuration at velocities as low as a few cm/s, a fact that is long known and well established (see for instance, Mukunda *et al.* (1984)). The reason for the difference lies in the observation by Evans & Emmons (1977) that the extinction begins by a heat loss at the edges. In a spherical configuration such an opportunity for heat loss is absent and hence combustion occurs even in the free convective mode at effective low velocities. While they have used a model for char combustion involving kinetics, large data of char spheres in conditions of the kind contemplated therein show that *the process is diffusion controlled* (Dasappa *et al.* (1994)). An examination of the experimental data with their curve-fit shows that the $p_{O_2,w}$ is between 1 to 5 %. Instead of the curve-fit $\dot{m}'' = 25.4 p_{O_2,w} e^{-9000/T}$ and an expression for $p_{O_2,w}$, the data lends itself to a simpler presentation based on the consideration of diffusion limitedness: $\dot{m}'' = 3.6 \times 10^{-6} Re^{0.5}$ and $\dot{m}'' = 4.7 \times 10^{-2} e^{-5180/T}$ with the Re based on char diameter. Issues of clear laminar-like behaviour for regression dependence on the flow even though inflow is turbulent has also been brought out by the investigators and needs considerations beyond the scope of this thesis. Experiments and modelling studies on single char spheres and packed bed have been made by Dasappa *et al.* (1998) and Dasappa & Paul (2001). These are related to the movement of air from the top of the particle bed downwards. Thunman & Leckner (2005) and Saastamoinen *et al.* (2000) have conducted studies on particle beds lit from the top with air flowing from the bottom, a configuration similar to the one considered here. Thunman & Leckner (2005) observe in their paper that *"..conversion rate of fixed biofuel bed, operated in counter-current mode, is not much affected by density. This is somewhat surprising since the conversion of the single particles constituting the bed could be expected to depend on their density"*. This is simply a

consequence of the surface boundary conditions in the conservation equations, that relate the mass flux from the surface to thermo-chemistry and fluid flow. Further, their studies have been conducted in a manner that does not distinguish between the char mode and flaming mode of functioning and hence the crucial aspects uncovered in the present work are missed out in their studies. This is partly related to the difference in nature of applications - their work is related to large scale combustor operations where in the fuel can be continuously fed from the top, whereas in the present work, it is related to domestic stove with the bed of a fixed amount and all the mass is expected to be consumed.

The modelling study on packed-bed of coal char particles by Cooper & Hallett (2000) makes a passing observation that char density does not affect the mass burn rate, a fact that is contradicted by the present data. Perhaps, their analysis did not focus on significant changes in the density of chars since they were concerned with coal char particles only. There are a number of modelling studies on single coal char particles (Makino & Law (2009), Yu & Zhang (2009), Lee *et al.* (1995), Phuoc & Annamalai (1999)) on ignition and steady combustion, but restricted to small sizes, less than a few mm.

From this it is clear that there is lack of experimental data for char bed gasification-combustion in the superficial velocity range of 3-6 cm/s, relevant to stove operation. Hence, in the present work, measurements of exit gas composition and bed temperatures are obtained in the V_s range of 3-6 cm/s and a detailed experimental analysis of the combustion of single char particles of wood and pellet under different ambient conditions is presented. A simple diffusion controlled combustion model is developed to explain the experimentally observed d^2 law and the similarity between wood char and pellet char combustion. The importance of including the effect of ash is also brought out. Finally the observed effect of density is shown to be related to the bed dynamics and not found in the combustion of single particles of different densities.

4.2 Experiments on packed bed

Experiments were conducted at air flow rates of 15, 20 and 25 g/min with wood chips of density 615 kg/m^3 and pellets of 1260 kg/m^3 with ash content of 1 % respectively. These experiments showed that flaming combustion occurred at the same rate of 10,

13.3 and 16.7 ± 0.5 g/min for all biomass considered, at 15, 20 and 25 g/min air flow rate respectively. However, the char combustion process initiated after 80 to 85 % mass consumption showed that wood char (360 kg/m^3) burnt at 2, 2.5 and 3.5 g/min and pellet char (990 kg/m^3) burnt at 2.6, 3.6 and 4 g/min respectively in the flow rate range chosen. An additional confirmation was obtained by using wood pieces of a higher density, 800 kg/m^3. This exhibited a behaviour for flaming mode same as for other biomass and a char consumption rate of 2.8 g/min at 20 g/min air flow rate, a result that lies in between those of wood and pellet char. Further experiments were restricted to low density wood and high density pellets.

4.2.1 Mass loss and bed temperature

Mass loss with time along with computed mass loss rate for 20 g/min gasification air flow rate is shown in Figure 4.2.

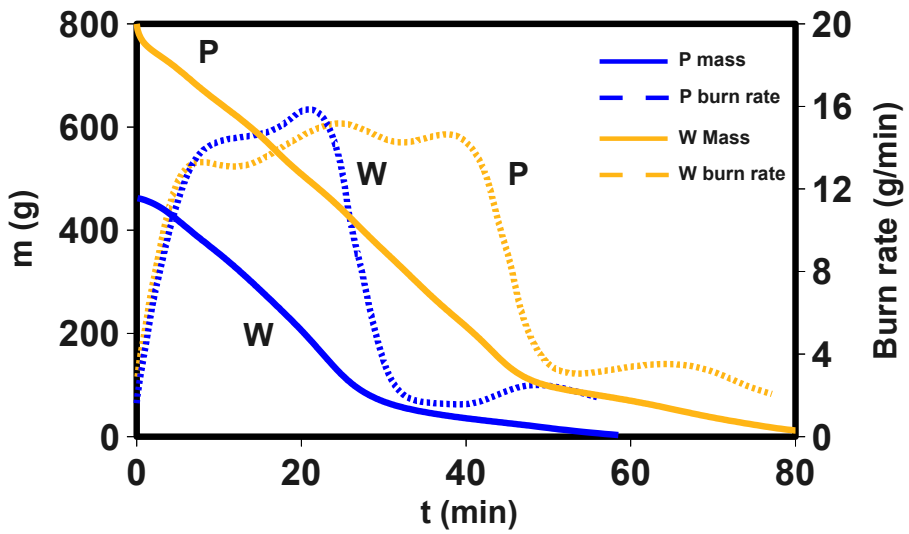

Figure 4.2: Mass with time and burn rate for wood (W) and pellets (P) for 20 g/min air gasification air flow rate in flaming and char mode

The temporal temperature profile as the flame front propagates through the bed for 20 g/min gasification air flow is shown in Fig. 4.3. The temperature plots (see Fig 4.3) clearly show the propagation of the reaction front through the packed bed. The important features are marked on the plot. The flame front reaches the

thermocouples W2 and P2 located 30 *mm* above the grate first at 900 and 1800 s respectively. The short peaks seen at this time are related to the location of the oxidative pyrolysis zone. The immediate dip in the profile is related to the reduction process (leading to gasification). One particular feature which needs attention is that W1 which does not show a dip like other thermocouples. The flame front reaches thermocouples W1 and P1 after about 285 and 450 s respectively from W2 and P2. This gives a local propagation rate of 245 $\pm$ 30 and 134 $\pm$ 25 *mm*/hr for wood and pellets respectively. The extraction of mean values from experimental data lead to 220 and 127 *mm*/hr respectively. The inaccuracy in local propagation measurement has been traced to particle movements in the bed close to the thermocouple. Perhaps, these issues may have led Thunman & Leckner (2005) to their results that show wide variations in air-to-fuel ratio in the gasification mode, something not found in earlier work and not easy to justify.

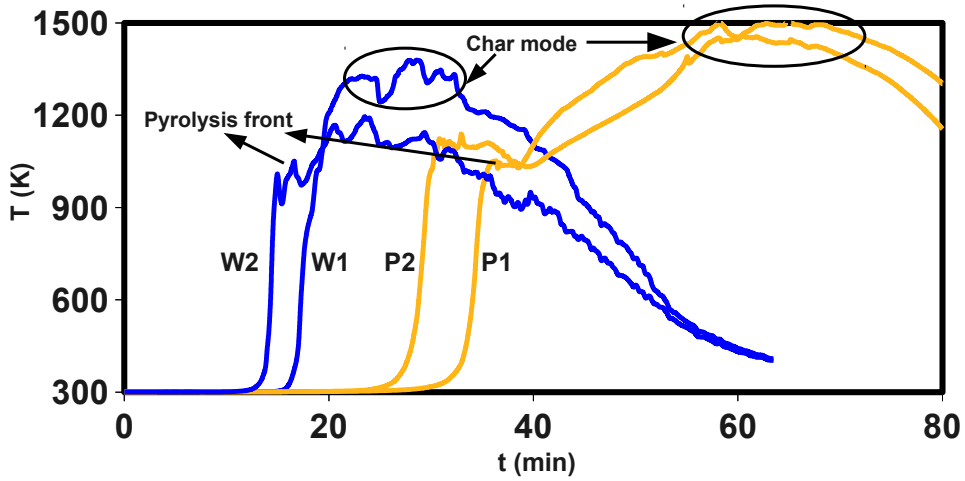

Figure 4.3: Bed temperature profiles at 20 g/min gasification air flow. Thermocouples W1, W2 and P1, P2 refer to wood and pellets positioned 10 *mm* and 30 *mm* above the grate

Mass burn rates and peak bed temperatures for all the three flow rates are compiled in Table 4.1. The data clearly shows the similarity of the flaming mode and the differences in the char mode.

Table 4.1: Mass burn rate and peak bed temperatures in flaming and char mode

V_{ga} (g/min)	$\dot{m}_{fla}$ (g/min)	T_{fla} (K)	$\dot{m}_{char}$ (g/min)	T_{char} (K)
Wood				
15	10.1	1027	2	1361
20	13.3	1065	2.7	1380
25	16.7	1093	3.7	1436
Pellets				
15	10.3	1042	2.4	1408
20	13.5	1099	3.6	1502
25	16.6	1120	4.2	$>1533^{\#}$

4.2.2 Exit gas composition

Figures 4.4 and 4.5 shows the gas composition measured during the operation of the reactor at 20 g/min gas flow air flow for wood and pellets.

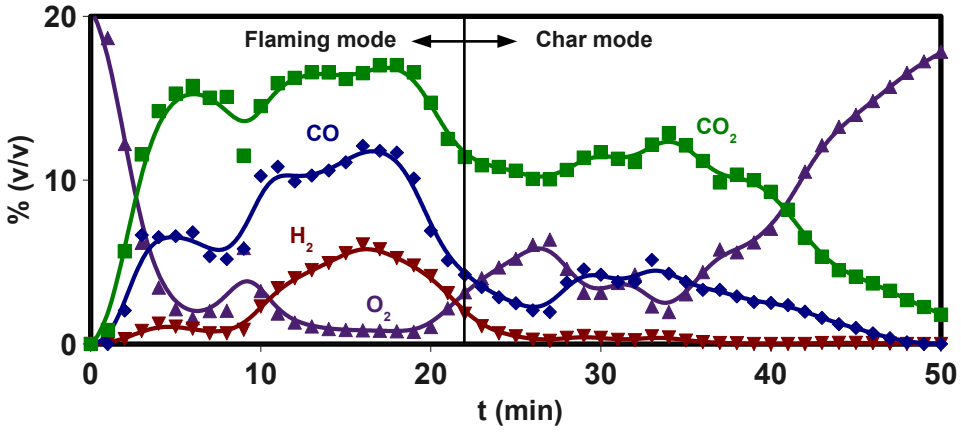

Figure 4.4: Exit gas composition for wood char bed at 20 g/min gasification air flow

Though the flaming mode shows differences in the variation of composition between wood and pellets, char mode shows up serious differences. In the char mode that begins after about 25 mins for the case of wood chips and 30 mins for pellets, the fraction of CO in the gas is 5-10% more in the case of pellets and this is clearly responsible for a prominent pale blue flame on top of the pellet char bed; however,

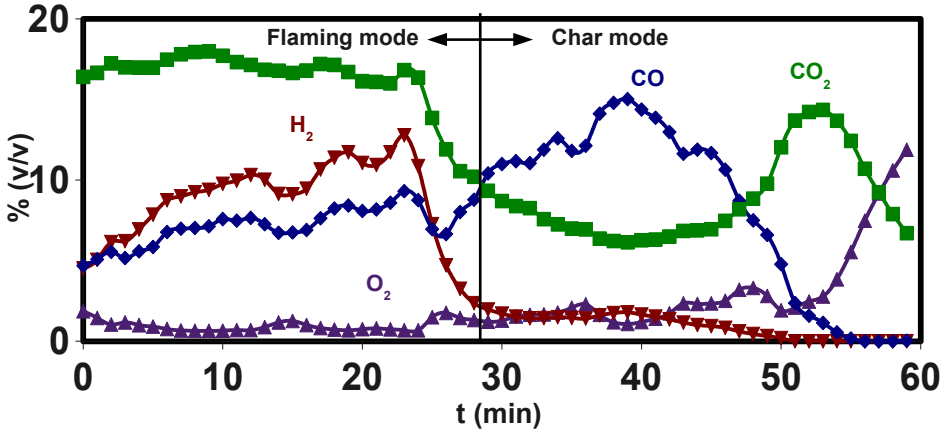

Figure 4.5: Exit gas composition for pellet char bed at 20 g/min gasification air flow

in the case of wood it is much weaker (see Fig. 4.1). The oxygen fraction in the case of wood char increases from near 0 at the time the volatile combustion is completed to ambient mole fractions nearly linearly up till the end, whereas in the case of pellet char it remains near 0 till the end. This implies that the wood chip char bed is too porous to intersect and consume all the oxygen in the air stream. Since the oxidation reactions are diffusion controlled, this result explains the difference in the char burn rates between wood and pellets.

Even though these experimental facts explain the differences between wood and pellet char beds, it is not clear whether these effects are just because of the differences in the bed properties (bed porosity and bed density) or *the way single char particles burn differently*. To understand these effects, experiments were conducted on single particles under different conditions and these are discussed in the following section.

4.3 Experiments on single particles

Wood spheres in the diameter range of 10-12 mm (615 kg/m^3) and pellet cylinders of diameter 8 mm and length 15 mm (1260 kg/m^3) were mounted on a fine needle and placed on a weighing balance with a precision of 1 mg. The particles were ignited with a LPG flame. Wood spheres take 10-15 s to ignite and pellet cylinders about 25 s. Pellets take more time to ignite because of high thermal inertia compared to wood (see for instance, Quintiere (2006)). Mass loss with time was continuously

acquired by interfacing the balance with a data acquisition system and a typical mass loss with time plot is shown in Fig. 4.6.

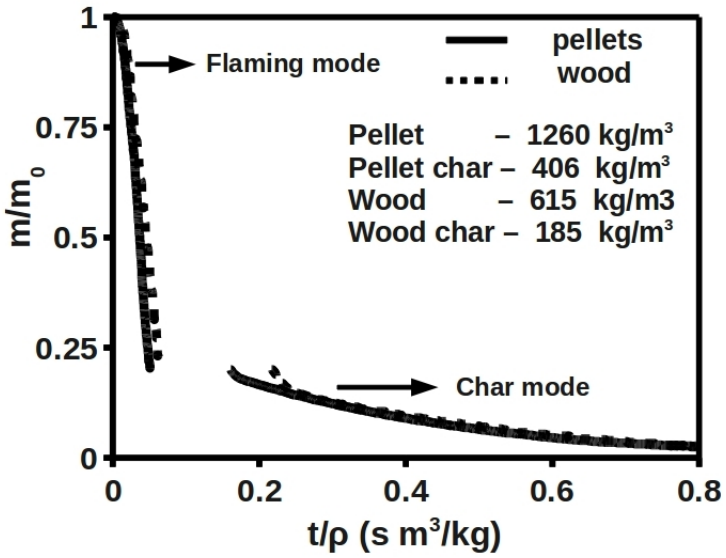

Figure 4.6: Mass loss with time for a wood and pellet under ambient conditions - time axis scaled with densities of corresponding particles

Similar to a packed bed, single particles also show two distinct modes of combustion, namely, flaming and char mode. Note the mass is scaled by the initial mass and burn time with densities of the particles in the corresponding modes. The break in the plot is because of the difference in densities between a virgin biomass particle and its corresponding char (see Table 4.2).

Table 4.2: Volatile fraction of fuel and Char properties

Item	Wood sphere	Pellet cylinder
Density, kg/m^3	615	1260
Size, *mm*	11.5 dia	8 dia, 15 length
Volatile fraction %	87	81
Char density, kg/m^3	185	406
Char Size, *mm*	10 dia	7 dia, 13.7 length

It is clear that both pellets and wood behave the same way in flaming as well as char mode. Therefore single particle behaviour in flaming and char mode is independent of particle density and the fact that surface heat flux balance is responsible

for this kind of behaviour is clearly demonstrated by this simple experiment. Since the experiments focus on determining the effect of ambient temperature and stream speed on the char particles, all the particles were lit under ambient conditions (300 K) and were allowed to burn in the flaming mode under ambient conditions, to ensure uniform initial condition for the char combustion. Once all the volatiles are consumed and the particle enters the char mode, the conditions were changed appropriately by introducing streams of different velocities and temperatures. The surface and the core temperature of the particles were measured using a 100 μm R-type thermocouple, by placing one pressed against the surface and one at the center through a 400 μm hole. To determine the properties of the fuel and the char obtained, a few of them were quenched after the flaming mode by passing N_2. Both wood and pellets shrink from their original dimensions. The properties are shown in Table 4.2. Experiments were also conducted on wood spheres of larger and smaller diameters at ambient conditions to specifically evaluate the Grashoff number effect.

It was observed that the ash layer builds up on the glowing particle and is retained throughout the burn duration. The ash layer appears porous for wood and dense for pellets, these features consistent with their structure; the natural cell construction in wood looses the contents and makes the structure more porous (see for instance, Dasappa *et al.* (1998)). The pellets have no organized structure and hence such a structural change is not obtained. This ash layer is retained in all the cases studied here. Exploring the region of stream speeds at which the ash layer is blown away showed the lower limit as 3 m/s, which is much above the velocities encountered in the stove operation.

4.3.1 Burn times and surface temperatures

The different conditions used, and the burn times measured are shown in Table 4.3. The choice of low velocities is consistent with the velocities encountered by the particle in the stoves, where the velocities are small to ensure little ash particle carry over from the stove.

Table 4.3: Burn time and surface temperature of wood and pellet char particles, m = measured; other temperatures estimated

d	V	T_0	t_b	T_{si}	t_b, model
mm	m/s	K	s	K	s
Wood spheres					
10.0	0	300	255	983 (m)	240 to 260
10.0	0.06	300	243	1003	
10.2	0.1	300	246	1005	235 to 255
10.5	0.15	300	262	1023 (m)	
9.0	0.04	400	190	1033	
9.0	0.08	400	183	1038	
9.0	0.13	400	176	1040 (m)	180 to 190
Pellet char,					
10.0	0	300	556	983 (m)	
10.0	0.06	300	530	1003	
10.0	0.09	300	500	1005	
10.0	0.15	300	490	1025 (m)	
9.0	0.04	400	419	1033	
9.0	0.08	400	392	1038	
9.0	0.113	400	366	1044 (m)	

Some experiments made at ambient conditions with wood spheres of 6.6, 6.8, 11.5, 14.9 mm, scaled with Grashoff number as $t_b/\rho_{char} = 0.064 \times Gr^{0.25}$ where $Gr = 223 \times 10^9 d_s^3$ with t_b in s, d_s in m, ρ_{char} in kg/m^3. For a 11.5 mm wood sphere (leading to 10 mm char sphere), the burn time is 255 s.

4.3.2 d^2 behaviour

Seeking confirmation of the diffusion controlled behaviour of char combustion, the data on char diameter for wood and equivalent diameter for pellet char are presented in Fig. 4.7. The time is normalized with initial char density from Table 4.2 accounting for the differences between wood and pellet char.

The variation shows a sharper drop of d^2 in the initial phase before joining the d^2 slope. This is due to the transition from flaming to char mode. As soon as the

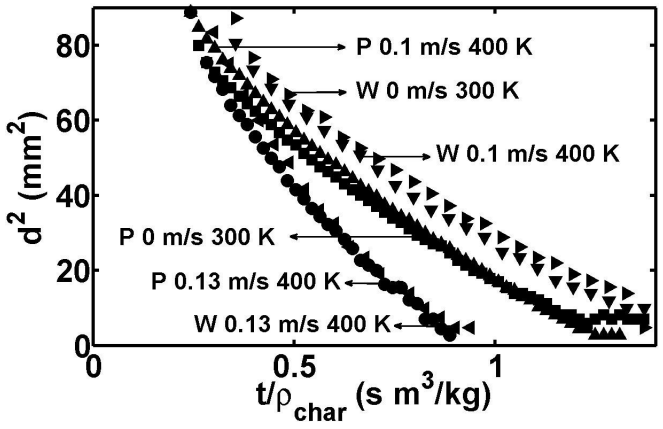

Figure 4.7: The variation of d^2 vs t/ρ_{char} for wood and pellet char with different air stream velocity and temperatures

gaseous flame extinguishes, the surface moves from 823 K to about 1050 K at which stage there is a sharp drop to 973 K (see Fig. 4.8). This is a transient process during which the ash forms on the surface; also the radiant heat loss from the surface drops sharply and settles down to a relatively slow drop rate due to increasing ash layer thickness. Beyond this transient process, the data show the linearity of d^2 vs. time behaviour.

Figure 4.8 shows the variation of the measured surface temperature of wood and pellet chars during the burn process at ambient temperature and under quiescent conditions with the time. The plot clearly shows that both the surface temperatures are the same at 973 K; The measured core temperature (not shown here) shows a similar trend with temperatures 50-60 K less than the surface temperature in the char mode. Further, the burn times shown scale with the char density. Also plotted are the outer surface temperatures corresponding to the ash layer with time. It is clear from the plot that the ash temperature drops linearly with time.

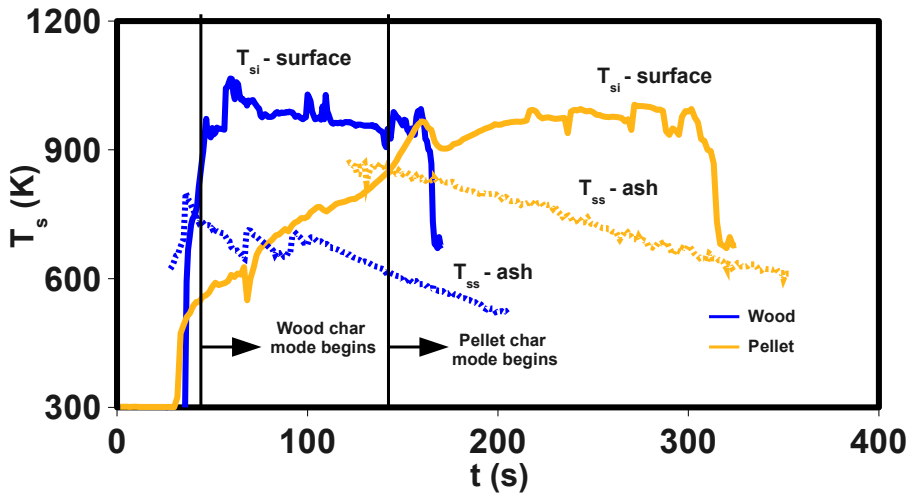

Figure 4.8: The variation of T_{si}, the surface temperature of the regressing char combustion surface, T_{ss}, the surface temperature of the ash layer with time for wood and pellet chars

4.4 Model for single particle combustion

The evolution of the model is dependent on the observation of ash build-up on wood (Glassman (1987)) and char spheres that seems to be retained largely. In this process, the surface becomes whitish with ash such that the effective temperatures at which it radiates is much lower than the red hot surface that can be seen through the porous ash layer. In the current problem the presence of the ash layer is imperative, as otherwise the radiant heat loss experienced at the kind of temperatures - 973 K or more is such that the char combustion cannot occur. Even if the ash layer is removed physically, the char oxidation creates immediately an ash layer reducing the heat loss from the surface. In addition, increased ash layer thickness implies lower emissivity; both the reduced temperature and emissivity combine to make radiant heat loss small in comparison to convective heat transport. A convective balance is drawn at the surface of the ash layer. The present model does not include the few seconds when the ash layer would be getting formed. The heat balance at the receding surface is given by

$$\rho_{char} c_{pchar} \dot{r} (T_{si} - T_c) = \dot{q}_s'' \tag{4.1}$$

Where $\dot{r}$ is the surface regression rate, T_{si} is the temperature at the reaction surface that is receding, T_c is the core temperature and $\dot{q}_s''$ includes the heat generated from surface reaction and the gas phase heat transfer flux due to free and forced convection at the reacting surface as well as heat loss due to radiation. Making use of the result of diffusion limited reaction derived from the experimental data and also supported by earlier work (Mukunda *et al.* (1984), Dasappa *et al.* (1994), Dasappa *et al.* (1998), Mukunda *et al.* (2007)) it can be written as

$$\dot{q}_s'' = D\rho \frac{H}{s} \left[\frac{dY_{ox}}{dr}\right]_{r=r_{si}^+} - k \left[\frac{dT}{dr}\right]_{r=r_{si}^+} - \epsilon\sigma(T_{ss}^4 - T_0^4) \tag{4.2}$$

where the first term on the right hand side is due to C-O_2 reaction and the second term is due to conductive heat transfer at the radius $r = r_{si}$, the surface radius (d_{si} = 2 r_{si}). The radiant loss term is based on the outer surface temperature, T_{ss}. The outer surface diameter is fixed at d_{ss}. ($d_{ss} = 2r_{ss}$)

We use the idea of classical boundary layer and rewrite the results as

$$\dot{q}_s'' = D\rho \frac{H}{s} \frac{Y_{ox,0}}{\delta_{ffc} + \delta_{ash}} - \frac{k}{c_p} \frac{c_p(T_{si} - T_0)}{\delta_{ffc} + \delta_{ash}} - \epsilon\sigma(T_{ss}^4 - T_0^4) \tag{4.3}$$

Where H is the heat released due to C - O_2 reaction, $Y_{ox,0}$ is the free stream oxidizer fraction = 0.232 in the present experiments, δ_{ffc} is the boundary layer thickness due to free and forced convection, δ_{ash} is the ash layer thickness. We invoke $D\rho = k/c_p$ and the transfer number B as

$$B = \frac{HY_{ox,0}}{sc_p(T_{si} - T_0)} \tag{4.4}$$

We can now write the flux equation as

$$\dot{q}''_s = \frac{k}{c_p d_{ss}}(B-1)\frac{c_p(T_{si} - T_0)}{\delta_{ffc}/d_{ss} + \delta_{ash}/d_{ss}} - \epsilon\sigma(T_{ss}^4 - T_0^4) \tag{4.5}$$

The balance equation can also be written as

$$\frac{\rho_{char}\dot{r}d_{ss}c_{pchar}}{k} = C_2\frac{(T_{si} - T_0)}{(T_{si} - T_c)}\frac{(B-1)}{\delta_{ffc}/d_{ss} + C_1\delta_{ash}/d_{ss}} - \frac{\epsilon\sigma(T_{ss}^4 - T_0^4)d_{ss}}{k(T_{si} - T_c)} \tag{4.6}$$

It can be noted that the left hand side is essentially a regression Reynolds number (we take that $\mu = k/c_p$) that is obtained from a balance of heat release, convective and radiative fluxes. The constants C_1 and C_2 are invoked due to lack of understanding of the precise extent of thermal diffusional resistance as a function of ash thickness. They need to be chosen to fit at least one set of experimental data.

$$\frac{d_{ss}}{\delta_{ffc}} = Nu = \frac{Nu}{Nu_0}Nu_0 \tag{4.7}$$

Based on the earlier work Mukunda *et al.* (2007), the correlations can be set as

$$\frac{Nu}{Nu_0}(B-1) = 0.7B^{0.75} \text{ and } \mathrm{Nu_0} = 2 + 0.3\mathrm{Re}^{0.5} + 0.7\mathrm{Gr}^{0.25} \tag{4.8}$$

The ash layer thickness is simply $\delta_{ash} = \int \dot{r}dt$. Connecting the temperature T_{ss} with T_{si} requires the solution of the conduction problem of the spherical region bounded by $r = r_{ss}$ and $r_s - \int \dot{r}dt$. While a conduction analysis with a fixed boundary temperature T_{si} at $r = r_{si}$ and a flux condition at $r = r_{ss}$ can be used to get the temperature profile a simple relationship for T_{ss} is assumed due to uncertainties in the heat transfer processes in the porous ash layer,

$$\frac{T_{si} - T_{ss}}{T_{si} - T_0} = \frac{\int_0^t \dot{r}dt}{r_{ss}} \tag{4.9}$$

This model has been run for several cases of wood and pellet char particles with the following data - H = 32 MJ/kg (assuming C $\rightarrow$ CO_2, see Evans & Emmons (1977), Scala (2009)), s = 2.67, $Y_{ox,0}$ = 0.232, c_p = 1000 J/kg K, and $c_{p,char}$ = 700 J/kg K. The calculated B from these and other data from earlier tables varies between 4.19 to 4.44 for various cases. The effect of transfer number can be expected to be very small. This was confirmed from specific experiments (not described here) in which single wood char spheres were burnt in a furnace at temperatures from 300 to 600 K with little variation in burn time. In the model T_{si} is set at 973 K and T_{ss} is taken to decrease linearly with time. The emissivity is taken to reduce from 0.85 to about 0.02 exponentially in about 15 s. The results of the calculation are set out in Table 4.3. A range of values is shown against predictions. It was not the aim to fix the choice of parameters to get the desired result, but to examine if some chosen set of reasonable parameters will allow predictions in a reasonable range. The constants C_1 and C_2 are chosen as 15 and 0.1. A 10% change, each in C1 and C2 leads to a 9% change in burn time; 1% change in T_{ss} changes the burn time by 2.5%. Fig. 4.9 shows the plot of various fluxes in the burn duration and the variation of d^2 with time.

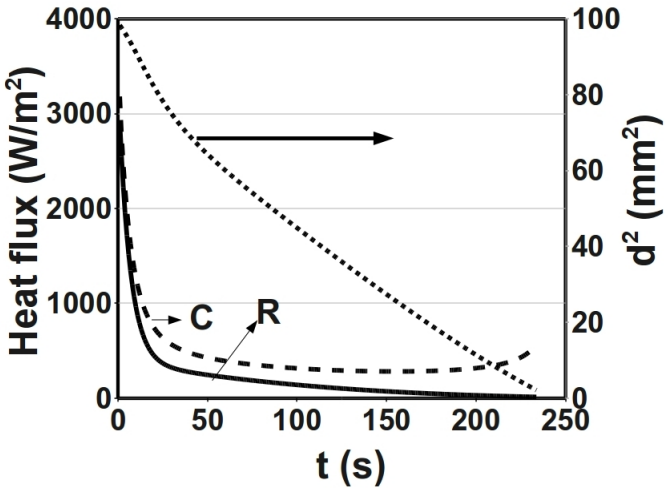

Figure 4.9: Convective and Radiative flux in ambient conditions with d^2 variation with time

The plot clearly shows two slopes for the d^2 variation with time. The initial higher slope is associated with the dynamics before the formation of the ash layer and the correspondingly high convective and radiative fluxes. The second part shows

lower value for the slope and clearly indicates the role played by the ash layer in bringing down the fluxes and increasing the burn time significantly. If the dynamics of the ash layer is not included then the wood sphere of 10 mm diameter will burn in about 27 seconds with d^2 showing a perfect linearity with time if we neglect radiative loss. Even if the radiative loss is incorporated, without the ash layer the model will be very sensitive to chosen parameters and burn times of the order determined in the experiments cannot be explained with such a model. Hence this model which includes the role of ash is close to realistic conditions experienced by the sphere.

4.5 A simple correlation for single particles

Seeking a correlation of the data in terms of known scaling features was attempted. The burn time, t_b (s) scales with char density and diameter as $\rho_{char} d_s^2$, with ρ_{char} in kg/m^3 and d_s in m. It depends on the heat transfer characteristics controlled by forced and free convection. These are represented by a quantity $Re^{0.5}/Gr^{0.25}$. Figure 4.10 shows that the data is well correlated (Eqn.4.10) and the kind of scaling clearly emphasizing the fact that the phenomena is transport controlled.

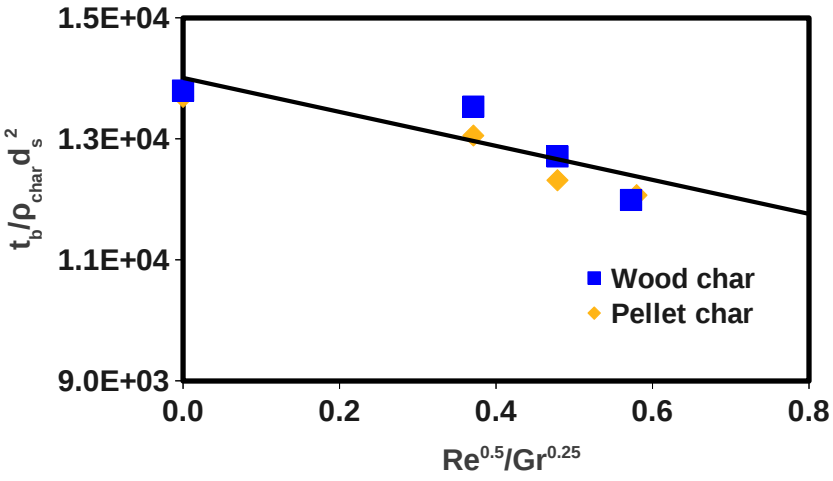

Figure 4.10: The normalized burn time, $t_b/(\rho_{char} d_s^2)$ with $Re^{0.5}/Gr^{0.25}$

$$\frac{t_b}{\rho_{char} d_s^2} = 1.38 \times 10^4 (1 - 0.19 Re^{0.5}/Gr^{0.25}) \tag{4.10}$$

From these set of experiments and modelling, it is clear that the single particles behave in a similar way. Therefore the explanation for higher burn rates in the char bed lies in the fact that the bed properties are different for wood and pellets.

4.6 Bed operation

The bed operation is controlled by the air stream speed past the particles in the bed. Further, each particle sees other particles in close proximity, much closer in the case of pellet char than in wood char. The properties of the char bed at the time it enters into char mode of combustion is presented in Table 4.4. Single particles of wood and pellets under ambient conditions burn with a mass loss rate of 0.1 g/min. In a bed the wood char consumption rate is 2.5 ± 0.5 g/min and pellet consumption rate is 3.5 ± 0.5 g/min. Equivalent consumption in bed per particle is 0.16 g/min for wood and 0.23 g/min for pellets. Convection combined with reduced radiation loss in the bed compared to single particles is responsible for higher burn rates in the bed. Also the heat release rate per unit combustor volume is lower for wood char bed compared to pellet char bed as is evident from the fact that packing density of pellet char bed is 38 % higher than that of wood char bed. At the same air flow rate this difference is because, closely packed pellet char particles see each other in close proximity than wood char particles leading to less radiation loss. This leads to higher surface temperatures (T_{si}) for pellet char compared to wood char (see Fig. 4.3) leads to better thermal environment for the pellet char operation. Bed temperature is an important parameter in diffusion controlled regime here because it determines the dynamics of radiation heat transfer in the bed. The radiation loss in wood char bed is intermediate between single particle combustion and dense pellet char bed. These enable higher combustion rates in pellet bed compared to wood char bed. Establishing the precise magnitudes calls for modelling the char bed operation, a subject for future study.

Table 4.4: Char bed properties

Item	Wood char	Pellet char
Char bed depth, mm	51	76
Mass of char bed, g	55	105
Bed Density, kg/m^3	110	176

4.7 Summary

Noting the significant difference in char burn rates between wood and pellet char particles in a packed bed used as a part of a domestic biomass based stove, the work on single particles was undertaken. This has shown that mass burn rates are the same; the linear burn rates scale as the density. The regressing surface temperatures are the same. The combustion behaviour obeys the d^2 law after an initial period region of adjustment.

Modelling the combustion behaviour of the single char particles shows that the ash layer that naturally forms on the surface during the combustion process is essential to explain the burn behaviour. Experimental data on the core, regressing surface as well as the outer ash surface with time are used as an important input for the model aimed at explaining the combustion behaviour. The scaling of burn time with density and d_s^2 and the relative independence with regard to ambient temperature (B effect) are condensed into a correlation with fluid flow variables - the Reynolds and Grashoff number as $t_b/\rho_{char}d_s^2 = 1.38 \times 10^4(1 - 0.19Re^{0.5}/Gr^{0.25})$.

Explaining the differences of bed combustion behaviour needs the observation that the bed densities are much higher for pellet char in comparison to wood char with significant heat release rate differences (of a factor of 1.6). This difference allows much higher adiabaticity in the functioning of a pellet char compared to wood char in the stove and hence the differences in the burn rates. While modelling approach outlined here captures the combustion behaviour of single char particles properly, there is need to extend this understanding to the combustion behaviour in a bed.

Chapter 5

Universal flame propagation behaviour in a packed bed of biomass

Chapter 3 and 4 dealt in detail with flaming and char mode dynamics of reverse downdraft (TLUD) system operating in the superficial velocity range of 3-6 cm/s, a range which offers favourable operating conditions for stoves. Other packed bed systems like gasifiers and moving grate boilers operate at a superficial velocity range of 10-15 cm/s and beyond 15 cm/s respectively. A detailed review of relevant literature on counter-current packed bed gasification-combustion, presented in Section 1.5, revealed the existence of conflicting perceptions on the propagation of flame front through the bed.

In order to resolve the conflicting perceptions of the bed behavior and establish the true picture of the behavior, experimental studies have been conducted to determine the propagation rate, fuel consumption rate, bed temperature and exit gas composition. Fuel consumption rate and bed temperature taken from literature for about fourteen biomass of various sizes, shapes, ash, moisture content etc., were put together along with the experimental results of the current study to seek an unified explanation. In addition to this, gas phase and condensed phase temperatures along with reaction front thickness and oxygen drop across the propagating flame front from experiments on transparent reactor are also obtained. A composite picture of the thermo-chemical behavior of the bed has been constructed; this shows that the behavior is substantially close to one presented by Fatehi & Kaviany (1994). Some exceptional features are also brought out. The propagation rate variation with superficial velocity is shown to follow a universal trend irrespective of the biomass used. A simple model is developed to capture the observed universal behaviour and inclusion of ash effect is shown to play a critical role in modulating the radiative

heat transfer from flame front to the fresh biomass.

5.1 Compiled propagation rate

Figure 5.1 shows the propagation rate for sixteen types of biomass obtained from literature along with the experimental results of the current work.

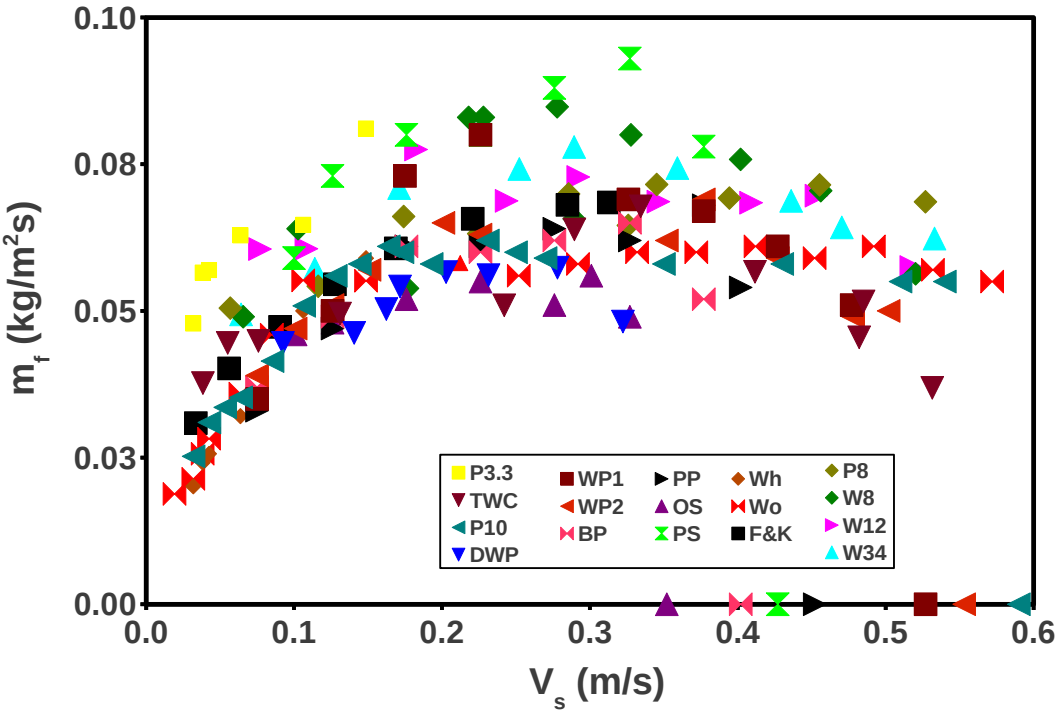

Figure 5.1: Fuel consumption rate ($m_f = \rho_p \dot{r}$) with air superficial velocity. P3.3 - pellets (3.3% ash), P10 - pellets (10% ash), Wh - wheat, Wo - wood, from current work. WP1, WP2, BP, PP, OS, PS - Porteiro *et al.* (2010*a*). F&K - Fatehi & Kaviany (1994), P8 - pellets 8 mm, W8, W12, W34 - wood 8 mm, 12 mm, 34 mm - Ronnback *et al.* (2001). DWP - digester waste pellets - Gnanendra *et al.* (2012). TWC - Harttanainen *et al.* (2002)

The data shows an universal trend: if we allow for experimental uncertainties including the moisture content totalling to about 5 %, it appears that the plot can be taken to be represented by a single curve with propagation rate increasing with superficial velocity up to about 16 cm/s and then saturates. But this data

required correction because of two issues, one related to the fuel consumption rate measurement method and other related to the variation in the ash and moisture fraction of the fuel used. These issues are explained in the following paragraphs.

5.1.1 Mass loss measurement method

An important point to be emphasized is that in the current study $\dot{r}$ measurements are made using thermocouples introduced into the bed from the wall (Method 1) and weight loss measurement as well (Method 2). Typical mass loss with time for wood for different air flow rates is shown in Fig. 5.2 and two distinct phases of conversion, namely, *flaming* and *char* mode can be discerned. In the flaming mode, the *average slope* calculated from the mass loss curve, neglecting the start-up phase of the initial 100 s, is a measure of the fuel consumption rate. The fuel burn rate increases with increase in air flow rate in the range shown.

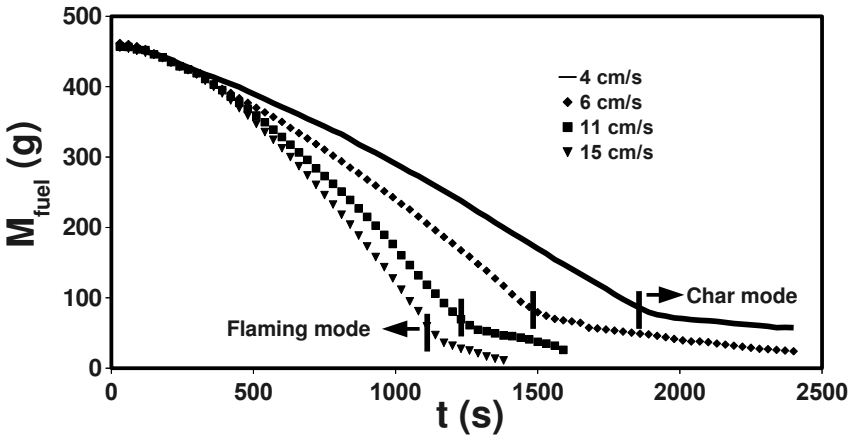

Figure 5.2: Mass loss vs. time of wood for different air superficial velocities

The $\dot{r}$ from both these approaches matched as long as the fuel was dense and did not have sharp edges. When thin wood chips or flakes were used, the $\dot{r}$ measured using thermocouples was larger than that from weight loss method (by 20 to 30 %). Figure 5.3 shows the difference between the two methods. For wood and wheat the propagation rate obtained from the two methods match. But for thin wood flakes, which has sharp edges compared to wood and wheat (see Fig. 2.1), propagation rate measured using method 1 is at least 20% greater than the results obtained from method 2.

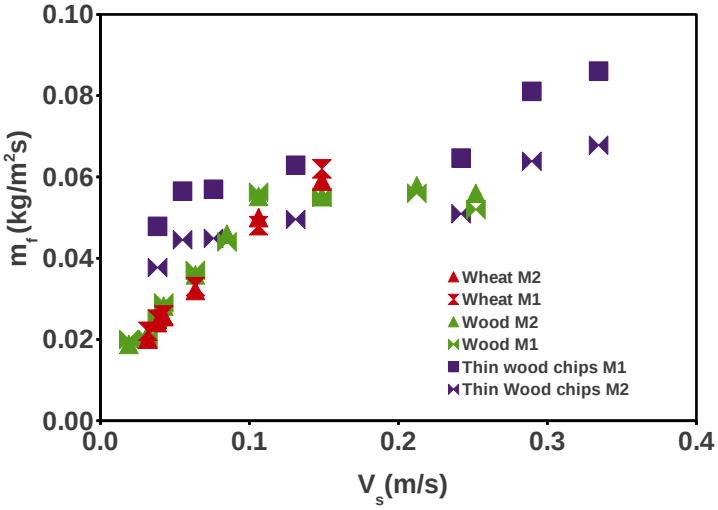

Figure 5.3: Propagation rate estimated from two methods - M1 - method 1; M2 - method 2

Visual observation of the propagation behaviour in the transparent reactor showed that for dense fuels, the propagation occurred after each layer lost its volatiles and entered the char conversion condition, but with flakes and sharp edged fuels, the jump occurred even when all the layer had not lost its volatiles. This is related to the thermal inertia of the biomass particle ($\rho c_p \Delta T$). Sharp edged flakes with individual mass being lower will ignite faster compared to others; ignition of the lower layer occurs even without proper consumption of the current layer. This is reflected in the difference in flaming to ignition time ratio; for thin wood flakes it is 5 and for dense biomass it is 2.

5.1.2 Correction for ash and moisture content variation

The fuel consumption rate is also influenced by the presence of inerts (ash) and moisture. The inerts remain in the condensed phase and contribute to absorption of heat. The heat release in the gas phase is reduced by the fraction of inerts. Moisture in the condensed phase draws energy for both sensible enthalpy rise and evaporation. The vapor will get heated up to the flame temperature in the gas phase and reduce the peak temperature. Since both ash and moisture contribute to reduction in propagation rate, it was thought that they be correlated in terms

of $\rho_p \dot{r}(1 + \alpha f_{ash} + \beta f_w)$ where ρ_p, f_{ash} and f_w are the density of the biomass, ash fraction and moisture fraction in the biomass. The coefficients α and β introduced here because the enthalpy absorbed by inerts and moisture may acquire different values; for simplicity, both are set to 1 here. Equation 5.1 is used to correct the measured propagation rate for the presence of ash and moisture.

$$m_f = \rho_p \dot{r}_c = \rho_p \dot{r}_m (1 + \alpha f_{ash} + \beta f_w), \ \alpha = 1, \ \beta = 1 \tag{5.1}$$

The corrected data from all the available sources (Fatehi & Kaviany (1994); Ronnback *et al.* (2001); Harttanainen *et al.* (2002); Porteiro *et al.* (2010*a*)) and from the present work are shown in Fig. 5.4.

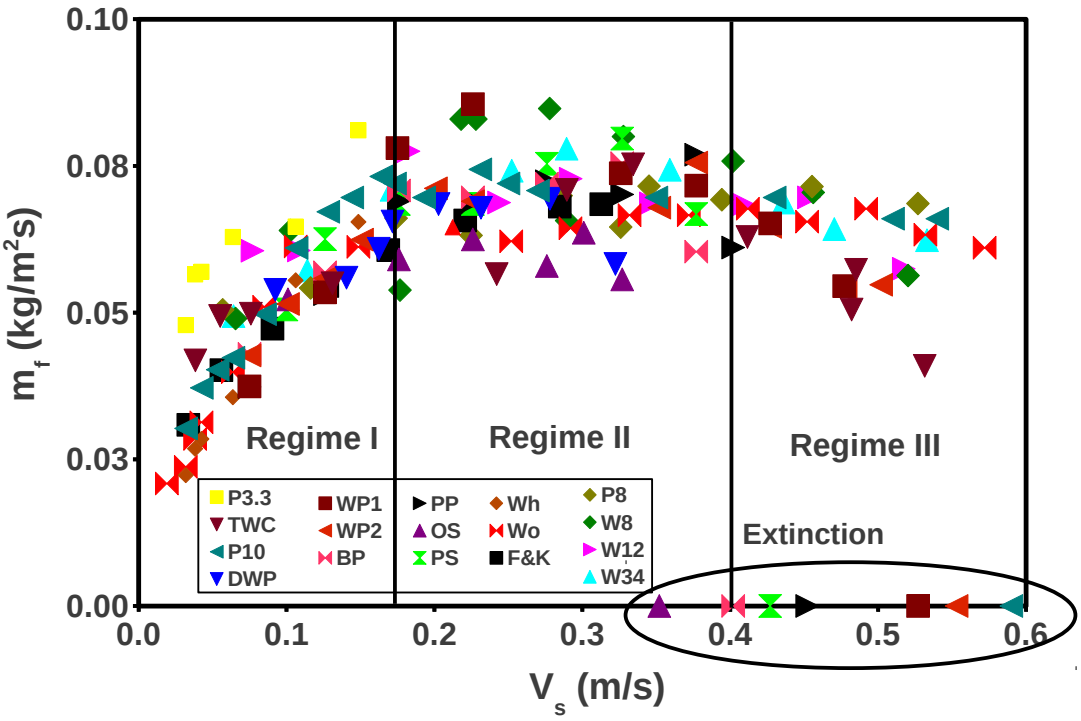

Figure 5.4: Corrected fuel consumption rate variation with superficial velocity

Figure 5.4 shows that with the incorporation of the corrections the scatter in the data has come down and the variation of fuel mass flux with V_s is nearly independent of the biomass used within the experimental limitations. Extinction occurs at around 55 cm/s with a sharp drop in $\dot{m}_f$ for all the fuels used in this study. Experimental results of Porteiro *et al.* (2010*a*) show extinction limits for some fuels being as low

as 35 cm/s. Experiments conducted to explore the possible causes at high V_s showed that the extinction velocity depended on the rate at which V_s is raised. It was found important to make sure that at least a couple of hot char layers are formed before the air flow can be increased to beyond 30 cm/s. Gradual increase in V_s in small steps led to extinction at $\sim$ 55 cm/s for all fuels used in present experiments. It is therefore inferred that observed extinction speeds lower than this value must be an artifact of the experimental procedure. This view is also supported by the work of Fatehi & Kaviany (1994).

Figure 5.5 shows the three major classifications of propagation regimes which were explained in detail in Section 1.5.

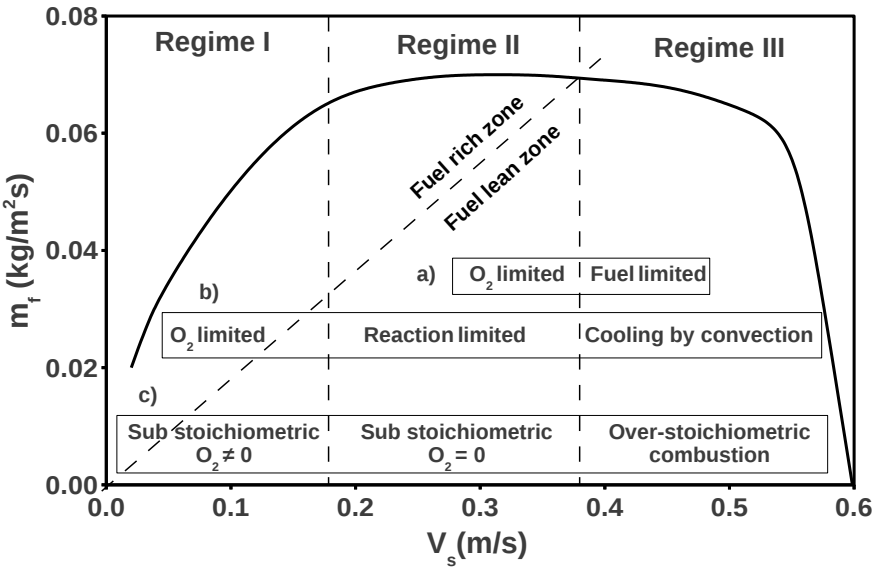

Figure 5.5: Classification of operating regimes in packed bed combustion - (a) Fatehi & Kaviany (1994), (b) Ronnback *et al.* (2001), (c) Porteiro *et al.* (2010*a*)

5.1.3 A/F and char yield variation with V_s

Figure 5.6 shows the air-to-fuel ratio variation and amount of char left at the end of flaming mode as percentage of the initial mass with superficial velocity estimated from the air flow rate and fuel consumption rate presented in Fig. 5.1.

Air-to-fuel ratio increases with increase in superficial velocity. Stoichiometric A/F is attained at V_s = 38 cm/s and matches with the experimental results from

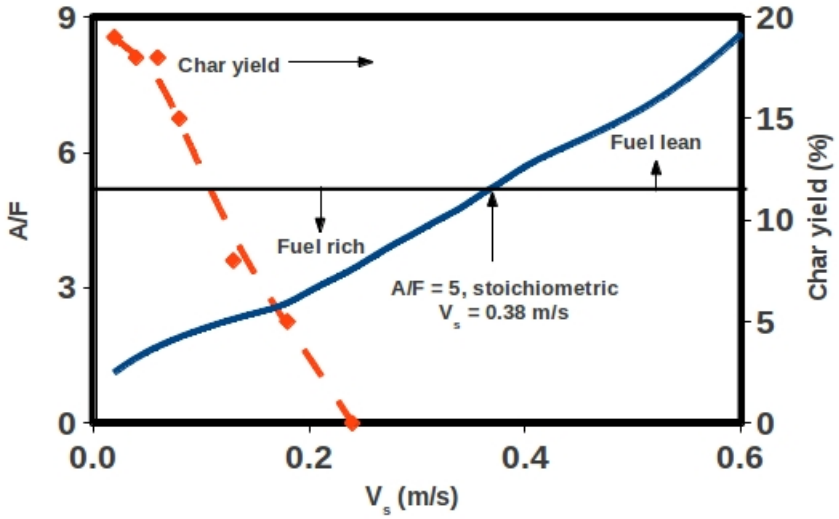

Figure 5.6: A/F and char yield variation with superficial velocity

other studies shown in Fig. 5.1. An important point to note is that the char left over after the flame front reaches the grate decreases from 18% at 5 cm/s to almost zero at 22 cm/s. Implications of increase in A/F combined with decrease in char left over on elucidating the processes in the flame front propagation through the bed will be brought out later.

5.1.4 Exit gas composition

Figure 5.7 shows the exit gas composition measured for pellets over a range of V_s. Data for wood and other fuels used in the current work and that of Gort (1995) also show a similar trend. Both CO and H_2 are at reasonably high levels between 10 to 16% up to a V_s of about 16 cm/s and drop subsequently. CH_4 is around 2.5% at low V_s and drops continuously through 16 cm/s. CO_2 goes up through $V_s = 16$ cm/s. O_2 remains very negligible throughout with below measurable levels beyond 16 cm/s. From these observations, it appears that $V_s = 16$ cm/s marks a transition point. More evidence to this transition will be presented subsequently.

The plot shows little O_2 throughout the range of V_s and it can therefore be concluded that the operation is entirely sub-stoichiometric even beyond 25 cm/s because the amount of H_2 and CO are not very low. To further explore how O_2 is depleting through the bed, it was thought important to use a sensor with a better

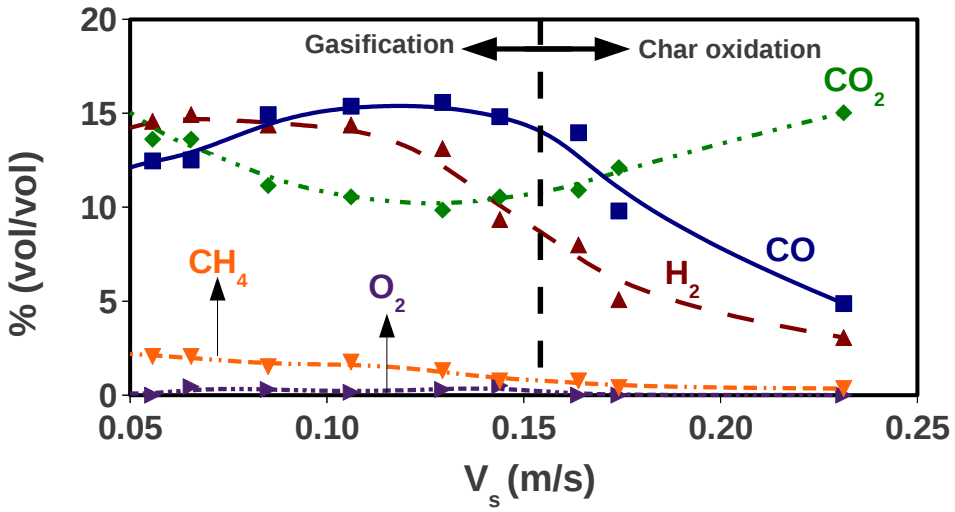

Figure 5.7: Variation of outlet gas composition with superficial velocity

response time than Maihak analyzer (response time is around 4 mins). Hence, λ sensor with a response time of < 10 s was used to measure the O_2 drop across the reaction zone. The data obtained from the simultaneous output of λ sensor and thermocouple with time are set out as a cross-plot between them in Fig. 5.8. These show that for all the cases considered, the O_2 fraction transitions sharply with temperature (to be emphasized later).

A simultaneous visual examination (including video) showed that this occurred as soon as there was a streak of gaseous flame past the measurement point (sample videos are posted at `http://cgpl.iisc.ernet.in`) up to $V_s = 16$ cm/s and beyond this the drop coincided with the ignition of char surface.

5.1.5 Gas phase vs. condensed phase temperature

Figure 5.9 shows gas phase, condensed phase and peak bed temperature measured in the superficial velocity range of 5-26 cm/s. Reaction zone thickness (δ_f) is set out in terms of the number of particle depths. The error bar on δ_f is larger at smaller thickness because it is not possible to distinguish below one particle size thickness.

Gas phase temperature (T_g) is constant (1600 K) up to about a V_s of 17 cm/s. It is important to note that in this range of V_s the A/F increases from 1.5 to 2.7 (see Fig. 5.6). This is a clear indication of diffusion flame behaviour because any

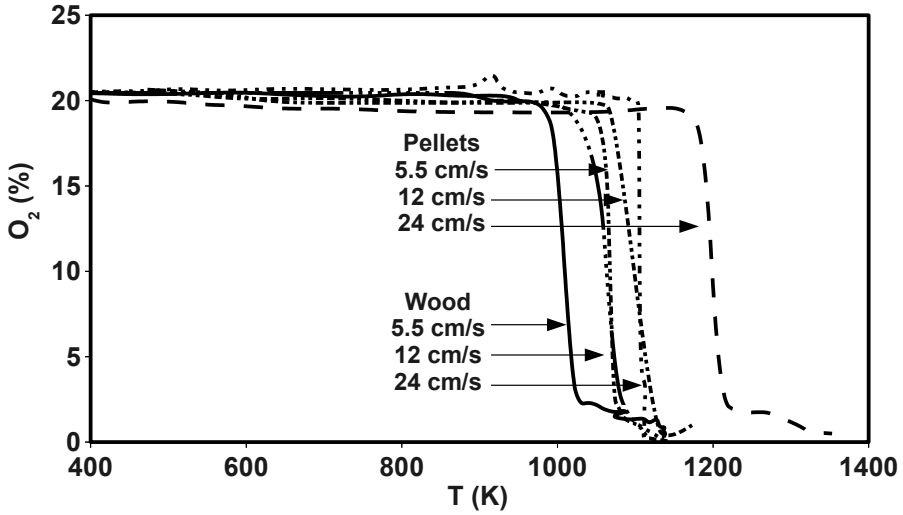

Figure 5.8: O_2 drop as a function of temperature increase across the propagating flame front

level of premixing should lead to a corresponding increase in gas phase temperature with the A/F moving towards stoichiometry. Also the fact that the condensed phase surface temperature (T_{su}) is less than T_g is a feature observed in diffusion flame surrounding the devolatalising particle similar to single particle combustion. T_{su} increases from 973 K to 1600 K as V_s is increased from 5 to 17 cm/s. Visual observation showed that the biomass particle undergoes loss of volatiles with a flame surrounding it. This combined with the fact that the O_2 drops from 21% to 0% within one particle depth shows that the char left behind by the ignition front participates only in reduction reactions with CO_2 and H_2O. Therefore this regime is classified as *gasification dominated*.

Beyond 17 cm/s, measured values of T_g and T_{su} were equal and same as the peak bed temperature. Therefore, only T_{pb} is reported for $V_s > 17$ cm/s. At $V_s = 17$ cm/s, the measured T_{pb} is 1600 K and increases with further increase in V_s. As was shown earlier, the maximum temperature attainable in the gas phase when there is no oxygen access to char surface is 1600 K. So measured temperatures of more than 1600 K for $V_s > 17$ cm/s show that the char participates in oxidation reactions. Visual examination in this regime showed that the gas phase flame of volatiles

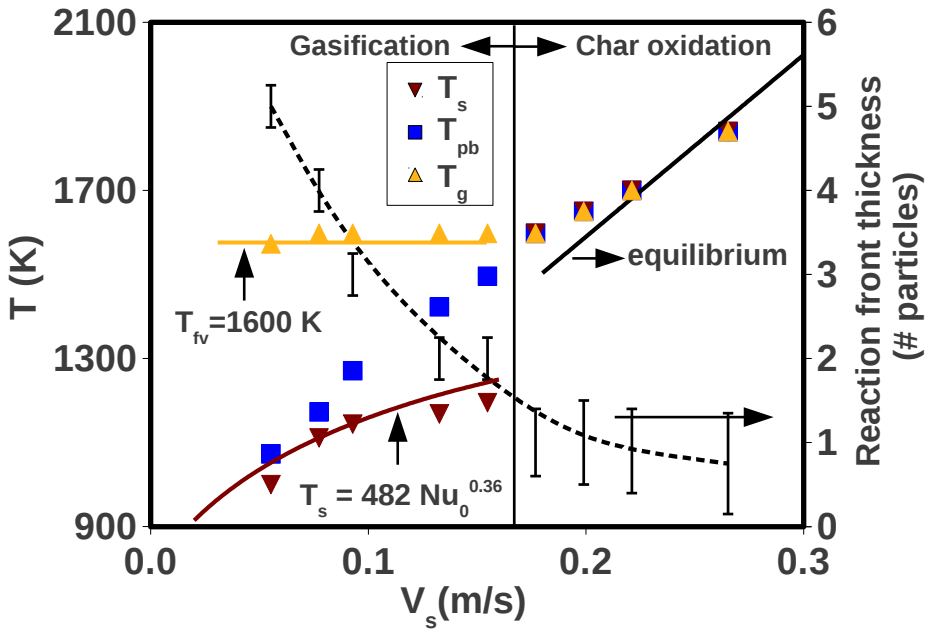

Figure 5.9: Variation of gas, surface and peak bed temperatures (T_g, T_{su}, T_{pb}), reaction zone thickness with V_s. Solid lines - $T_{su} = 482Nu_0^{0.36}$ (model) in the gasification regime and equilibrium temperature in char oxidation regime and volatiles flame temperature (T_{fv}) = 1600 K in gasification regime. Data points are from experimental results. Dotted line represents the mean behavior of reaction zone thickness, δ_f

generated from the fresh biomass gets blown off because of high local velocities and the un-burnt volatiles burn above the devolatalising layer biomass along with the hot char layer. Experiments with single particles in a stream of air showed that the volatile flame surrounding the single particle gets blown off at a Reynolds number of around 100 ($\mathrm{Re} = Vd/\nu$, V is the free stream velocity (m/s), d is particle diameter (10-15 mm), ν is kinematic viscosity of air (m^2/s)). This occurs in a bed at a Reynolds number of around 150 ($\mathrm{Re}_{bed} = V_s d/\nu(1-\phi)$, V_s is the superficial velocity (m/s), d is diameter of single fuel particle (10-15 mm), ϕ is the bed porosity = 0.3). The Reynolds number at which volatiles flame blow off is slightly higher in the case of bed understandably because of better thermal environment compared to a single particle in ambient stream.

Also since the gas phase reactions are faster than the condensed phase surface reactions, participation of char in oxidation can only mean that stoichiometry is reached in the gas phase at around $V_s = 17$ cm/s and it becomes lean beyond this superficial velocity. This also shows that the claim of Porteiro *et al.* (2010*b*) based on air excess ratio scaling using char fraction and char stoichiometric A/F that char stoichiometry is attained at $V_s = 17$ cm/s is inconsistent with this observation. Conditions at $V_s = 17$ cm/s are closer to attainment of volatile stoichiometry and scaling the air excess ratio with volatile fraction in biomass and volatile stoichiometric A/F instead of values corresponding to char led to a value of 1 for air excess ratio. So the conclusions of Porteiro *et al.* (2010*b*) are coincidental and the actual conditions are closer to attainment of volatile stoichiometry at $V_s = 17$ cm/s.

These features combined with the fact that the gas phase and condensed phase temperatures are equal imply *simultaneous oxidation of volatiles and char*. This is the reason for very little char left at the end of flaming mode beyond $V_s = 17$ cm/s (see Fig. 5.6). This regime is termed *char oxidation dominated*. The reaction zone in this regime is like a stirred reactor with heterogeneous surface reactions. Since the dominant process is char surface reaction and is controlled by diffusion of oxygen to the surface this regime is also *diffusion controlled*.

From the videos taken at various values of V_s, two typical conditions of the bed (at $V_s = 7$ and 20 cm/s) have been described in Fig. 5.10. At low V_s, δ_f is many particles deep. At high V_s, it reduces to one particle depth. An interesting feature of this behavior is that $\delta_f V_s$, is constant for the range of data shown (27 ± 3 cm^2/s), a feature similar to what is observed in premixed flames. This should not be taken to imply that premixed flame theory will describe the processes, because the thermochemical dynamics involves diffusion limitedness significantly as discussed earlier. Also for $V_s < 17$ cm/s ignition occurs in the gas phase and the ignition temperature is around 650 K. For $V_s > 17$ cm/s the volatiles are convected up and the char surface ignites the volatiles implying that the char surface ignites first and therefore the ignition temperature is around 850 K. This is the reason for the 200-300 K difference in the temperature at which O_2 drop from 21% to 0% between 12 cm/s and 24 cm/s (see Fig. 5.8).

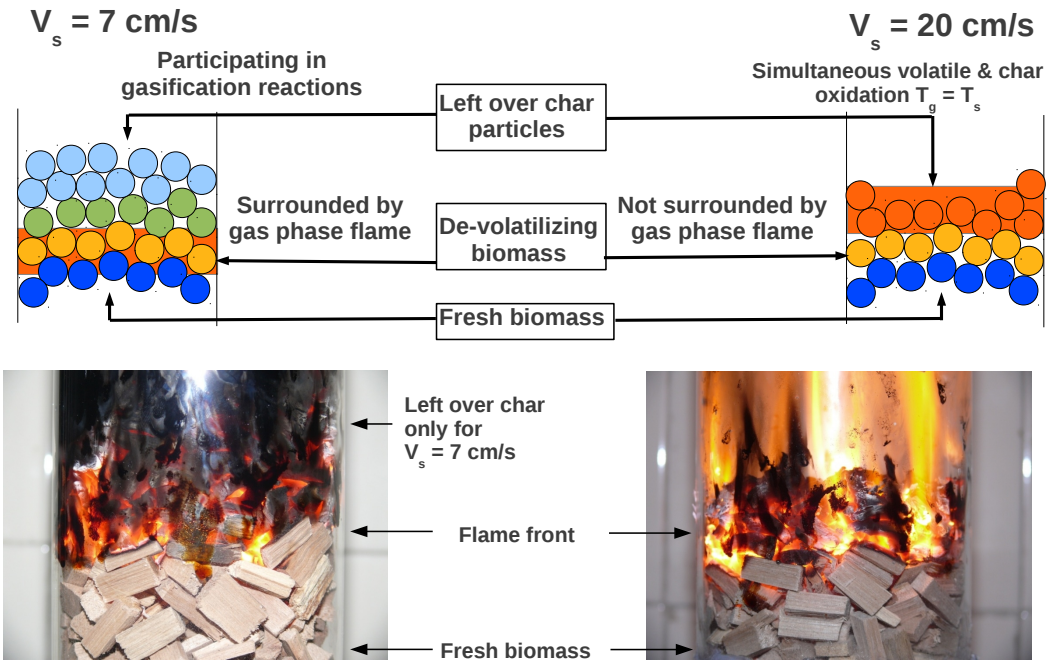

Figure 5.10: Schematic of the reaction zone at V_s = 7 cm/s and 20 cm/s

5.1.6 Classification of operating regime

Using the experimental data shown till now, the operating regime can be classified into *gasification dominated* for $V_s < 17$ cm/s and *char oxidation dominated* for $V_s > 17$ cm/s. Characteristic features of these regimes are given below.

Gasification dominated regime

i. CO and H_2 in the exit gas composition are both 15% (see Fig. 5.7)

ii. Gas phase temperature remains constant at 1600 K even though A/F increases from 1.5 to 2.7 as V_s is increased from 5 cm/s to 17 cm/s (see Fig. 5.9)

iii. Condensed phase temperature increases from 973 K to 1600 K as V_s is increases from 5 cm/s to 17 cm/s (see Fig. 5.9)

iv. It is inferred from the last two points combined with visual examination that in this regime the de-volatilising biomass particle is surrounded by a flame similar to a single particle

v. The reaction zone thickness is 5-6 particles deep at V_s = 5 cm/s and drops to 1-2 particles deep at 17 cm/s (see Fig. 5.9)

vi. Lambda sensor data combined with visual examination shows O_2 drops from 21% to 0% within one particle depth (see Fig. 5.8). This feature combined with the presence of diffusion flame around the particle indicates that all the incoming O_2 is consumed by the volatiles and the surface of the devolatalising particle as well as the char left over above the ignition front do not have access to oxygen. Hence they participate only in reduction of CO_2 and H_2O and so the regime is termed gasification dominated

Char oxidation dominated regime

i. CO and H_2 drop sharply to less than 10% with a corresponding increase in CO_2 faction as V_s is increased beyond 17 cm/s (see Fig. 5.7)

ii. Gas phase temperature and condensed phase surface temperatures are equal and match closely with the equilibrium temperature corresponding to the A/F (see Fig. 5.9).

iii. $T_g > 1600$ K in this regime indicates attainment of gas phase stoichiometry and beginning of char oxidation.

iv. This combined with the fact that the reaction zone is just 1-2 to particles deep (see Fig. 5.9) indicates simultaneous oxidation of volatiles and char.

v. In this regime also O_2 drops from 21% to 0% within one particle depth (see Fig. 5.8). This combined with close agreement of bed temperature with equilibrium temperature indicates that the reaction zone resembles a stirred reactor with heterogeneous surface reaction of char. Diffusion controlled nature of char oxidation makes the dynamics transport controlled in this regime as well.

vi. Participation of char in oxidation reaction and its importance in causing ignition of the volatiles justifies classifying this regime as *char oxidation dominated*.

5.1.7 Peak bed temperature variation with V_s

Figure 5.11 shows the peak bed temperature variation with superficial velocity from the current work along with the data obtained from earlier studies.

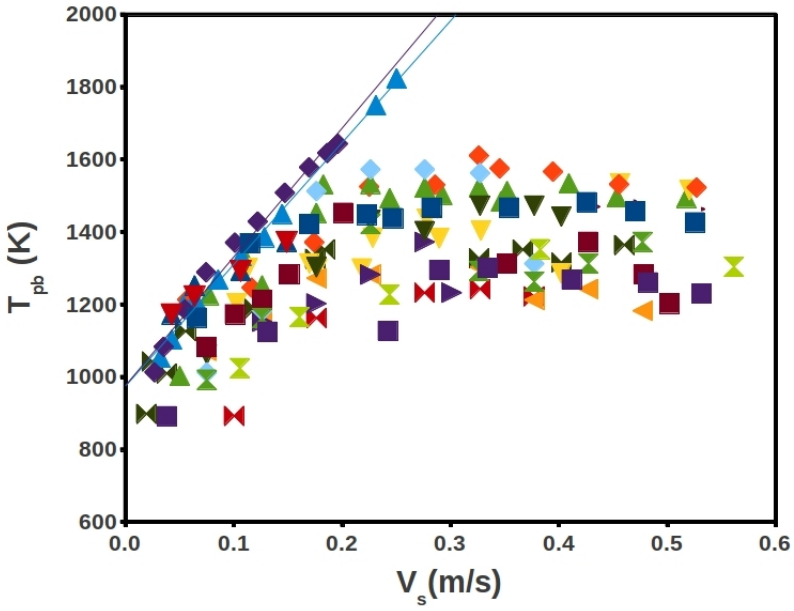

Figure 5.11: Peak bed temperature (T_{pb}) variation with superficial velocity

Most of the data show a trend similar to the fuel consumption rate variation : bed temperature increases with increase in superficial velocity up to 16 cm/s and then saturates. But experimental data obtained from the current study and from that of Fatehi & Kaviany (1994) shows a monotonic increase in temperature with increase in superficial velocity and matches closely with the semi-empirical predictions of Saastamoinen *et al.* (2000). This difference was found to be related to the type of thermocouples used for measurement. Except Fatehi & Kaviany (1994) all others have used chromel-alumel (Type-K) thermocouple which can measure only up to 1500 K. The saturation of temperature data at 1500 K shown in Fig. 5.11 is related to this. Fatehi & Kaviany (1994) have used Pt Rh 30%/Pt Rh 6% (Type-B - max 2000 K) and a Pt/Pt Rh 13% R-type (max 1873 K) is used in this study. So most of the data had to be discarded and the rest containing data from the present work, Fatehi & Kaviany (1994) and Saastamoinen *et al.* (2000) along with the equilibrium calculations using an overall equivalence ratio (ϕ) is shown in Fig. 5.12.

The temperatures measured go up to as high as 1850 K at V_s = 0.25 m/s (ϕ = 0.63). Measured data shows a linear variation of T_{pb} with V_s and ϕ ; it gets increasingly close to equilibrium values with increasing V_s. This is essentially due to the fact that with increasing ϕ, thermo-chemical conversion process leads to reduced

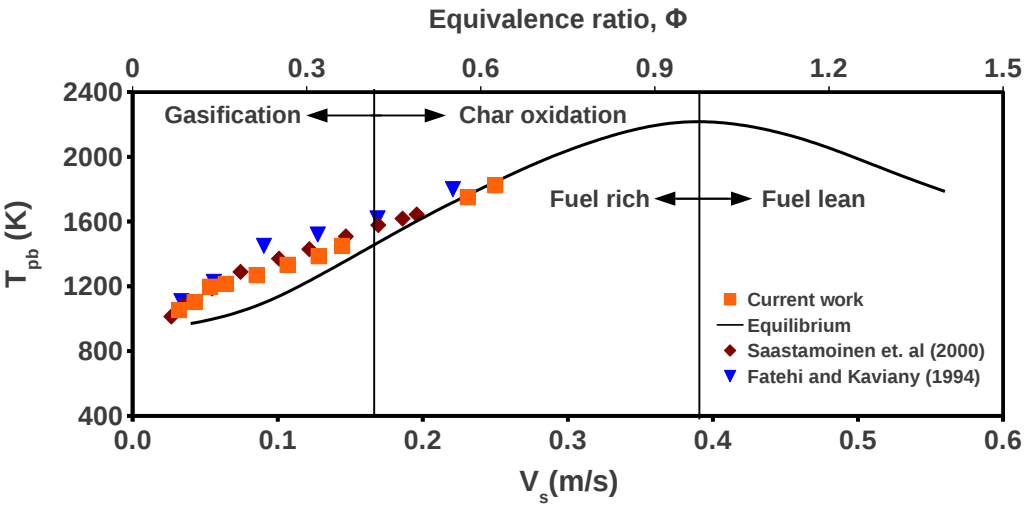

Figure 5.12: Bed temperature with V_s from current work, Fatehi & Kaviany (1994), Saastamoinen *et al.* (2000) and equilibrium calculations

fraction of complex compounds (tars) thereby reducing the residence time to reach equilibration. This is in fact supported indirectly by the experimental data on composition (Fig. 5.7) which shows that CH_4 fraction comes down significantly with increasing ϕ. CH_4 fraction less about 1.5% ensures minimal higher hydrocarbons (see Dasappa *et al.* (2003)). This result allows us to conclude that for $\phi > 0.4$, one can use equilibrium calculations to obtain T_{pb}.

5.2 Resolution of perceived differences in process behavior

It is now possible to clarify the differences in the perception of the bed behavior expressed in Porteiro *et al.* (2010*a*); Fatehi & Kaviany (1994) and Ronnback *et al.* (2001). The depiction of reaction limitedness for V_s between 17 and 38 cm/s is incorrect because as seen from Fig. 5.7, it is O_2 limited. In fact, O_2 drops to 0% in one particle depth in an operating bed as can be noted from Fig. 5.8. Volatile oxidation in diffusion flame mode dominates for $V_s < 16$ cm/s and char surface oxidation dominates for $V_s > 16$ cm/s. Since both these processes are diffusion controlled regimes I and II have the same behavior, namely O_2 limitedness.

The depiction of Ronnback *et al.* (2001) that regime I is sub-stoichiometric with

$O_2 \neq 0$ is incorrect as it is in conflict with the data on O_2 discussed just above. The reason for their conclusion was inferred from their description of experimental procedure. Their data is sampled over 4 minutes. This is in fact close to the response time of the analyzer. If sufficient time for the measurements to become steady had been allowed, they would have also observed zero oxygen fraction. Hence, regime I and II are essentially fuel rich, O_2 limited regimes. The depiction by Fatehi & Kaviany (1994) is indeed correct. Finally, Gort (1995) defines another term called partial gasification to connote regime 1 where some char will remain unconsumed. This is consistent with the experimental observation (see Fig. 5.6) but to emphasise the importance of char reduction reactions this regime is best termed *gasification*.

5.3 The Model

The heat balance for a fresh biomass particle immediately upstream of the reaction zone can be written as,

$$mc_p \frac{dT_p}{dt} = A(f\epsilon\sigma(T_{su}^4 - T_p^4) - h(T_p - T_0)) \tag{5.2}$$

where m is the mass of the particle assumed spherical here (diameter d). The term due to particle temperature, T_p^4 is very small compared to T_s^4 and is ignored. The time for ignition can be calculated by integrating the equation from $T_p = 300$ K (ambient temperature) to $T_p = T_{ign}$. The resulting expression is,

$$\dot{r} = \frac{d}{t_{ign}} = \frac{6h}{\rho c_p ln\frac{1}{1-z}} \tag{5.3}$$

where, $\dot{r}$ is the flame propagation rate, $z = h(T_p - T_0)/(f\epsilon\sigma T_{su}^4)$ and f is the view factor.

$$h = Nu\ k/d;\ Nu = 2 + 0.9Re^{0.5};\ Re = V_s d/(\nu(1-\phi)) \tag{5.4}$$

where Re is Reynolds number, ϕ is the void fraction and k is the thermal conductivity of air. Equation 5.3 requires T_{su} as an input. In the gasification regime ($V_s < 16 \pm 1$ cm/s), the de-volatilizing layer of biomass is surrounded by a gas phase diffusion flame and an energy balance at the surface of the char particle surrounded by the flame that relates the regression rate Reynolds number to the difference between heat release and radiant heat loss. Drawing from Mukunda *et al.* (2007) the heat

balance equation for the surface due to flow past it (see Eq. 5.5) T_{su} is obtained from

$$\frac{\epsilon\sigma(T_{su}^4 - T_0^4)}{[\frac{\mu c_p}{d_0}](T_{su} - T_0)} = (B-1)\frac{Nu}{Nu_0}Nu_0 \tag{5.5}$$

where,

$$B = \frac{H_v Y_{ox,0}}{s_v c_p (T_s - T_0)} \tag{5.6}$$

H_v is the caloric value of the volatiles (14 MJ/kg) and s_v is the stoichiometric coefficient (3.6). By solving the above equation iteratively for T_{su} assuming $Nu_0 = 2 + 0.9\ Re^{0.5}$, we get $T_{su} = 482 Nu_0^{0.36}$; the properties are chosen at 600 K and char emissivity value of 0.85. The theoretical results are shown along with the experimentally determined T_{su} in Fig. 5.9. The model results deviate from the experimental results by less than 5%. For $V_s > 16$ cm/s, T_{su} is taken from equilibrium calculations (see Fig. 5.12).

5.3.1 Ignited mass and choice of ignition temperature

As was discussed earlier, in the gasification dominated regime up to $V_s = 17$ cm/s, fresh biomass devolatalises due to heat transfer from hot char layer above it; the volatiles coming out mix with the incoming air and burn around the devolatalising particle in diffusion flame mode. Ignition essentially occurs in the gas phase and further heat for devolatalisation is supplied by the surrounding flame similar to single particle combustion. Therefore the mass of fresh biomass that needs to be heated for ignition is very small compared to the mass of a fresh biomass particle. Consistent with this observation Eq. 5.3 over predicted the propagation rate by six times. So the mass to be heated for ignition of gas phase flame is significantly smaller perhaps one-sixth the mass of the particle and once the gas phase flame is established, further devolatilisation occurs by heat transfer from the flame to the biomass particle. This also implies that the ignition temperature that must be used in Eq. 5.3 should correspond to the gas phase ignition temperature of volatiles, which is around 650 K (see Quintiere (2006)). Therefore in the calculations the numerical factor 6 in Eq. 5.3 is dropped and 650 K is used for the ignition temperature.

But for $V_s > 17$ cm/s as was shown earlier the gas phase flame gets blown off from around the devolatalising particle; the volatiles coming out get convected upwards

and burn around the hot char particle leading to simultaneous oxidation of volatiles and char. Therefore the entire fresh biomass gets heated only because of heat transfer by radiation from the hot char on top till the surface reaches temperature sufficient for the char oxidation reactions to begin. So the mass to be heated for ignition in this case is very close to the mass of a fresh biomass particle and the ignition temperature is that of the char, around 850 K. Another factor which must be taken into account once the char starts to oxidise is the formation of ash layer on the char surface which will alter the emissivity. This aspect is dealt with in the following section.

5.3.2 Role of ash on the propagation behaviour

The source of ignition for flame propagation is radiation from the hot char surface just above the fresh biomass. The emissivity can be chosen to be close to unity (say 0.85) up to $V_s = 16$ cm/s as the char surface is not covered by ash. But beyond 16 cm/s, as discussed earlier, char oxidation starts to dominate and the ash formed stays on the surface of the char (see Varunkumar *et al.* (2011)). In the case of single char particles burning under ambient conditions, ash layer plays a dual role. It brings down the heat loss from the surface by bringing down the emissivity as well as the surface temperature and adds an extra resistance to the transport of O_2 to the surface of the char, thereby establishing a delicate balance between convection and radiation (see Varunkumar *et al.* (2011)). But in a packed bed, for $V_s > 18$ cm/s, the temperature drop across the ash layer is taken negligible; the ash layer brings down the effective emissivity at which the particles emit radiation to the fresh biomass or char. The emissivity data for hot ash layer is obtained from the work of Wall *et al.* (1993) and Zbogar *et al.* (2005) on coal combustion in boilers. The emissivity is shown to decrease with an increase in temperature; also it is shown in Wall *et al.* (1993) that the fraction of radiation transmitted through a 0.4 mm thick ash layer is just 5% and through a 1 mm thick layer is less than 1%. Therefore, in the present model, the ash layer is assumed to be opaque and radiate at T_{su} with the emissivity correlation given in Zbogar & Frandsen (2003), as $\epsilon(T_{su}) = 1 - 0.0004\, T_{su}$. This expression is extrapolated up to 2200 K.

Figure 5.13 shows the model results along with the emissivity data used; experimental data points are also shown. Uncertainty of 10% in the emissivity data leads to predictions that encompass most of experimental data. The agreement between

the model results and experiments is indeed good and clearly brings out the universal behavior of flame propagation through a packed bed of biomass. Measurements of $\dot{r}$ with steel and glass reactor are within 5% up to 50 cm/s; beyond 50 cm/s, it drops sharply leading to extinction in the glass reactor at $\sim$ 55 cm/s and in the insulated steel reactor at $\sim$ 65 cm/s. These imply that heat loss is the key factor initiating the extinction process. Further physical examination and videos show that extinction starts locally in some region near the wall and spreads around. This is understood as follows. Coupled effects of (a) enhanced voidage near the wall, (b) sharp local increase in velocity due to bed adjustment and (c) reactive heating of the incoming stream lead to high local velocities of 2.5 to 3 m/s. This causes ash local blow off and enhanced radiation loss and cooling-off(Varunkumar *et al.* (2011)). This spreads around leading to overall extinction.

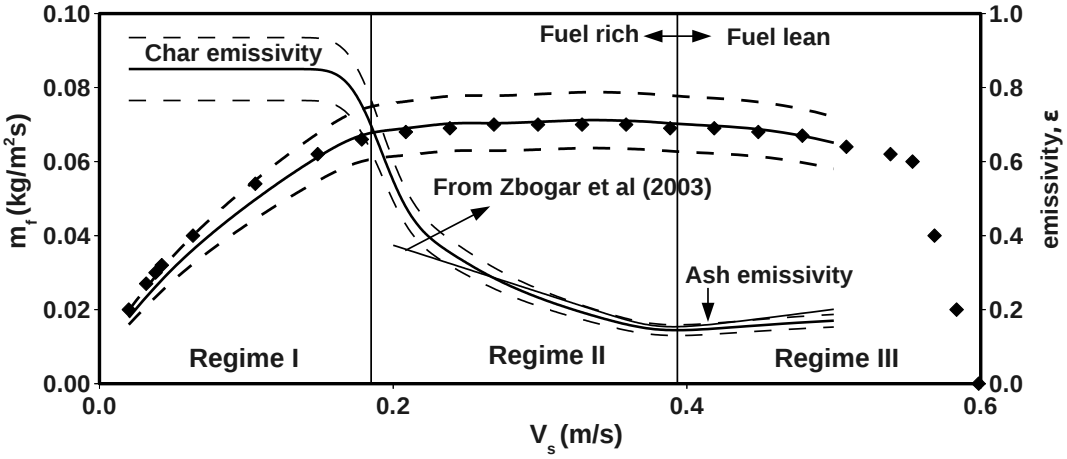

Figure 5.13: Model results. Solid line - model results; dashed lines - fuel mass flux calculated by incorporating ± 10% uncertainty in emissivity; data points - experimental results; emissivity values with bounds and correlation of Zbogar & Frandsen (2003) are also shown

5.4 Summary

This chapter has considered the processes in the thermo-chemical conversion of a packed bed of biomass particles. There have been various perceptions of the conversion process mostly arising out of inadequate exploration of crucial thermo-

chemical behavior. The data on exit gas composition and the change in O_2 fraction through the bed are used to show that the operation is sub-stoichiometric over a large range of V_s (up to 40 cm/s). Visual examination of thin gaseous flames between particles and their flame temperatures close to the adiabatic flame temperature for the volatiles (1600 K) over a range of V_s up to 18 cm/s are taken to indicate the diffusion limitedness of the process; in this regime, the surface temperature is less than the gas phase temperature. For $V_s > 18$ cm/s, the difference between T_{su} and T_g vanishes due to simultaneous volatile and char oxidation processes. Based on these observations two regimes of operation are identified, namely, gasification reactions dominated ($V_s < 16 \pm 1$ cm/s) and char oxidation dominated ($V_s > 16 \pm 1$ cm/s). In both these regimes, λ sensor data shows that O_2 drops from 21% to near 0% within one particle depth, indicating *fast chemistry and transport limited dynamics*. These inputs are used to develop a model which considers the thermal evolution of fresh biomass from ambient to ignition conditions. In the gasification regime, it is coupled with the surface heat balance equation for the flaming particle above the fresh biomass and the predicted propagation rates match excellently with the experimental results. In the char oxidation regime, ash plays an important role in regulating the radiant heat transfer to the fresh biomass and the variation of ash emissivity is shown to be crucial in explaining the observed behavior. This is the second instance in which the role of ash in regulating radiant heat transfer is shown to be crucial in explaining the observed conversion behavior. In this regime also, the agreement between model results with experiments is shown to be very good. Finally, the observed variation of fuel consumption rate with air flow rate is shown to follow an universal trend irrespective of the biomass used; it is important to realize that this is primarily a consequence of diffusion limitedness of the conversion process.

Chapter 6

Concluding remarks

This thesis has contributed to the fundamental experimental and computational investigations on gasification and combustion in a packed bed. Its contributions are both at the level of improving the understanding and clarifying issues around conflicting features in literature as well as providing design inputs for high efficiency low emission stoves of reverse downdraft class of combustion devices.

To restate the basic features, when a packed bed of pellets or wood chips is lit at the top as uniformly as possible and air flow is created through the bed, a flame propagates through the bed in a direction opposite to the direction of the mean air flow leading to either release of volatiles from the biomass or in addition, conversion of char in gasification mode. The fuel-rich gases are subsequently burnt with additional air at the top to release all the heat in the gases. Another class of applications involves of use of a packed bed for combustion-on-grate for boiler application that has the same mode of gasification-combustion. It is important to recognize the difference between the two applications noted above. It lies in the magnitude of the superficial velocity (V_s) in the bed - for domestic stoves between 3.5 and 6 cm/s and for packed bed on grates between 15 and 30 cm/s. The lower values of V_s for domestic stoves are chosen to limit the particulate emissions; the higher values of V_s for operations of combustion-on-grate to maximize the conversion rate. A fundamental property that changes when the superficial velocity (V_s) is increased is the flame propagation rate through the bed ($\dot{r}$, mm/s). This increases nearly linearly with V_s till V_s = 16 cm/s and levels-off beyond this value of V_s till it is 50 to 60 cm/s; beyond this V_s, the propagation ceases (alternately stated, flame extinction occurs).

It is important to note that a significant part of the effort has been devoted to domestic stoves. In this respect, it progresses the work performed earlier and takes

the status of stove operations much closer to the revered LPG stove (except for turn-off and turn-on whenever required as well as large turn down features).

Recognizing that even the large water boiling efficiency of 50 % and the low emissions of 0.75 g/MJ are limited by the char mode of operation, this mode of operation was addressed in this work as it was seen as a possibility for enhancing efficiency and reducing the emissions. In the process, it was observed that

i. The optimal value of R for flaming mode is 5 and for char mode is 2.

ii. The water boiling efficiency (η_{wb}) of existing systems can be raised to 60 % through operation of char mode at higher V_s (corresponding to R=2) and with similar ideas on large power systems have shown η_{wb} of 70 % using R ratio noted earlier.

iii. The contribution of flaming mode to total CO is 40 % (0.4 g/MJ) under stoichiometric conditions. Char mode contribution to efficiency is just 4% with 60% CO contribution (0.6 g/MJ); total CO under stoichiometric conditions is 1 g/MJ.

iv. The overall CO emissions can be brought down from 0.7 g/MJ to about 0.5 g/MJ for domestic stoves and 0.3 g/MJ in large systems using the R ratio noted above.

v. Under these conditions the recommendation that grate blockage area should be kept to a minimum was evolved so as to minimize ash fusion problems.

vi. Operating the stove at various equivalence ratio showed that it was not possible to operate in lean-mode.

vii. To understand this feature, reactive flow CFD (RCFD) calculations were performed. These studies showed that increased air flow from the top caused enhanced recirculation around the fuel bed brings in more oxygen that reacts closer to the surface and transfers additional heat enhancing the pyrolysis in the fuel bed. This brings the equivalence ratio towards stoichiometry.

viii. RCFD calculations are also used to predict the efficiency components and utilised in creating a heat balance for the stove.

ix. The heat balance that included the heat released, heat transferred to the vessel by convection and radiation, heat lost to the walls of the vessel and the heat lost through the flue gases showed that the balance could be closed to within 5 %. This

vast improvement in the heat balance is due to the fact that the unaccounted losses in the earlier estimates were essentially due to poor combustion and were not so recognized.

Studies on single piece of wood and pellet as well as in a packed bed were conducted to elucidate the commonalities and differences between the volatile and char mode combustion regimes over a range of V_s. These studies showed that,

i. There are no differences in the volatile combustion mode beyond the role played through $\rho_p \dot{r}$, where ρ_p is the density of wood pieces or pellets.

ii. No differences in char mode combustion of single particles as well.

iii. The differences noticed in the packed bed combustion of char were traced to poor thermal environment faced by wood char pieces compared to pellet char pieces.

iv. In attempting to understand the phenomenology, the single particle char conversion process was modeled. It was found that unless the presence of ash layer was properly accounted for, it was not possible to explain the burn time of the char pieces.

The flame propagation rate through the bed was experimentally obtained using thermocouples at various distances into the bed through the wall and from weight loss time data. It was shown that both the approaches provide consistent data as long as the density of the biomass used was high (typically above 400 kg/m^3). For light biomass pieces or flakes, the thermocouple strategy gave a higher propagation rate compared to weight loss time data. This was explained in terms of the differences in the ratio of ignition time to volatilization time between flakes and dense wood pieces/pellets.

A major question on the operational behavior of the bed was brought up because several earlier studies (all European) had inferred differently about the nature of packed bed functioning at various V_s. To understand and rationalize the bed behavior specifically designed experiments that captured as many features as could be explored were conducted. A composite picture was obtained from the measurements of composition over the bed, temperatures in the bed, fine thermocouple temperatures in the gas phase and on the hot char, lambda sensor measurement of oxygen fraction as a function of V_s. These showed a distinctive superficial velocity domain. In the first domain of $V_s < 17$ cm/s,

i. The fractions of CO, H_2 increase, CH_4 fraction decrease,

ii. The oxygen fraction is near zero,

iii. The gas temperature remains at about 1600 K,

iv. The surface temperatures increase from 850 K to 1600 K and

v. Transition of the oxygen fraction from 0.21 to 0.0 occurs in a single particle depth when gas flame arrives at this level.

The inferences drawn from these data are that,

- The bed operates in fuel rich mode,
- Diffusive combustion dominates the propagation, and
- The propagation is controlled by the heat transferred from a current layer to an upstream layer.

In the second domain of 17 cm/s $< V_s <$ 50 cm/s,

i. The mass fractions of CO and H_2 decline,

ii. CH_4 decreases further,

iii. Oxygen fraction remains near zero,

iv. CO_2 increases,

v. Gas and surface temperatures are nearly equal and increase from 1600 K to 2200 K,

vi. Oxygen fraction drops from 0.21 to 0 in one particle depth,

vii. The gas efflux from biomass is drawn up to upper layer for combustion without a local flame, and

viii. The flame temperature is close to equilibrium flame temperature for the overall equivalence ratio

The inferences from these data are that diffusive combustion dominates and reactions are fast.

Beyond $V_s = 50$ cm/s, the propagation ceases to occur. The precise value of the extinction V_s depends on the rate of increase of V_s in this range. A faster change initiated the extinction earlier. Observations showed that extinction would begin at some location around the periphery and spread laterally. Extinction at one layer is adequate to complete the extinction process.

The observed flattening of propagation rates at 17 cm/s needed to be explained. In order to do this modeling efforts on single particle combustion and the bed propagation were made. These showed that unless ash layer that is built on the surface as soon as char oxidation commences it is not possible to explain the magnitude of the radiation flux from the surface to maintain the observed burn rate. That this is responsible for flattening of propagation rate variation with superficial velocity and not fuel limitedness beyond $V_s = 17$ cm/s was not recognized till now. Combining theory and experiments was needed to explain the extinction. The features are:

- The presence of the ash layer over the surface that is shown as responsible for maintaining a steady char conversion in a single char particle at low stream speeds,
- The feature that the ash layer would be blown away at stream velocities of 2.5 to 3 m/s in a single particle combustion,
- With V_s close to 50 cm/s, local velocities of air flow through the bed can reach 2 to 3 m/s, this value being sensitive to the bed arrangement, with slight shifting or settling of one particle leading to increase of the local velocity at the periphery. Thus, the high local speeds of flow through the bed (more than 2 m/s) was considered responsible for removal of ash layer such that radiation losses would be dominant and cause local extinction of the reaction front at the char surface.
- A model for propagation rate was set up based on the heat transfer by radiation from one layer to the upcoming layer of biomass with convective cooling around the fresh biomass from the air flow through the bed.
- The results of the model were compared with experimental data from all reported studies including the present one over a range of biomass on a propagation rate vs. V_s accounting for moisture fraction and ash fraction and *this showed a behavior that is universal.*

Thus this study has led to a comprehensive understanding of the gasification-combustion behavior of packed bed in stoves and on grates. It has also led to the evolution of parameters for obtaining high efficiency and low emissions from stoves. Finally, it is important to point out that these features were incorporated into larger combustion devices with water boiling efficiencies close to 70 % and CO emissions of 0.35 0. 4 g/MJ. These values closely approximate those of LPG stoves and about 2500 of these devices are in current use. The contributions are best summarized in the following figures.

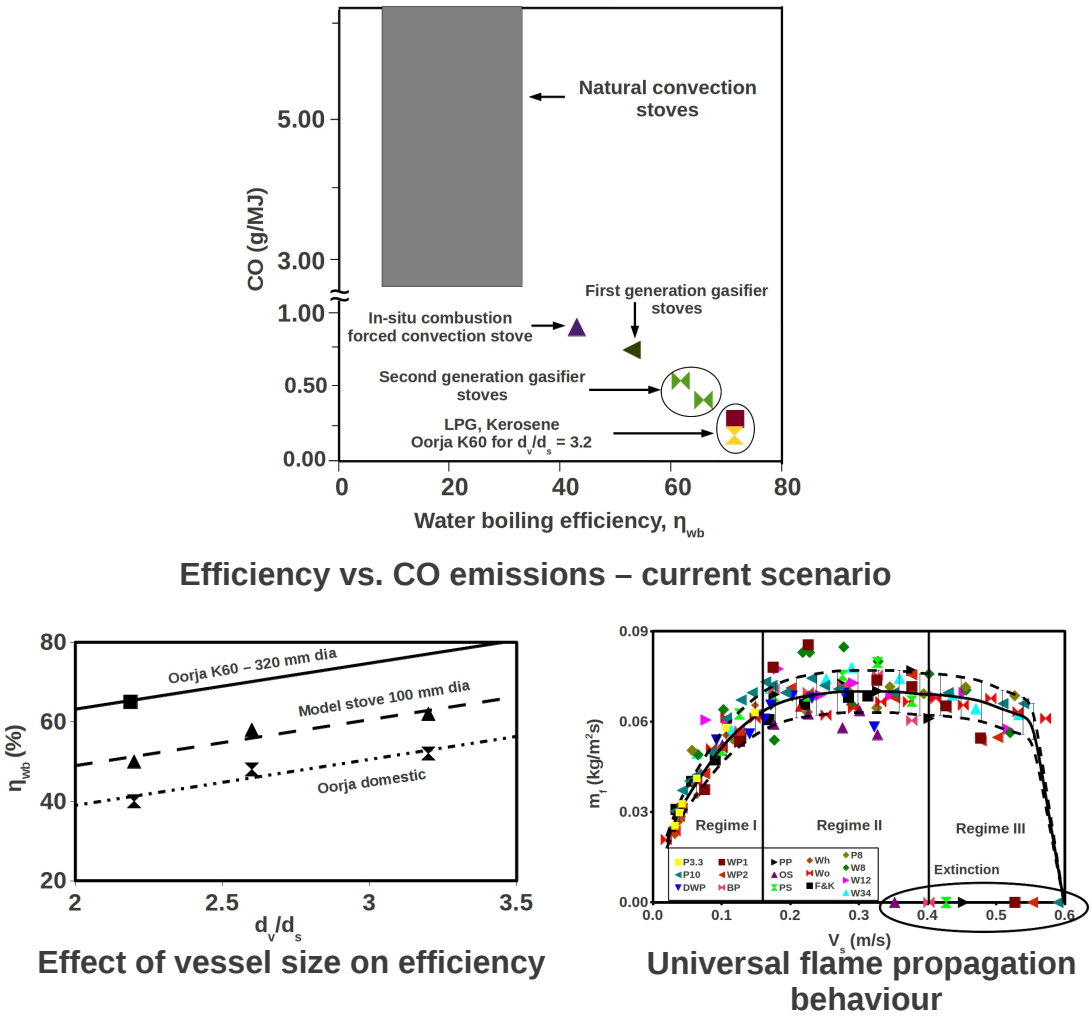

Figure 6.1: Contribution of the thesis - Top: The current thesis is essentially on second generation biomass burning devices; bottom left. The top square data point is from experiment conducted with a cylindrical vessel twice as large as the stove combustion chamber and the line at the top is drawn parallel to the lower curve; the bottom right figure is the universal law on the propagation rate through a packed fuel bed of biomass pieces

In the authors' mind what remains to be done is to develop a fundamental approach to predicting the CO emissions from the stove and this work is in currently under-way.

Appendix A

Measured gas composition and propagation rates

Table A.1: Measured exit gas composition

V_s (m/s)	CO (%)	CO_2 (%)	CH_4 (%)	H_2 (%)	O_2 (%)
0.06	12.5	13.6	2.1	14.6	0
0.09	14.9	11.2	1.5	14.4	0.3
0.11	15.4	10.6	1.8	14.4	0.2
0.13	15.6	9.8	1.3	13.1	0.3
0.14	14.8	10.6	0.8	9.3	0.5
0.16	14.0	10.9	0.8	8.0	0
0.17	9.8	12.1	0.4	5.1	0
0.23	4.9	15.0	0.4	3.1	0

Table A.2: Measured propagation rates for different fuels

	$\rho_p \dot{r}$ (kg/m^2 s)			
V_s (m/s)	P10	P3.3	Wo	Wh
0.032	0.025	0.022	0.021	0.02
0.043	0.031	0.029	0.028	0.026
0.053	0.034	-	-	-
0.064	0.035	0.036	0.036	0.032
0.085	0.041	-	0.046	-
0.107	0.051	0.051	0.055	0.05
0.128	0.056	-	-	-
0.144	0.058	0.056	0.055	0.059
0.164	0.061	-	-	-
0.173	0.06	-	-	-
0.193	0.058	-	0.056	-
0.231	0.062	-	-	-
0.25	0.06	-	0.056	-
0.270	0.059	-	0.057	-
0.350	0.058	-	0.06	-
0.430	0.058	-	0.059	-
0.510	0.055	-	0.058	-
0.540	0.055	-	0.057	-
0.590	0.000	-	0.000	-

P10 - 10% ash pellets; P3.3 - 3.3% ash pellets
Wo - wood chips; Wh - wheat

Publications

1) S Varunkumar, NKS Rajan, and HS Mukunda. Single particle and packed bed combustion in modern gasifier stoves density effects. *Combustion Science and Technology*, 183(11):1147-1163, 2011.

2) S Varunkumar, NKS Rajan, and HS Mukunda. Experimental and computational studies on a gasifier based stove. *Energy Conversion and Management*, 53(1):135-141, 2012.

Bibliography

Agenbroad, J., DeFoort, M., Kirkpatrick, A. & Kreutzer, C. 2011 A simplified model for understanding natural convection driven biomass cooking stoves part 1: Setup and baseline validation. *Energy for Sustainable Development* **15** (2), 160–168.

Anderson, P.S., Reed, T.B. & Wever, P.W. 2007 Micro-gasification: What it is and why it works. *Boiling Point* **53**, 35.

Bhattacharya, SC 2005 Biomass gasification in asia. *Handbook biomass gasification. Enschede: BTG* pp. 162–80.

Bhattacharya, S C, Albina, D O & Khaing, A M 2002 Effects of selected parameters on performance and emission of biomass-fired cookstoves. *Biomass and Bioenergy* **23**, 387–395.

Bogdanski, A., Dubois, O., Jamieson, C. & Rainer, K. 2010 Making integrated food-energy systems work for people and climate. *Environment and natural resources management working paper* **45**.

Bryers, R.W. 1996 Fireside slagging, fouling, and high-temperature corrosion of heat-transfer surface due to impurities in steam-raising fuels. *Progress in Energy and Combustion Science* **22** (1), 29–120.

Collazo, J., Porteiro, J., Patiño, D. & Granada, E. 2011 Numerical modeling of the combustion of densified wood under fixed-bed conditions. *Fuel* .

Cooper, J. & Hallett, WLH 2000 A numerical model for packed-bed combustion of char particles. *Chemical engineering science* **55** (20), 4451–4460.

Cordes, Leslie 2011 Igniting change : A strategy for universal adoption of clean cookstoves and fuels. http://cleancookstoves.org/blog/ignitingchange/, last accessed Jan 17, 2012.

Dasappa, S & Paul, P J 2001 Gasification of char particles in packed beds: analysis and results. *Int. J. Energy. Res.* **25**, 1053–1072.

Dasappa, S, Paul, P J, Mukunda, H S & Shrinivasa, U 1994 The gasification of wood-char spheres in carbon-dioxide - nitrogen mixtures : Analysis and experiments. *Chem. Eng. Sci* **49**, 223–232.

Dasappa, S, Paul, P J, Mukunda, H S & Shrinivasa, U 1998 Combustion of char. *Proc. combust. Instit* **27**, 1335–1342.

Dasappa, S., Sridhar, HV, Sridhar, G., Paul, PJ & Mukunda, HS 2003 Biomass gasification–a substitute to fossil fuel for heat application. *Biomass and Bioenergy* **25** (6), 637–649.

Dosanjh, Sudip S, Pagni, Patrick J & Fernandez-Pello, Carlos 1987 Forced cocurrent smoldering combustion. *Combustion and flame* **68**, 131–142.

Dutta, K., Shields, K.N., Edwards, R. & Smith, K.R. 2007 Impact of improved biomass cookstoves on indoor air quality near pune, india. *Energy for Sustainable Development* **11** (2), 19–32.

Emmons, H.W. & Atreya, A. 1982 The science of wood combustion. *Sadhana* **5** (4), 259–268.

Evans, D D & Emmons, H W 1977 Combustion of wood charcoal. *Fire research* **1**, 57–66.

Fatehi, M & Kaviany, M 1994 Adiabatic reverse combustion in a packed bed. *Combustion and flame* **99**, 1–17.

Glassman, I 1987 *Combustion*, chap. 6, pp. 407–409. New york: Academic press.

Gnanendra, PM, Ramesha, DK & Dasappa, S. 2012 Preliminary investigation on the use of biogas sludge for gasification. *International Journal of Sustainable Energy* .

Gort, R 1995 On the propagation of a reaction front in a packed bed: thermal conversion of municipal waste and biomass. PhD thesis, University of Twente.

Gort, R & Brouwers, J J H 2001 Theoretical analysis of the propagation of a reaction front in a packed bed. *Combustion and flame* **124**, 1–13.

Harttanainen, M, Saastamoinen, J & Sarkomaa, P 2002 Operational limits of ignition front propagation against airflow in packed beds of different wood fuels. *Energy and Fuels* **16**, 676–686.

IEA 2006 World energy outlook. http://www.iea.org/textbase/nppdf/free/2006/weo2006.pdf, last accessed Jan 17, 2012.

Incropera & Dewitt 1996 *Fundamentals of Heat and Mass transfer*. Wiley.

Jetter, J.J. & Kariher, P. 2009 Solid-fuel household cook stoves: characterization of performance and emissions. *Biomass and Bioenergy* **33** (2), 294–305.

Johansson, R, Thunman, H & Leckner, Bo 2007 Influence of intraparticle gradients in modeling of fixed bed combustion. *Combustion and flame* **149**, 49–62.

Kaupp, A. 1983 *Gasification of rice hulls: theory and praxis.*. Deutsches Zentrum fur Entwicklungstecnologien. Braunschweig.

Kaupp, A & Goss, J R 1984 *Small scale gas producer - engine systems*. Braunschweig/Wiesbaden: Friedr. Vieweg & Sohn.

Kohli, S., Srinivasan, J. & Mukunda, HS 1993 Heat transfer to a horizontal disc using a buoyancy-induced jet. *International journal of heat and mass transfer* **36** (16), 4049–4066.

La Fontaine, H. & Reed, TB 1993 An inverted downdraft wood-gas stove and charcoal producer. In *Energy from Biomass and Wastes XV* (ed. D Klass).

Larson, E.D. & Kartha, S. 2000 Expanding roles for modernized biomass energy. *Energy for sustainable development* **4** (3), 15–25.

Lee, J C, Yetter, R A & Dryer, F L 1995 Trasnient modeling of carbon particle ignition and oxidation. *Combustion and flame* **101**, 387–398.

Lokras, SS, Sudhakar Babu, DS, Bhogle, S. & Jagadish S, K.R. 1983 Development of an improved three-pan cookstove. In *Cook stoves - firewood burning. Designing and transfer*. Consortium on Rural technology.

MacCarty, N., Still, D. & Ogle, D. 2010 Fuel use and emissions performance of fifty cooking stoves in the laboratory and related benchmarks of performance. *Energy for sustainable development* **14**, 161–171.

Makino, A & Law, C K 2009 Combustion of graphite. *Proc. combust. Instit* **32**, 2067–2074.

MNES & IIT, Delhi 1993 Indian improved cookstoves: A compendium. http://www.fao.org/docrep/006/AD585E/ad585e00.pdf, last accessed Jan 17, 2012.

Mukunda, H S, Basani, J, Shravan, H M & Philip, B 2007 Smoldering combustion of "incense" sticks, experiments and modeling. *Combustion science and technology* **179**, 1113–1129.

Mukunda, H S, Dasappa, S, Paul, P J, Rajan, N K S, Yagnaraman, M, Kumar, D Ravi & Deogaonkar, M. 2010 Gasifier stove - science, technology and outreach. *Current Science* **98** (5), 627–638.

Mukunda, H S, Paul, P J, Shrinivasa, U & Rajan, N K S 1984 Combustion of wooden spheres. *Proc. combust. Instit* **20**, 1619–1628.

Mukunda, H S, Shrinivasa, U & Dasappa, S 1988 Portable single-pan wood stoves of high efficiency for domestic use. *Sadhana* **13** (4), 237–270.

Philips 2006 Password - philips research technology magazine issue 28 p 28 - 31. http://www.research.philips.com/password/, last accessed Jan 17, 2012.

Phuoc, T X & Annamalai, K 1999 A heat and mass transfer analysis of the ignition and extinction of solid char particles. *Journal of heat transfer* **121**, 886–893.

Porteiro, J., Patino, D., Collazo, J., Granada, E., Moran, J. & Miguez, JL 2010*a* Experimental analysis of the ignition front propagation of several biomass fuels in a fixed-bed combustor. *Fuel* **89** (1), 26–35.

Porteiro, J., Patino, D., Moran, J. & Granada, E. 2010*b* Study of a fixed-bed biomass combustor: Influential parameters on ignition front propagation using parametric analysis. *Energy & Fuels* **24**.

Quintiere, J.G. 2006 *Fundamentals of fire phenomena*. Wiley Online Library.

Ravi, MR, Kohli, S. & Ray, A. 2002 Use of cfd simulation as a design tool for biomass stoves. *Energy for Sustainable Development* **6** (2), 20–27.

Reed, TB & Larson, R. 1996 A wood-gas stove for developing countries. *Energy for sustainable development* **3** (2), 34–37.

Reed, TB, Walt, R., Ellis, S., Das, A. & Deutch, S. 1999 Superficial velocity–the key to downdraft gasification. In *Fourth Biomass Conference of the Americas, Oakland, USA*, pp. 343–356.

Ronnback, Marie, Axell, Monica, Gustavsson, Lennart, Thunman, Henrik & Leckner, Bo 2001 Combustion processes in a biomass fuel bed - experimental results. *Progress in thermochemical biomass conversion* pp. 743–757.

Ryan, J.S. & Hallett, W.L.H. 2002 Packed bed combustion of char particles: experiments and an ash model. *Chemical engineering science* **57** (18), 3873–3882.

Ryu, C., Yang, Y.B., Khor, A., Yates, N.E., Sharifi, V.N. & Swithenbank, J. 2006 Effect of fuel properties on biomass combustion: Part i. experiments–fuel type, equivalence ratio and particle size. *Fuel* **85** (7-8), 1039–1046.

Saastamoinen, J J, Taipale, R, Harttanainen, M & Sarkomaa, P 2000 Propagation of ignition front in beds of wood particles. *Combustion and flame* **123**, 214–226.

Scala, F 2009 A new technique for the measurement of the product co/co_2 ratio at the surface of char particles burning in fluidized bed. *Proc. combust. Instit* **32**, 2021–2027.

Sharma, S K 1993 Improved solid biomass burning cookstoves: A development manual, regional wood energy development programme in asia. *Tech. Rep.* 44. FAO Field Document.

Shastri, CM, Sangeetha, G. & Ravindranath, NH 2002 Dissemination of efficient astra stove: case study of a successful entrepreneur in sirsi, india. *Energy for Sustainable Development* **6** (2), 63–67.

Smith, K.R. 1994 Health, energy, and greenhouse-gas impacts of biomass combustion in household stoves. *Energy for sustainable development* **1** (4), 23–29.

Smith, K.R. 2002 In praise of petroleum? *Science* **298** (5600), 1847.

Smith, K.R., Dutta, K., Chengappa, C., Gusain, PPS, Masera, O., Berrueta, V., Edwards, R., Bailis, R. & Shields, K.N. 2007 Monitoring and evaluation of improved biomass cookstove programs for indoor air quality and stove performance: conclusions from the household energy and health project. *Energy for Sustainable Development* **11** (2), 5–18.

Smith, K.R., Uma, R., Kishore, VVN, Zhang, J., Joshi, V. & Khalil, MAK 2000*a* Greenhouse implications of household stoves: an analysis for india. *Annual Review of Energy and the Environment* **25** (1), 741–763.

Smith, K.R., (US), National Risk Management Research Laboratory & Center, E.W. 2000*b* *Greenhouse gases from small-scale combustion devices in developing countries, Phase IIa: Household Stoves in India*. US Environmental Protection Agency, Office of Research and Development, National Risk Management Research Laboratory.

Thunman, H & Leckner, Bo 2005 Influence of size and density of fuel on combustion in a packed bed. *Proc. combust. Instit* **30**, 2939–2946.

Varunkumar, S., Rajan, NKS & Mukunda, HS 2011 Single particle and packed bed combustion in modern gasifier stoves density effects. *Combustion Science and Technology* **183** (11), 1147–1163.

Wall, TF, Bhattacharya, SP, Zhang, DK, Gupta, RP & He, X. 1993 The properties and thermal effects of ash deposits in coal-fired furnaces. *Progress in energy and combustion science* **19** (6), 487–504.

Yang, YB, Sharifi, VN & Swithenbank, J. 2004 Effect of air flow rate and fuel moisture on the burning behaviours of biomass and simulated municipal solid wastes in packed beds. *Fuel* **83** (11-12), 1553–1562.

Yu, J & Zhang, M C 2009 Experimental and modeling study on char combustion. *Energy and Fuels* **23**, 2874–2885.

Zbogar, A. & Frandsen, F. 2003 Surface emissivity of coal ashes. *IFRF Combustion Journal* pp. 1–5.

Zbogar, A., Frandsen, F.J., Jensen, P.A. & Glarborg, P. 2005 Heat transfer in ash deposits: A modelling tool-box. *Progress in energy and combustion science* **31** (5-6), 371–421.